INVESTIGATING THE SPATIOTEMPORAL VARIABILITY OF NO_2 AND PHOTOCHEMISTRY IN URBAN AREAS

A Dissertation

Presented to the Faculty of the Department of

Earth and Atmospheric Sciences

University of Houston

In Partial Fulfillment

of the Requirements for the Degree

Doctor of Philosophy

By

Laura Margaret Judd

May 2016

INVESTIGATING THE SPATIOTEMPORAL VARIABILITY OF NO_2 AND PHOTOCHEMISTRY IN URBAN AREAS

_____

Laura M. Judd

APPROVED:

_____

Dr. Xun Jiang, UH EAS, Chairman

_____

Dr. Yunsoo Choi, UH EAS

_____

Dr. Shuhab D. Khan, UH EAS

_____

Dr. James H. Crawford, NASA Langley

_____

Dr. Barry L. Lefer, NASA Headquarters

_____

Dean, College of Natural Sciences and Mathematics

ACKNOWLEDGEMENTS

There are many individuals and teams without whom this research and Ph.D. degree would not be possible. I would like to start off by sharing my sincere gratitude to Dr. Barry Lefer for guiding me through the first few years of my graduate career, and Dr. Xun Jiang for taking me under her wing in the last year and helping me finish my degree requirements and research. I would not have finished without them both. Next, I want to thank the rest of my dissertation committee—Dr. Yunsoo Choi (UH), Dr. Shuhab Khan (UH), and Dr. James Crawford (NASA Langley)—for their time and guidance with respect to this research and my education. These projects would also not be possible without the data collection and analysis from the science teams for OMI, CalNex, and DISCOVER-AQ, as well as Hyun Cheol Kim (NOAA), Mark Estes (TCEQ), and David Westenbarger (TCEQ). Grants from NASA, TCEQ, and AQRP also made funding for the research possible. Finally, I want to acknowledge the numerous other scientists, classmates, friends, and family for their support in getting me through graduate school and earning my degree.

INVESTIGATING THE SPATIOTEMPORAL VARIABILITY OF NO_2 AND PHOTOCHEMISTRY IN URBAN AREAS

An Abstract of a Dissertation

Presented to the Faculty of the Department of

Earth and Atmospheric Sciences

University of Houston

In Partial Fulfillment

of the Requirements for the Degree

Doctor of Philosophy

By

Laura Margaret Judd

May 2016

ABSTRACT

The spatial distribution of nitrogen dioxide (NO_2) is difficult to measure due to sparse ground-base monitoring and the poor spatial-resolution of space-based sensors. A better understanding of how satellite-derived NO_2 columns compare to surface conditions will help in the assessment of regulations for improving air quality and reducing health risks. This dissertation addressed questions on the spatial and temporal variability of NO_2 as monitored from the ground, aircraft, and space, as well as how emission reductions influenced the photochemical environment in Houston, Texas. Part one compared satellite (OMI), airborne photometry (GeoTASO), and *in situ* P-3B aircraft measurements of NO_2 columns to those measured by a network of eleven ground-based Pandora spectrometers in Houston, TX during the NASA DISCOVER-AQ Texas campaign in September 2013. Results showed how the spatial resolution of measurements influenced the intercomparison due to the strong spatial variability of NO_2 in urban areas. Part two studied the spatial heterogeneity of NO_2 during the CalNex 2010 campaign in California by comparing three OMI tropospheric column retrievals (NASA Standard Product, KNMI DOMINO, and BEHR) and a new OMI downscaling technique to *in situ* aircraft measurements. Near urban environments, the aircraft measurements were not representative of the OMI observations as a result of the spatial heterogeneity of NO_2 and the different spatial coverage of these two different observations. When OMI NO_2 measurements were downscaled, the aircraft-to-downscale comparisons showed improvement for areas with high NO_2 pollution.

Finally, in part three, the LaRC photochemical box model was used to evaluate how ozone photochemistry had changed between 2000 and 2014 in Houston, Texas. The model results showed that the decline in the number and severity of ozone events in the Houston Ship Channel was due to significant decreases in highly reactive volatile organic carbons (HRVOCs). Furthermore, on high-ozone days, this chemical system transitioned to a more VOC-sensitive regime resulting in a decrease in the instantaneous ozone production efficiency. These results suggest that further reducing HRVOC emissions is the most efficient way to bring the Houston metropolitan area into compliance with the EPA's ozone National Ambient Air Quality Standards (NAAQS).

TABLE OF CONTENTS

LIST OF FIGURES

LIST OF ACRONYMS

AMF: Air Mass Factor

ARCTAS-CA: Arctic Research of the Composition of the Troposphere from Aircraft and Satellites-California

Auto-GC: Automatic Gas Chromatograph

BEHR: Berkeley High Resolution NO_2 tropospheric column product

CAMS: Continuous Ambient Monitoring Sites

CMAQ: Community Modeling and Analysis System model

CO: Carbon Monoxide

DANDELIONS: Dutch Aerosol and Nitrogen Dioxide Experiments for Validation of OMI and SCIAMACHY

DEM: Digital Elevation Model

DISCOVER-AQ: Deriving Information on Surface conditions from COlumn and VERtically resolved observations relevant to Air Quality

DOAS: Differential Optical Absorption Spectroscopy

DOMINO: Dutch OMI NO_2 product

EOS: Earth Observing System

ECMWF: European Center for Medium range Weather Forecasting

FOV: Field of View

FWHM: Full-Width Half-Maximum

GeoTASO: Geostationary Trace gas and Aerosol Sensor Optimization

GMI CTM: Global Modeling Initiative Chemical Transport Model

GoMACCS: Gulf of Mexico Atmospheric Composition and Climate Study

GOME/GOME-2: Global Ozone Monitoring Experiment

HCHO or CH_2O: Formaldehyde

HGB: Houston-Galveston-Brazoria

HNO_3: Nitric Acid

HRVOC: Highly-Reactive Volatile Organic Carbon

INTEX-A and INTEX B: Intercontinental Chemical Transport Experiment Phase A and B

IOPE: Instantaneous Ozone Production Efficiency

jNO_2: NO_2 photolysis rate

KNMI: Koninklijk Nederlands Meteorologisch Instituut

LaRC: Langley Research Center

LIDAR: Light Detection And Ranging

LST: Local Standard Time

LUT: Look-Up Table

MAX-DOAS: Multi-Axis Differential Optical Absorption Spectroscopy

MDA8: Maximum Daily Average 8-hr

MODIS: Moderate Resolution Imaging Spectroradiometer

NAAQS: National Ambient Air Quality Standards

NAQFC: National Air Quality Forecasting Capability

NASA: National Aeronautics and Space Administration

NO: Nitric Oxide

NO_2: Nitrogen Dioxide

NOAA: National Oceanic and Atmospheric Administration

NOx: Nitrogen Oxides ($NO+NO_2$)

O_3: Ozone

OMI: Ozone Monitoring Instrument

OPE: Ozone Production Efficiency

P-Cl: Photolysis-Chemiluminescence

PAN: Peroxyacytyl nitrate

PM: Particulate Matter

RMSE: Root-Mean-Square Error

SCIAMACHY: SCanning Imaging Absorption spectroMeter for Atmospheric CHartographY

SP: NASA Standard Product

TCEQ: Texas Commission for Environmental Quality

TEMPO: Tropospheric Emission: Monitoring of Pollution

TexAQS: Texas Air Quality Study (2000 and 2006)

TROPOMI: TROPOspheric Monitoring Instrument

UTC: Universal Time Coordinated (+ 6 hours from Houston LST)

UV: Ultraviolet

Vis: Visible

VOC: Volatile Organic Carbon

WAS: Whole Air Sampler

1. INTRODUCTION

While Earth's stratospheric ozone layer is essential for living organisms to thrive on our planet, ozone near the surface is harmful to life and detrimental to human health, particularly those in sensitive-health groups. Since the 1970s, ozone levels, along with other criteria pollutants (including nitrogen dioxide, or NO_2), have been monitored and regulated in the United States with the implementation of the Clean Air Act (https://www.epa.gov/laws-regulations/summary-clean-air-act).

While Houston is compliant with the NO_2 National Ambient Air Quality Standards (NAAQS), ozone still falls above the threshold for the EPA's NAAQS. Compliance for 8-hr ozone NAAQS is defined by a design value: the three-year average of the annual 4^{th} highest maximum daily 8-hr average (MDA8) ozone level. Although the number and severity of ozone events have decreased since the late 1990s, Houston still has occurrences of unhealthy ozone levels with a design value currently around 80 ppbv for the region (Figure 1-1). The threshold for compliance is 70 ppbv as of 2016.

Ozone is produced in the presence of sunlight, NOx ($NO + NO_2$), and volatile organic carbons (VOCs, also referred to as hydrocarbons). The naturally occurring ozone null-production cycle, as indicated by reactions R1.1, R1.3, and R1.4 below, results in zero net ozone production:

(R1.1) $NO + O_3 \rightarrow NO_2 + O_2$
(R1.2) $NO + RO_2 \rightarrow NO_2 + RO$ (where R can be H, CH_3, C_2H_5, etc.)
(R1.3) $NO_2 + h\nu \rightarrow NO + O$
(R1.4) $O + O_2 \rightarrow O_3$

During this cycle, ozone is only produced when another ozone molecule is destroyed for the production of NO_2, thus keeping ozone levels in equilibrium. However, in the presence of oxidized VOCs (peroxy radicals, RO_2), NO_2 is created without ozone destruction (R1.2). High rates of ozone production are common in areas with significant anthropogenic activities that produce NOx and hydrocarbon emissions, resulting in ozone-exceedance events.

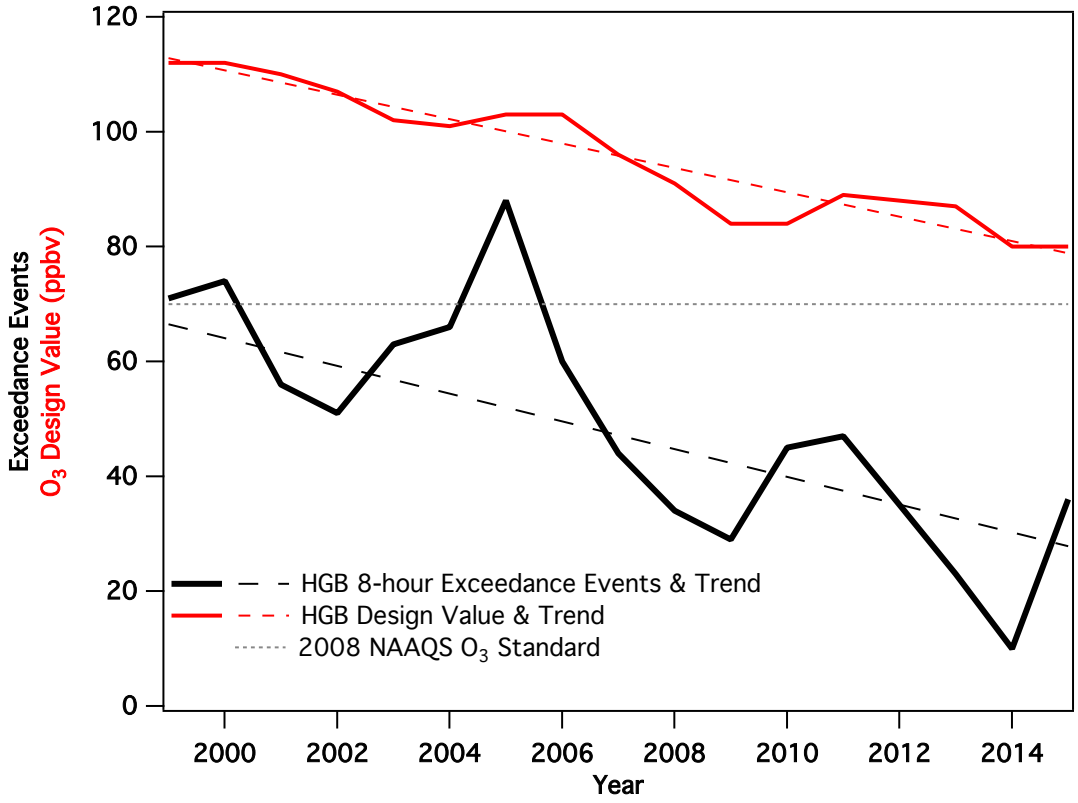

Figure 1-1: The number of ozone exceedances each year in the Houston-Galveston-Brazoria (HGB) region (solid black) with a best-fit linear trend (dashed black), design value for the HGB region (solid red) and its trend (dashed red), along with the 2016 8-hr NAAQS ozone standard (grey dots).

When meteorological conditions are conducive for ozone production (low-wind speeds and strong sunlight), either NOx or VOCs limit reaction R1.2. When NOx is in excess, ozone production is VOC-limited or NOx-saturated. When NOx levels are low and VOCs are in excess, ozone production is NOx-limited or VOC-saturated. Identifying whether an area is NOx or VOC-limited is important from a regulatory standpoint, as it defines the quickest way to decrease ozone pollution for that area. Limiting ingredients for ozone production vary from place to place and depend on the ratio of NOx and VOC emissions. Urban areas dominated by primarily mobile emissions are usually VOC-sensitive throughout the day, such as in New York City (Mao et al., 2010). An area like Houston is unique with its higher emissions of highly reactive VOCs (HRVOCs) from the petrochemical facilities located near the Ship Channel (Kleinman et al., 2002; Mao et al., 2010). Previous studies near downtown Houston had shown a diurnal pattern shifting from VOC-limited to NOx-limited in the late-morning hours during the fall months of 2000, 2006, and 2009 (Flynn, 2013; Mao et al., 2010; Ren et al., 2013). This diurnal transition is driven by the morning rush hour resulting in excess NOx in the urban parts of the region. On high-ozone producing days in Houston, the temporal transition between sensitivity regimes often shifts to later in the day (Ren et al., 2013).

Houston has been the center of numerous air quality studies since the turn of the century. The Texas Air Quality Study 2000 (TexAQS 2000) included both ground and aircraft measurements with the goal of understanding the relationship between

emissions, meteorology, and air quality in the region (Daum et al., 2003). Similar to the 2000 study, the 2006 TexAQS II (and the Gulf of Mexico Atmospheric Composition and Climate Study (GoMACCS)) campaign in Houston also studied these relationships and investigated how changing emissions can influence air quality conditions (Parrish et al., 2009). High-ozone events in Houston occur during days of stagnation when there are opposing flows of the onshore sea breeze and offshore post-frontal winds (Banta et al., 2005; Daum et al., 2003; Lefer et al., 2010). The timing of these flows may also result in advected emissions during the morning to the Gulf of Mexico and resultant ozone being pushed back inland with the arrival of the sea-breeze front later in the day (Banta et al., 2005; Lefer et al., 2010). Fast ozone production rates are often observed over the Houston Ship Channel, where VOCs accumulate from the petrochemical facilities (Daum et al., 2003). Results from these research campaigns found that emission inventories vastly underestimated VOC emissions, and these emission inaccuracies were still present in the results from later research campaigns (Jiang et al., 2004; Parrish et al., 2009; Ryerson et al., 2003;Washenfelder et al., 2010). Fortunately, VOC emissions decreased from TexAQS 2000 to TexAQS II/GoMACCS (Daum et al., 2003; Ryerson et al., 2003; Zhou et al., 2014). Similar reductions in hydrocarbon reactivity were observed when comparing results from 2006 to 2010 for a central-Houston measurement location, the University of Houston's Moody Tower (Flynn, 2013).

The most recent air quality research campaign in the Houston region was the Deriving Information on Surface conditions from COlumn and VERtically resolved

observations relevant to Air Quality (DISCOVER-AQ) in September 2013. DISCOVER-AQ's primary goals were to (1) relate surface conditions of O_3, NO_2, and CH_2O to column measurements from ground and space-based platforms, (2) determine how the column-to-surface relationship changes diurnally, and (3) examine what conditions influence the spatial variability of these trace-gases (https://www.nasa.gov/mission_pages/discover-aq/science/index.html). This project was motivated by the future launch of the first geostationary air quality observing satellite, Tropospheric Emission: Monitoring of Pollution (TEMPO), over North America. This sensor will have unprecedented spatial resolution of ~ 2×4.5 km^2 at nadir, the center of the satellite-observing swath (Figure 1-2), and it will also be able to monitor air quality for most of North America hourly (Zoogman et al., submitted).

The first two parts of this dissertation will focus on the remote sensing of NO_2 for two different urban areas. Since the 1990s, NO_2 has been observed from space with the Global Ozone Monitoring Experiment (GOME), GOME-2, SCanning Imaging Absorption spectroMeter for Atmospheric CHartographY (SCIAMACHY), and the Ozone Monitoring Instrument (OMI) (Bovensmann et al. 1999; Burrows et al., 1999; Callies et al., 2000; Levelt et al., 2006; Valks et al., 2011). In late 2016, TROPOspheric Monitoring Instrument (TROPOMI) is expected continue these observations of global NO_2 similar to the sun-synchronous polar-orbiting sensors mentioned above, but at a smaller spatial scale (~ 7×7 km^2, Figure 1-2) (van Geffen et al., 2016). In addition to studying the magnitude and spatial distribution of NO_2, space-based measurements also

allow for a global view of how emission mitigations influence air quality (Duncan et al., 2015; Kim et al., 2006; Lamsal et al., 2015; Lu et al., 2015; Russell et al., 2012). Unfortunately, sun-synchronous polar-orbiting sensors cannot be utilized to explore diurnal patterns. OMI currently overpasses during the early-afternoon hours, which misses the daily rush-hour peaks in urban areas. This is where a geostationary sensor like TEMPO will aid in the study of diurnal patterns in air quality over North America.

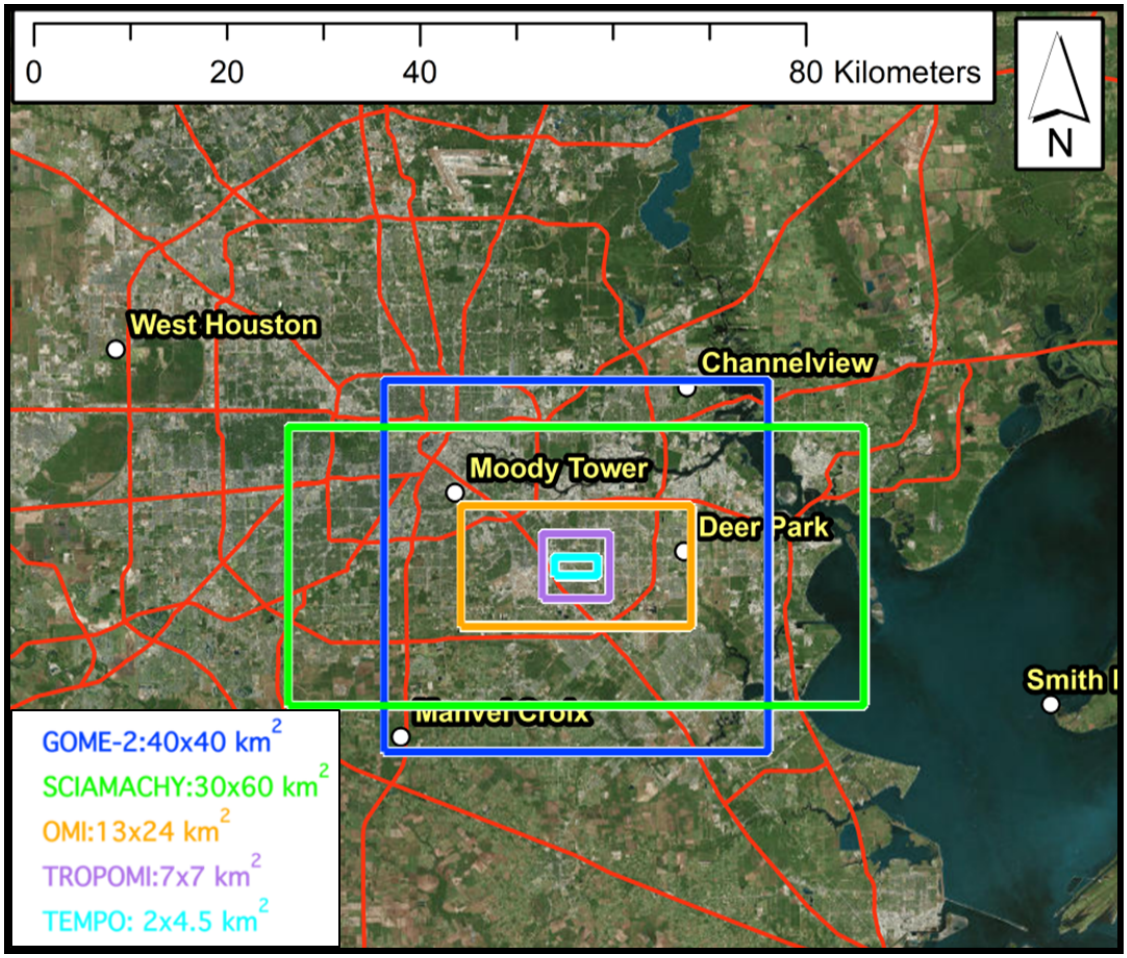

Figure 1-2: Map displaying typical pixel size for nadir NO_2 retrievals from GOME-2, SCIAMACHY, OMI, TROPOMI, and TEMPO in comparison to the Houston metropolitan area.

Validations of space-based observations are necessary to determine that sensor's capability for retrieving accurate data. Past validations included comparisons to other NO_2 measurements such as LIDARs, MAX-DOAS, Pandora direct-sun DOAS, and aircraft and ground *in situ* data (Boersma et al., 2008; Boersma et al., 2009; Brinksma et al., 2008; Bucsela et al., 2008; Bucsela et al., 2013; Celarier et al., 2008; Hains et al., 2010; Herman et al., 2009; Kramer et al., 2008; Martin et al., 2006; Russell et al., 2011; Tzortziou et al. 2013). These studies all made data-filtering assumptions to obtain the closest 'apples to apples' comparisons, which included time differences, cloud conditions, profile shapes, and boundary layer assumptions, among others. These studies also took pollution levels and spatial heterogeneity into consideration, but often stated spatial heterogeneity as exceptions where measurements did not compare well. This work will investigate how the spatial heterogeneity of NO_2 can influence measurement comparisons, and show that these influences change at varying instrument spatial resolutions near the urban environments of Houston and Los Angeles.

The improvements in future satellite NO_2 measurements will be considerably more useful to state regulators as observations enter the realm of the sub-urban spatial scale. Figure 1-2 demonstrates how current and previous sensors often encompassed multiple and highly varying pollution-environments ranging from rural to urbanized/ industrial. Understanding spatial heterogeneity will aid in urban studies on the spatial variability and emissions of NO_2, as well as future validations of TEMPO, TROPOMI,

and other sensors observing NO_2 and other short-lived trace-gases, as the spatial resolution approaches the scale of the environmental heterogeneity of NO_2.

As stated above, one of the purposes of DISCOVER-AQ was to study the surface-to-column relationship and spatial heterogeneity of NO_2 for monitoring purposes as space-based measurements enter sub-urban spatial scales. Before coming to Texas in September 2013, the DISCOVER-AQ team deployed in Maryland in 2011 and California earlier in 2013. In Maryland, the Pandora and OMI observations compared well with respect to NO_2 at times, but were influenced by clouds, aerosol layers, and OMI's wide field of view (Reed et al., 2013). The NO_2 column retrieved from the Community Modeling and Analysis System (CMAQ) model and Pandora measurements also spanned an order of magnitude spatially and diurnally, but the coarse resolution of OMI was unable to capture this variability (Tzortziou et al., 2013). Lamsal et al. (2014) also reported that during the Maryland DISCOVER-AQ campaign, the NO_2 column comparisons only had moderate correlation to surface and aircraft measurements, and OMI tended to underestimate NO_2 when compared with the more urbanized air quality measurement sites. Quantifying surface conditions from column information has proved to be difficult due to NO_2 often not being well-mixed through the boundary layer. Consequently, boundary layer height information was found to be useful in improving surface to column comparisons of NO_2 (Flynn et al., 2014a; Knepp et al., 2013). Boundary layer height accounted for ~ 75% of the variability between column and surface concentration datasets during DISCOVER-AQ Maryland (Knepp et al., 2013).

The following chapters will present analysis and results of the spatial variability of NO_2 and its influences on measurement intercomparisons, as well as how decreasing ozone precursor emissions had affected Houston's ozone photochemistry between 2000-2014. Chapter 2 compares all methods of NO_2 measurements from ground, aircraft, and satellite during DISCOVER-AQ Texas 2013. Chapter 3 focuses more on satellite retrievals for tropospheric NO_2 and how retrieval assumptions and environmental heterogeneity affect comparisons to aircraft data in southern California. Chapter 3 will also introduce a technique for downscaling satellite measurements to sub-satellite spatial resolutions using a chemical transport model. Finally, Chapter 4 shows results from the LaRC photochemical box model in the industrial, urban, and rural portions of Houston using continuous monitoring data from the Houston Ship Channel and aircraft data, when available. The model analysis of Houston's air quality through time will demonstrate how decreasing VOCs have influenced Houston's ozone photochemistry and provide advice on how to further decrease ozone pollution in the region.

2. INTERCOMPARISON OF NO_2 *IN SITU* AND COLUMN MEASUREMENTS DURING DISCOVER-AQ TEXAS

2.1 INTRODUCTION

Nitrogen oxides (NOx) are short-lived highly reactive trace-gases composed of nitric oxide (NO) and nitrogen dioxide (NO_2). The lifetime of NOx has been reported as less than half a day in the summer US boundary layer (Liang et al., 1998) leading to high spatial variability in NOx peaks near emission sources. NO_2 is one of the six criteria pollutants included in the Clean Air Act, and the EPA has defined NO_2 standards since 1971. In urban areas, NOx is emitted by combustion in power plants, industry, and mobile sources (http://www3.epa.gov/airquality/nitrogenoxides/index.html). Current NO_2 NAAQS are 100 ppbv for a 1-hour average (based on the 98th percentile averaged over 3 years) and an annual average of 53 ppbv.

While Houston's air quality does not exceed the NO_2 NAAQS, it is non-compliant with the ozone NAAQS and does not fall far below in PM 2.5 standards. Since NOx is one of the key ingredients needed to produce ozone and PM 2.5, continuous high-quality NO_2 surface monitoring is needed in urban areas like Houston. The current number of these NO_2 monitors is not nearly extensive enough to understand how NO_2 is influencing the atmospheric photochemistry in most metropolitan areas.

Since the mid 1990s, space-based instruments have measured the magnitude and spatial distribution of NO_2 globally with the Global Ozone Monitoring Experiment

(GOME), GOME-2, SCanning Imaging Absorption spectroMeter for Atmospheric CHartographY (SCIAMACHY), and Ozone Monitoring Instrument (OMI) sensors (Bovensmann et al. 1999; Burrows et al., 1999; Callies et al., 2000; Levelt et al., 2006; Valks et al., 2011). In addition to studying the magnitude and distribution of NO_2, space-based measurements also allow for a global view of how emission mitigations influence our environment with decreasing concentrations (Kim et al., 2006; Lamsal et al., 2015; Lu et al., 2015; Russell et al., 2012). Sensors such as OMI or SCIAMACHY also allow for emissions estimates from a top-down approach without the time consuming information needed for bottom-up methods (de Foy et al., 2015; Lamsal et al., 2011).

OMI is the latest space-based platform currently in use with a spatial resolution at nadir of 13×24 km^2 (Figure 1-2). In the near future, TROPOMI and TEMPO will be launched with improved spatial resolutions of 7×7 km^2 and 2×4.5 km^2, respectively, allowing for a view of NO_2 at sub-urban spatial scales (van Geffen et al., 2016; Zoogman et al., submitted). While TROPOMI will follow precedent and be located in a sun-synchronous orbit, TEMPO will be the first geostationary satellite dedicated to air quality monitoring, allowing scientists to study the diurnal evolution of air quality at an unmatched spatial scale over North America. The sensor will be able to measure columns of NO_2, O_3, HCHO, and other air quality parameters at hourly time steps over North America. As such observations are unprecedented, the DISCOVER-AQ campaign was dedicated to observing how air quality varies on a diurnal timescale and how

surface characteristics can be related to geostationary space-based column measurements (https://www.nasa.gov/mission_pages/discover-aq/).

This chapter aids in DISCOVER-AQ's goals (listed in Chapter 1) by intercomparing NO_2 measurements from DISCOVER-AQ Texas in September 2013. Analysis was focused on investigating the effect of the instruments' spatial resolutions and the spatial heterogeneity of NO_2 on the observations' relationships. Pandora spectrometer measurements were compared to other collocated NO_2 column and *in situ* measurements including: directly measured columns from OMI and the Geostationary Trace gas and Aerosol Sensor Optimization (GeoTASO), and derived-column measurements from *in situ* samples from the NASA P-3B and two ground sites (Moody Tower and Galveston).

Pandora has been used for previous validations of space-based sensors and had compared well over long-term measurement periods for column-to-column comparisons (Herman et al., 2009; Reed et al., 2013; Tzortziou et al., 2013). Differences in measurements were dependent on parameters such as cloud cover, aerosols, pollution environment, and OMI's wide field of view. Unfortunately, OMI only captures an early-afternoon snapshot of NO_2 and therefore misses the major rush-hour maxima. The relationship between surface and column measurements was more complex than ozone's, as it appeared to depend on additional factors, such as boundary layer height and mixing (Flynn et al., 2014a; Knepp et al, 2013).

For this study, measurements were spread throughout the region capturing urban, industrial, and rural environments from ground sites, aircraft, and satellites. Relationships were analyzed while taking into consideration the spatial footprint of the measurements and the spatial variability of NO_2. Finally, column and surface conditions were related at an urban site (Moody Tower) and a rural site (Galveston) to examine the capabilities of monitoring surface air quality from column observations of NO_2. This analysis will aid in the validation of TEMPO by demonstrating how Pandora compared to varying measurement spatial scales, as well as demonstrating how the shrinking field of view, with the launches of TROPOMI and TEMPO, will improve urban-scale studies for the spatial distribution and magnitude of NO_2.

2.2 DATA

All data used in this analysis can be downloaded at the DISCOVER-AQ DOI: http://doi.org/10.5067/Aircraft/DISCOVER-AQ/Aerosol-TraceGas

2.2.1 PANDORA SPECTROMETER

The Pandora Spectrometer measured NO_2 trace-gas columns using direct-sun spectra and Differential Optical Absorption Spectroscopy (DOAS) (Herman et al., 2009; Tzortziou et al., 2012). Information about this retrieval and instrument can be found in Herman et al. (2009). The Pandora instrument is composed of an optical head with two filter wheels (neutral density and band-pass filters) with an attached 1.6° field of view (FOV) collimator mounted on a solar tracker. The head sensor is connected to the UV-

VIS spectrometer via a fiber-optic cable measuring UV-VIS spectra from 290-500 nm with a full-width half-maximum (FWHM) of approximately 0.5nm.

In recent years, the Pandora spectrometer has been used for ground and satellite intercomparisons (Flynn et al., 2014a; Herman et al., 2009; Reed et al., 2013; Wang et al., 2010). The spatial and temporal variability of NO_2 columns had also been studied in Maryland using this instrument (Tzortziou et al., 2013). During DISCOVER-AQ Texas, Pandora spectrometers were located at 11 research sites (Figure 2-1). The spatial distribution of these sites enabled the study of the NO_2 column near rural, urban, and industrial sites. All data used in this analysis had normalized root-mean-square (RMS) of the spectral-fit residuals of less than 0.01 and column errors less than 0.05 DU.

Moody Tower's Pandora was different from the other Pandora locations because the instrument was located at a height of 70 m. Fortunately, NO_2 was measured at 70 m, as well as at the surface. The distribution of NO_2 between the surface and 70 m was assumed to be linear, and a surface to 70 m column was computed as a correction factor to the Pandora measurements at Moody Tower. Since this location is near the junction of three major freeways, there was a strong NO_2 signal from the mobile sources nearby, and this correction is significant at times. Figure 2-2 shows the diurnal average of the 70 m calculated columns, as well as its percent contribution to the total column. Early in the morning, 40% of the total column was below 70 m and decreased to approximately 10-15% later in the day.

2.2.2 OZONE MONITORING INSTRUMENT

The Ozone Monitoring Instrument (OMI) is aboard EOS-Aura, launched in 2004. This sun synchronous nadir-viewing spectrometer measures the daily spatial distribution of NO_2 in the early afternoon globally with an equator-crossing time of 13:30 LST. Its nadir resolution for NO_2 column is 13×24 km^2 (Figure 1-2) and OMI has a spectral resolution of 0.5 nm for the spectral range of 270-500 nm (Levelt et al., 2006). The NO_2 column is retrieved via DOAS from the 405-465 nm range (Bucsela et al., 2006; Bucsela et al., 2013). The NASA Standard Product (Version 2.1 Level 2) was used in this intercomparison, and the most recent information on this retrieval is found in Section 3.2.1.1 and Bucsela et al. (2013). The map in Figure 2-1a displays a typical view of a near nadir OMI NO_2 observation over the Houston region. There was little spatial variability or magnitude in the NO_2 columns. Pixels are filtered by OMI cloud fractions less than 20% and influences from the row anomaly (http://www.knmi.nl/omi/research/product/rowanomaly-background.php).

2.2.3 GEOTASO

The Geostationary Trace gas and Aerosol Sensor Optimization (GeoTASO) is a UV/VIS/NIR backscatter spectrometer similar OMI and is the test bed for future satellite air quality retrievals (Nowlan et al., 2015). During DISCOVER-AQ Texas, this instrument was deployed for the first time on the NASA Falcon. It measured during four days of the campaign while flying at approximately 11 km over the Houston region. The NO_2 retrieval utilized the DOAS technique using the spectral window of 420-465 nm

and a zenith sky measurement for its reference spectrum. O_3, water vapor, O_2-O_2, and the ring spectrum are considered in the spectral fitting for NO_2 slant columns (Nowlan et al., 2015). After correcting for across-track striping, the slant columns were converted to vertical columns using air mass factors (AMFs) calculated following Palmer et al. (2001). The final product consisted of 250×250 m^2 pixels and had been filtered for clouds. All above information, and a more in depth description of GeoTASO, its NO_2 retrieval, and validation can be found in Nowlan et al. (2015). The first flight in Houston for GeoTASO is mapped in Figure 2-1b. These measurements demonstrated the complexity of the spatial distribution of NO_2 over an urban region, especially when compared to the wider field of view from OMI in Figure 2-1a.

2.2.4 NASA P-3B

During this deployment of DISCOVER-AQ, the NASA P-3B flew nine research flights over the Houston region. Each flight consisted of spirals over eight ground sites repeated up to three times a day (morning, midday, and afternoon) (Figure 2-1c). This configuration allowed for the study of trace-gas column abundances both spatially and temporally. All spiral sites had co-located Pandora spectrometers at the surface (except for Moody Tower at 70 m). *In situ* NO_2 on the NASA P-3B aircraft was measured by the National Center for Atmospheric Research's (NCAR) 4-channel NOxyO_3 chemiluminescence instrument at one-second time resolution. To derive column densities from the *in situ* flight data, spiral data was averaged into 100 m bins and integrated from 0-3.5 km to produce a lower tropospheric NO_2 column for comparison

to other observations. In order for the derived column to be considered valid, 80% of the 100 m bins from 0-3.5 km must contain valid data. Gaps within the spiral were linearly interpolated from surrounding bins. End member gaps are extracted from the nearest bin and held as a constant to the surface or 3.5 km.

2.2.5 SURFACE DATA

The relationship between surface concentrations and NO_2 column measurements were investigated at the Moody Tower and Galveston ground sites. NOAA in Galveston and the University of Houston at Moody Tower measured NO_2 concentrations at the surface using a photolytic converter in-line with a chemiluminescence chamber (Pollack et al., 2010). Photolytic converters are more selective of converting NO_2 to NO, and its interferences are less than the standard molybdenum converters (Sather et al., 2006). The University of Houston measured the boundary layer height at Moody Tower and Galveston using a Vaisala CL31 ceilometer that measures aerosol backscatter using a 905 nm laser and identifies lower atmosphere layering by selecting maximum-backscatter gradients (Haman et al., 2012; Münkel et al., 2006). The yellow boxes in Figure 2-1 indicate the locations of the surface sites in this analysis. Moody Tower and Galveston have vastly different pollution-environments, with Moody Tower located in urban Houston, surrounded by numerous freeways, whereas the Galveston site is approximately 1 km from the Gulf of Mexico and experiences a predominantly clean onshore flow.

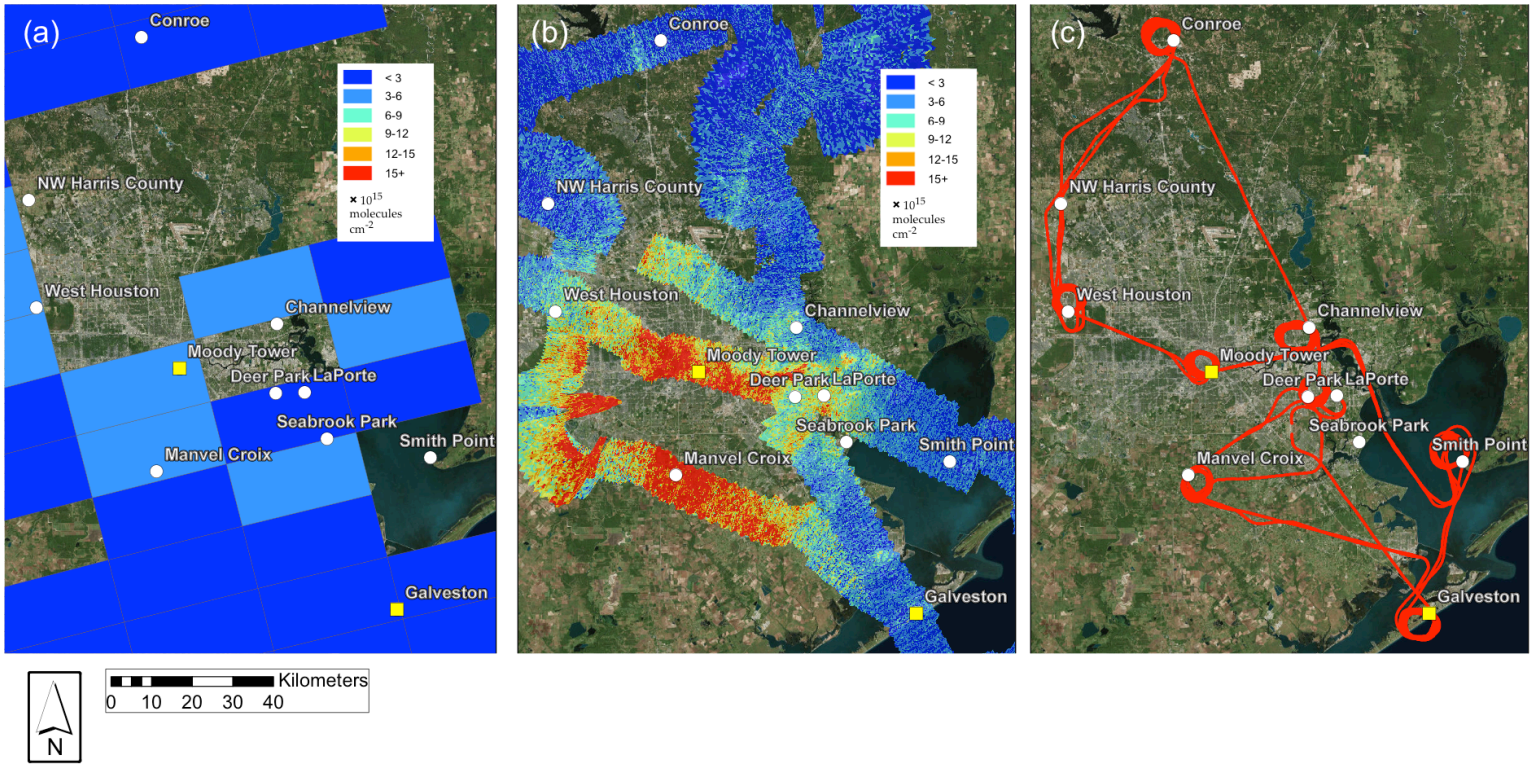

Figure 2-1: Locations of Pandora spectrometers (white circles) and Pandora spectrometers with Vaisala CL31s and in situ data (yellow squares) along with: (a) an OMI NASA Standard Product vertical NO_2 column example, (b) GeoTASO NO_2 vertical columns during on September 13th, and (a) flight path for the NASA P-3B on September 13th during DISCOVER-AQ Texas.

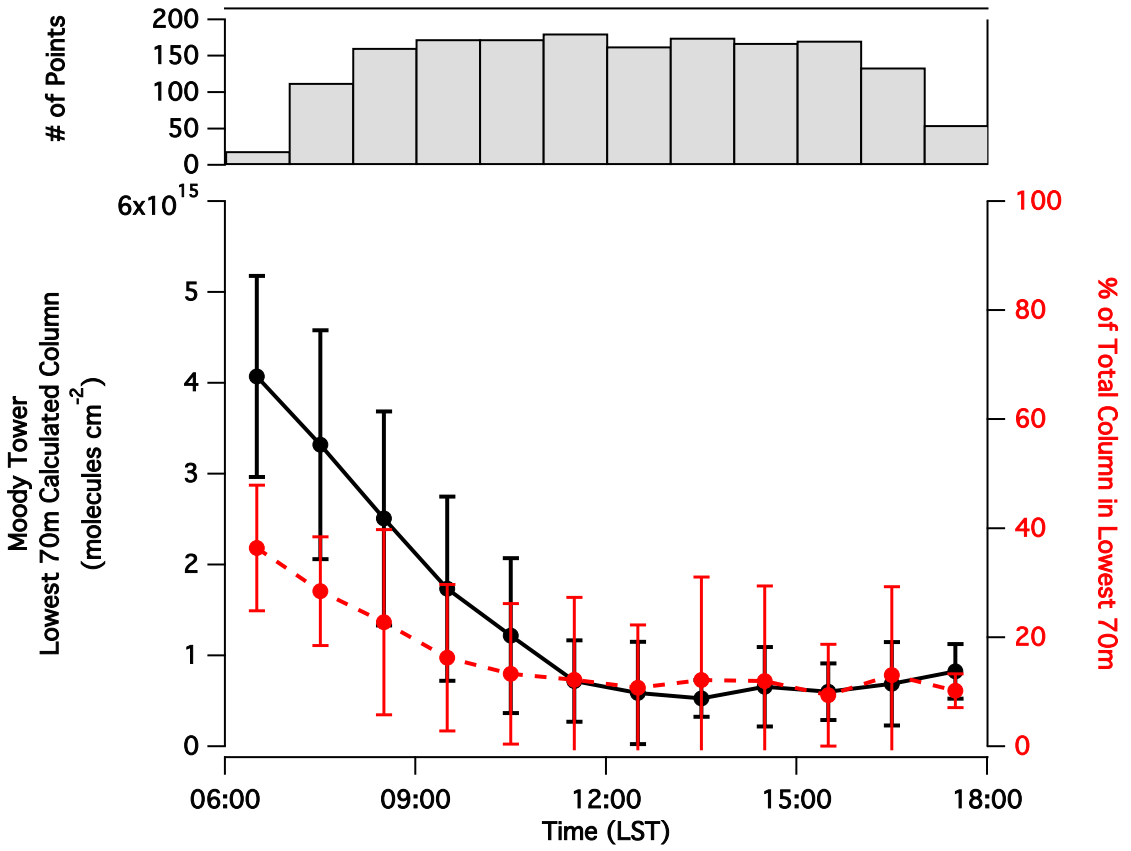

Figure 2-2: The diurnal average of the calculated 70 m column (solid black) and its percent contribution to the total column (dashed red) at Moody Tower. Error bars are ± 1 standard deviation. Grey bars indicate the number of points per hour in the diurnally averaged calculation.

2.3 RESULTS

2.3.1 SPATIAL RESOLUTION INFLUENCES ON COMPARISONS

2.3.1.1 OMI

OMI and Pandora both measured NO_2 columns from the Earth's surface to the top of the atmosphere. However, OMI was looking at reflected sunlight from space with a large footprint while Pandora was measuring direct solar radiation from the Earth's

surface. OMI observed at most two times daily over Houston, whereas Pandora measured a NO_2 column approximately every 90 seconds as it tracked the sun. To compare the two measurements, Pandora was averaged ± 30 min from the OMI overpass time and compared to the OMI pixel in which the Pandora was located. The occurrences of the row anomaly and cloudy conditions limited the dataset during this campaign. On average, each site had 16 coinciding data points with a total of 223 comparisons throughout the entire DISCOVER-AQ Texas deployment.

While there were times when OMI and Pandora matched each other, many comparisons throughout all sites showed scatter (Figure 2-3). The characteristics of this scatter seemed to vary due to the environmental heterogeneity and the spatial footprint mismatch between the two measurements. OMI measured over an area larger than 13×24 km^2 and, therefore, was measuring averaged mixtures of rural, urban, and industrial pollution at most sites. In contrast, Pandora measured a small cone between instrument and the sun that spanned only a few kilometers in the horizontal during the time of the OMI overpasses. As a result, OMI lacked dynamic range because of its wide field of view and the spatial averaging of the NO_2 signal over an urban region. In cleaner environments observed by Pandora, OMI tended to overestimate NO_2, and in the most polluted areas of the city, OMI did not capture the magnitude of NO_2 observed by Pandora.

Close comparisons were only expected if the Pandora footprint was representative of the pollution environment of the OMI pixel. The Galveston Pandora

site was considered a clean site with very little NO_2 emissions within the instrument's field of view. On September 11th, 2013, both OMI and Galveston's Pandora measured a NO_2 total column of ~ 3.6×10^{15} molecules cm^{-2} (Figure 2-4a). The placement of the coincident OMI pixel measured primarily rural/unpolluted environments similar the location of the Galveston Pandora. However, on September 13th (Figure 2-4b), the coincident OMI pixel also encompassed all of urban Galveston and the inlet to Galveston Bay in which many ships travel. The OMI total NO_2 column was almost twice what the Galveston Pandora measured at that time. Most unpolluted sites like Galveston displayed two results: (1) they matched well if the OMI pixel encompassed similarly unpolluted environments, or (2) the OMI measurement was found to be higher than Pandora due to OMI encompassing parts of the urban plume not within Pandora's field of view. In addition to Galveston, this pattern was seen in Manvel Croix, Smith Point, and NW Harris County (Figure 2-3). One exception to this pattern was on September 22-23rd at Smith Point, TX where the Pandora measurements were larger than OMI. However, a frontal passage the day before shifted local winds to predominantly offshore flow. In this case, Smith Point was downwind of the Ship Channel, and it was possible that the Pandora was measuring a local NO_2 pollution on these days and the intensity of this plume was diluted by the OMI wide field of view. Aircraft measurements were unavailable for confirmation of this hypothesis.

Pandora locations near urban areas were often influenced by fresh emissions of NO_2 leading to spatial heterogeneity. For example, the Channelview Pandora was

located at a NO_2-emission transition zone, with many sources to the south-southwest in the Ship Channel and urban Houston and less NOx sources to the northeast. The placement of the OMI pixel in this region always encompassed both polluted and unpolluted environments. Meteorological conditions determined whether the smaller-scale Pandora measurements were associated with densely polluted or cleaner portions of the OMI observation. For example, on September 3rd wind conditions resulted in the pooling of NO_2 over the Channelview location. As a result, the Pandora measured a very-polluted NO_2 total column in comparison to the spatially averaged OMI measurement (Figure 2-4c). Similar to the Galveston case, other days presented conditions where the Pandora measured relatively clean NO_2 columns even though OMI encompassed polluted air in other parts of the region (Figure 2-4b). Considering all these observations, there was an apparent transition across the 1:1 line for a Pandora measurement at approximately 6×10^{15} molecules cm^{-2} (Figure 2-3).

Comparison of smaller-scale Pandora measurements to the larger-scale observations from OMI demonstrated the difficulty in interpreting the spatial heterogeneity of NO_2 from current satellite retrievals. These results suggest expected improvement in capturing the spatial variability as observations approach a sub-urban spatial scale. The data from the future satellite sensors TROPOMI and TEMPO should show less scatter when compared to ground-based instruments such as Pandora, allowing for better applications to urban spatial variability studies.

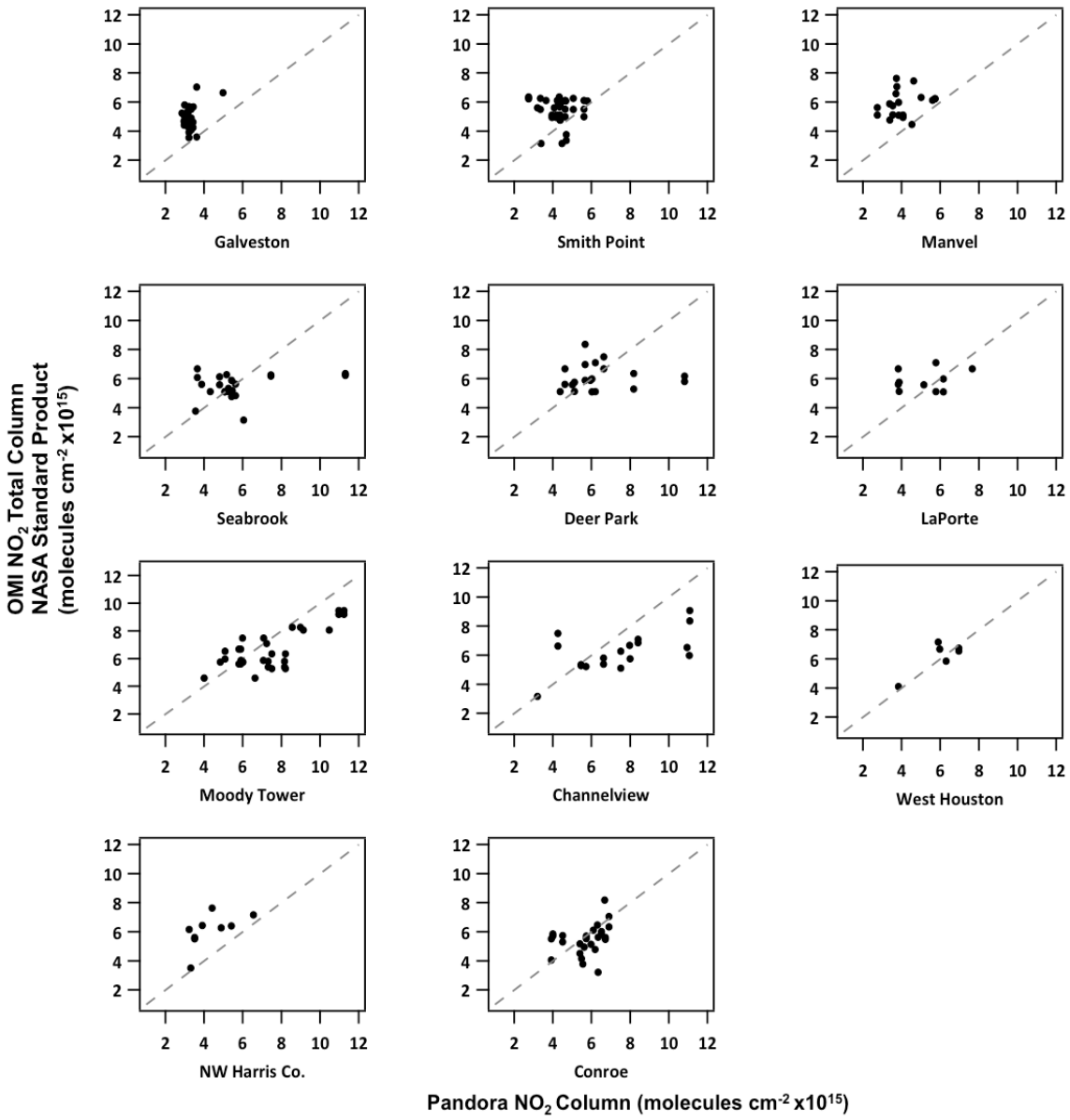

Figure 2-3: Scatter plots comparing the Pandora measurements to the OMI NASA Standard Product total NO_2 columns during DISCOVER-AQ Texas for all 11 Pandora locations. The grey dashed line indicates the 1:1 relationship.

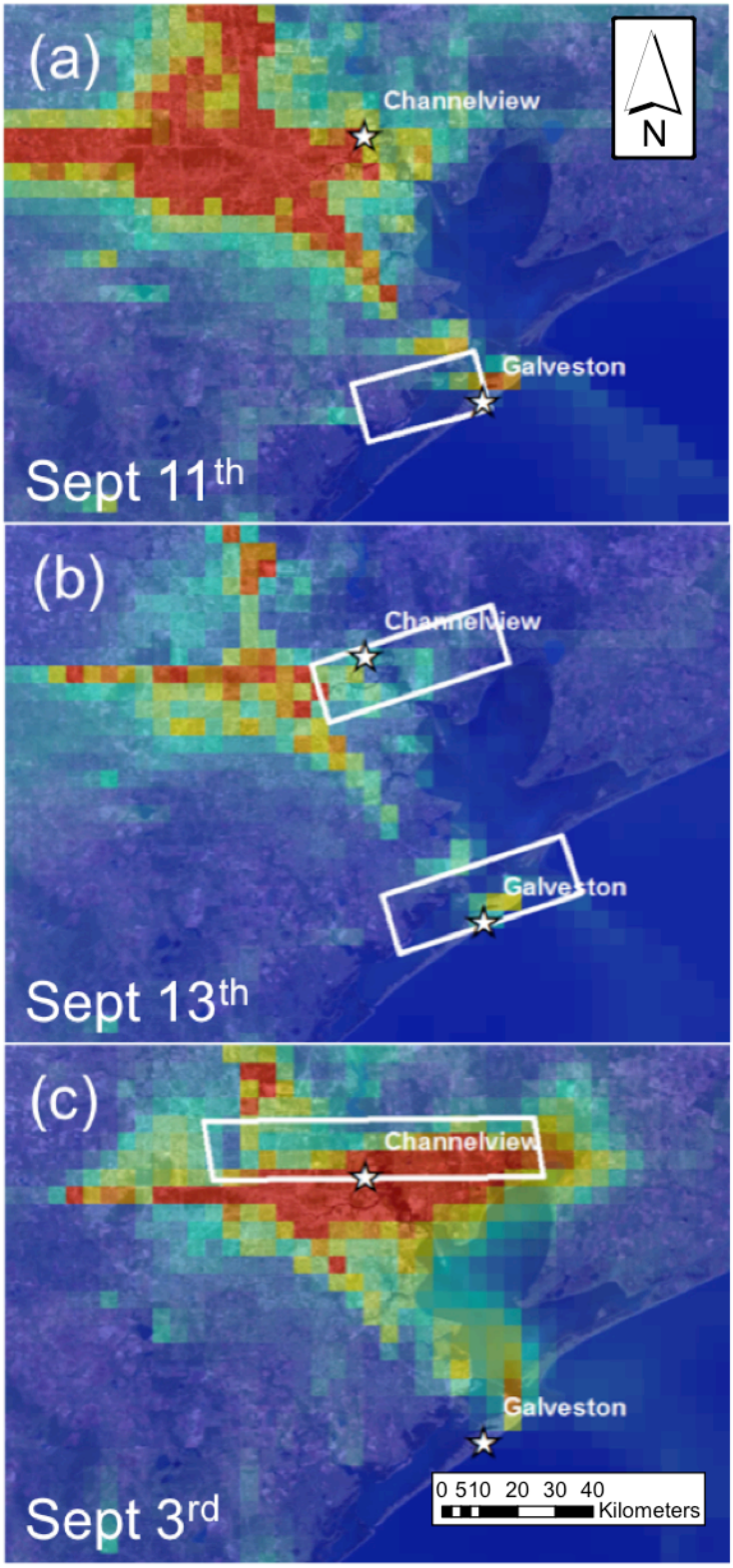

Figure 2-4: OMI pixels (white boxes) overlaid on 4 km CMAQ output of NO_2 concentrations at the surface. Stars indicate the Pandora locations at Galveston and Channelview.

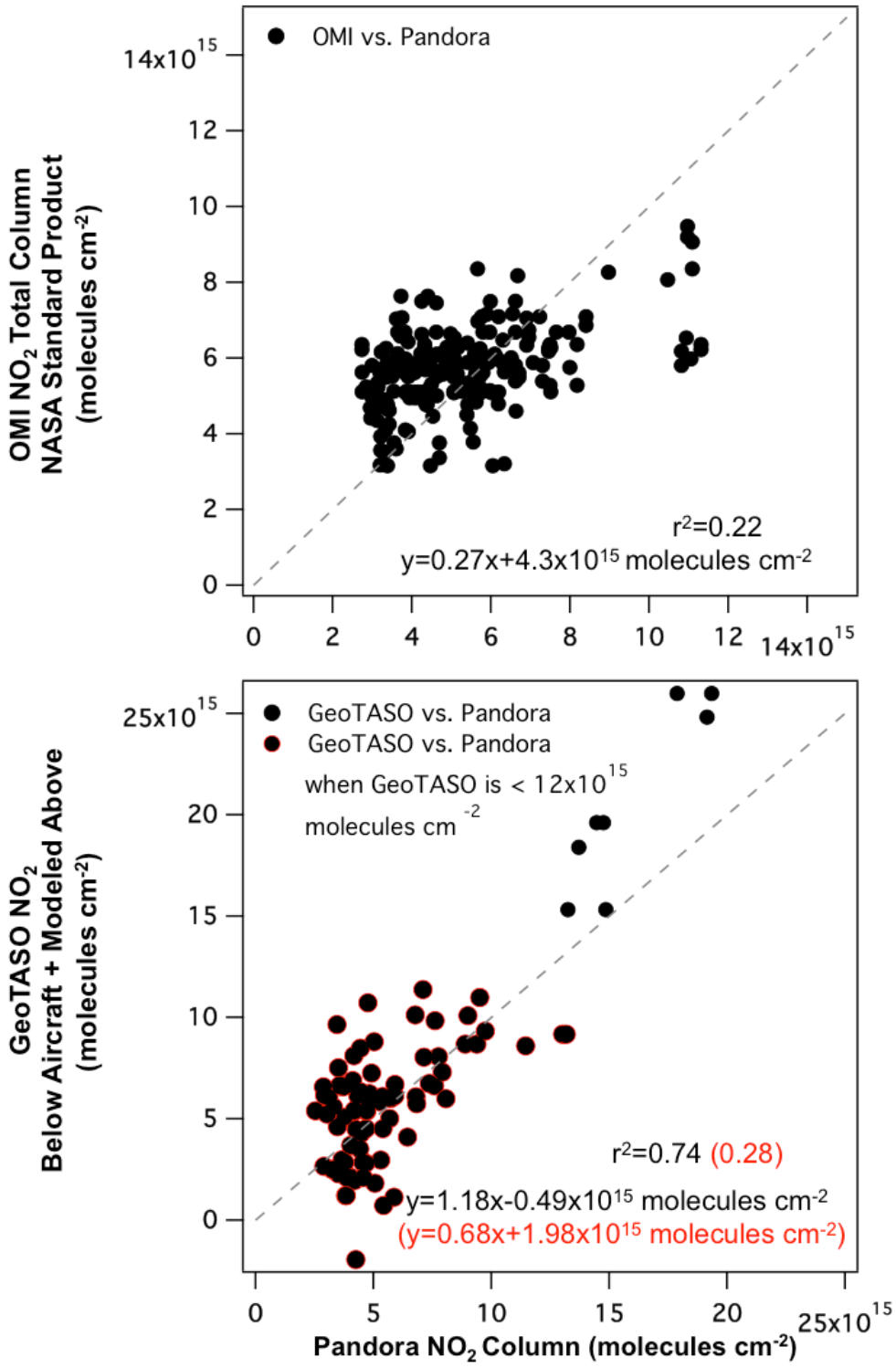

Figure 2-5: Scatter plots of Pandora vs. OMI (top) and Pandora vs. GeoTASO (bottom) with annotated linear regression fits and correlation coefficients for each. Red outlined circles in the bottom graph show a range similar to the dynamic range observed from OMI (statistics in red).

2.3.1.2 GEO-TASO

Pandora comparisons to GeoTASO demonstrated the hypothesis that finer-spatial resolution improved the intercomparison of the two measurements. Similar to the OMI comparison, valid Pandora measurements were averaged ± 30 minutes from the GeoTASO overpass for comparison. The smaller spatial footprint of GeoTASO resulted in fewer cases where there was a concern about observing multiple pollution-environments, like in the OMI comparison. As stated in the previous section, and shown in Figure 2-3, there was considerable scatter between coincident Pandora and OMI measurements ($r^2 = 0.22$). Unpolluted regions were often overestimated by OMI and polluted regions often measured as smaller by OMI, due OMI's wide field of view encompassing both polluted and unpolluted environments (linear regression: OMI = 0.27 [Pandora] + 4.3×10^{15} molecules cm^{-2}).

There was statistical improvement when comparing Pandora to the finer-scale measurements from GeoTASO, as seen in the bottom plot of Figure 2-5. The data was better correlated ($r^2 = 0.74$) and the linear regression slope was closer to a 1:1 comparison (GeoTASO = 1.18 [Pandora] - 0.49×10^{15} molecules cm^{-2}). However, the Pandora measurements during GeoTASO overpasses sampled a larger range than what occurred during OMI overpasses. This difference in range was due to the early-afternoon overpass of OMI not capturing the morning peak in NO_2, whereas GeoTASO obtained some morning observations. When considering GeoTASO data points below a threshold of $12x10^{15}$ molecules cm^{-2} (red outlines in Figure 2-5), the correlation did not

improve when compared to the OMI comparison ($r^2 = 0.28$). However, the linear regression between GeoTASO and Pandora at this reduced range was still better than the comparison to OMI (GeoTASO = 0.68 [Pandora] + 1.98×10^{15} molecules cm^{-2}). The lack of correlation at smaller NO_2 columns was possibly due to GeoTASO measurement noise from retrieval errors and a stray-light issue within its spectrometer. This comparison is expected to improve in later GeoTASO deployments (e.g. DISCOVER-AQ Denver 2014).

GeoTASO comparisons showed improvement in capturing the spatial variability of NO_2 in comparison to OMI because the spatial resolutions of the instruments were using a similar spatial scale. As seen in Figure 2-6, both GeoTASO and Pandora demonstrated their capability in capturing NO_2 heterogeneity. GeoTASO measurements were averaged every five seconds to compare to Pandora on a temporal axis. Five seconds of GeoTASO data covered approximately 2×10 km^2 (Figure 2-7). The GeoTASO and Pandora NO_2 columns correlated for all flights with coincident peaks in NO_2 observed by both instruments (Figure 2-6). The coincident measurements were better correlated on days with higher NO_2 pollution (September 16th and 18th). On the days with more NO_2 signal, the standard deviation of the GeoTASO measurements decreased in magnitude. On cleaner days, possible retrieval uncertainties and stray-light issues became more apparent. Despite these errors, results showed how finer-scale NO_2 column measurements could assist in future studies of urban emission and spatial heterogeneity.

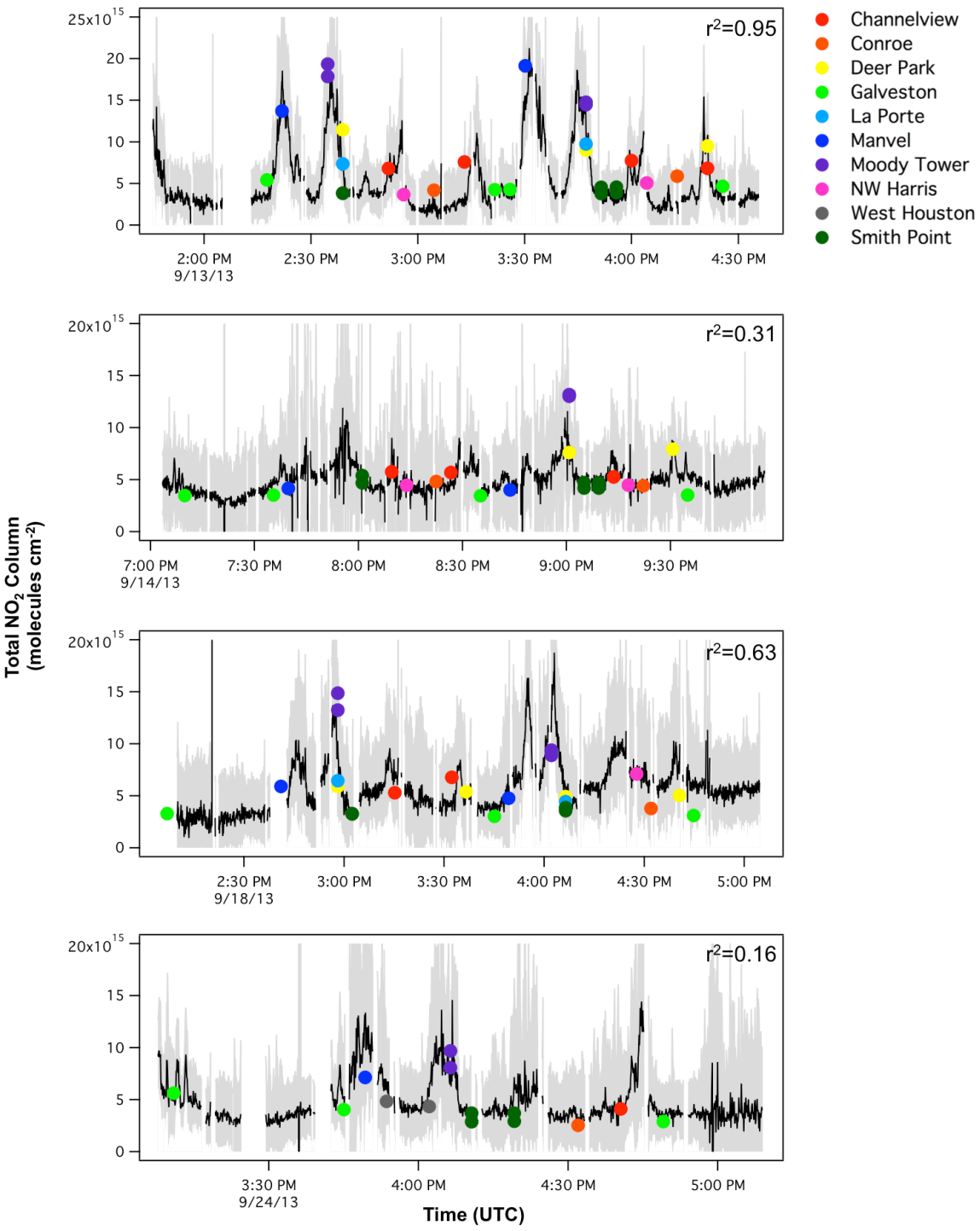

Figure 2-6: Time series of 5-second running averaged GeoTASO NO_2 total columns (black line), ± 2 standard deviations of the 5-second average (grey), and coincident Pandora retrievals (colored by site) for the four Falcon flights. All times are in UTC.

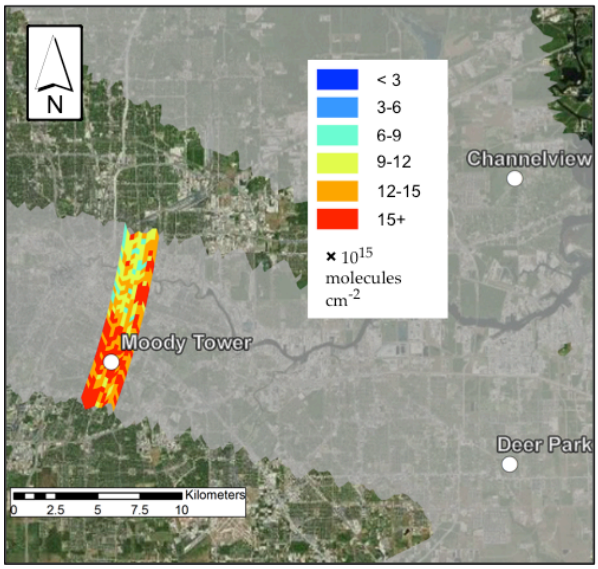

Figure 2-7: Colored GeoTASO data showing data coverage for five seconds of flight over Moody Tower. The coverage was approximately 2×10 km².

2.3.1.2 NASA P-3B

The spirals the NASA P-3B performed over the sites of interest (Figure 2-1c) were approximately 5 km in diameter. This footprint was the closest to the expected footprint of TEMPO over North America, and this comparison gave an idea of what Pandora-TEMPO validation may looks like across an urban area like Houston. To facilitate the comparison between the NASA P-3B *in situ* data and the Pandora column data, the *in situ* aircraft data was binned and integrated over the lower troposphere covered by the spiral as explained in Section 2.2.4. The P-3B integrated spirals included data from 0-3.5 km, which was considered a tropospheric column as most sources of NO_2 are within the boundary layer and the short lifetime of the trace-gas does not allow for a significant amount to reside in the free troposphere near urban areas. Coincident Pandora measurements were averaged over the time of each spiral (~15 minutes) and a monthly

averaged OMI stratosphere was subtracted from the Pandora data to become considered a tropospheric column.

Unlike the direct column measurements, aircraft data from the NASA P-3B spirals incorporated information about the vertical distribution of NO_2. However, the 5-km horizontal spatial coverage still led to influences from spatial heterogeneity over the region for these comparisons. In this analysis, spatial heterogeneity of NO_2 was quantified by the calculating the average standard deviation of NO_2 concentrations within each 100m bin in the lowest 1 km of the spirals. Spatial heterogeneity correlated to the scatter of the column comparisons around the 1:1 relationship (RMSE) (Table 2-1). Areas without large influences from fresh NO_2 emissions showed less scatter in the comparison between Pandora and the P-3B integrated profiles (scatter plots with circles in Figure 2-8 and Table 2-1 with RMSEs ~1×10^{15} molecules cm^{-2} and standard deviations within the 100m bins below 1 km of less than 1 ppbv). Locations near central Houston and the Houston Ship Channel (Moody Tower, Channelview, and Deer Park) showed much more variability with larger RMSEs and large near-surface spatial variability of NO_2. Deer Park had a few outliers, with an extreme case on September 25th having a standard deviation within the 100m bins of ~ 30 ppbv. The Deer Park Pandora was located on the southern edge of the spiral measurements, and many of the NOx sources in the region were to the northeast of the measurement site and not in the field of view of the Pandora.

All comparisons of Pandora to OMI, GeoTASO, and the NASA P-3B showed the

importance of spatial heterogeneity in urban regions when considering instrument intercomparisons and validations with respect to NO_2. Finer-scale measurements in the future will greatly improve our understanding of spatial distributions of short-lived trace-gases in areas with strong emission sources. Additionally, these comparisons showed how Pandora spectrometers could be useful for the future validation of TEMPO and TROPOMI as their spatial resolutions approach closer to a sub-urban scale.

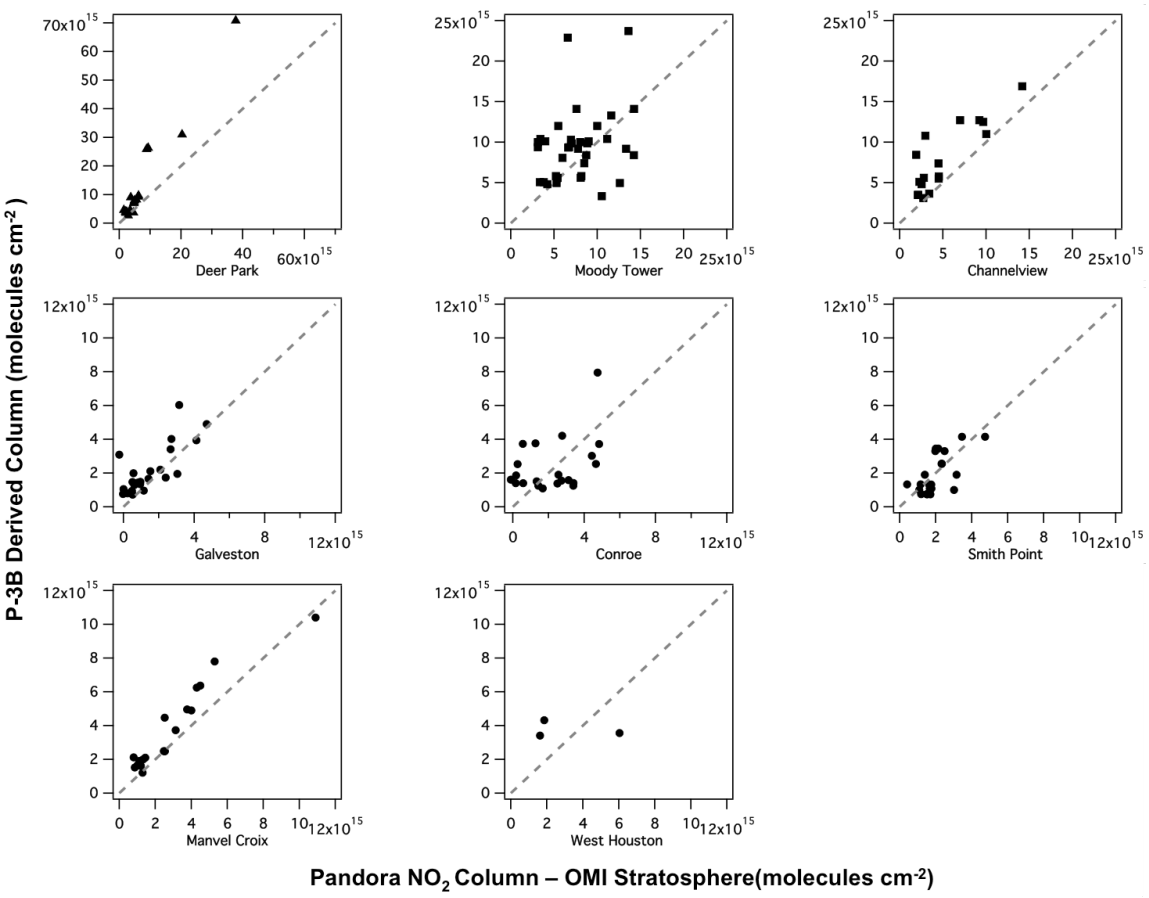

Figure 2-8: *Comparison of aircraft-derived tropospheric NO_2 columns from the NASA P-3B to Pandora. Each symbol indicates a different pollution scale where triangles are the most polluted, squares are mildly polluted, and circles are relatively unpolluted. The dashed line indicates a 1:1 relationship.*

Location	RMSE ($\times 10^{15}$ molecules cm^{-2})	Average standard deviation of each 100 m bin below 1 km (pptv)
Deer Park	10.2	5980
Moody Tower	4.88	1477
Channelview	5.71	2358
Galveston	1.15	826
Conroe	1.74	513
Smith Point	0.89	875
Manvel Croix	1.17	836
West Houston	2.27	976

Table 2-1: Statistical calculations of RMSE from the 1:1 comparison between the NASA P-3B and Pandora observations minus an OMI stratospheric column, and the average standard deviation of NO_2 from each 100 m P-3B bin below 1 km for the eight spiral locations during DISCOVER-AQ Texas.

2.3.2 SURFACE *IN SITU*: COLUMN-TO-SURFACE ANALYSIS

One of the primary objects for DISCOVER-AQ was to study the column-to-surface relationships and how parameters such as boundary layer height and time of day affect this relationship. The future launch of TEMPO and other currently measuring air quality sensors only observe column densities between the surface and the top of the atmosphere, however poor air quality is measured by its impacts at Earth's surface. Therefore, understanding how surface concentrations relate to a column measurement are critical for deriving air quality conditions from space-based sensors. Differences in diurnal patterns of NO_2 concentrations at the surface and NO_2 column observations make this a challenging feat. At Moody Tower, NO_2 concentrations at the surface peaked during the morning rush hour and decreased as the boundary layer grew and diluted the pools NO_2 near the surface and as photochemistry increased throughout the

morning (Figure 2-9). Although the Pandora did not show as strong of a diurnal change in NO_2 columns, there was a peak a few hours after the surface concentration maximum. Decreases in the column in the mid-morning and afternoon can be linked to increased photochemistry. Boundary layer growth and dilution did not influence the column measurement. Galveston's observations have a more muted diurnal shape, and both surface and column measurements were at smaller magnitudes in comparison to the polluted Moody Tower site.

Previously, Knepp et al. (2013) found that boundary layer height drove the relationship between surface-to-column comparisons for NO_2 in Maryland. This also seemed to be the case at Moody Tower. In Figure 2-10 (top), *in situ* surface concentrations showed a time-of-day based relationship with the local Pandora measurements. Integrating the surface concentration through the height of the boundary layer measured by a CL31 locally removed the time-of-day dependence (Figure 2-10 (middle)). This integration followed the assumption of a well-mixed boundary layer column (shown in red in Figure 2-9). Although there was moderate correlation for this well-mixed assumption ($r^2 = 0.59$), the slope was quite low (slope = 0.43) suggesting that in urban areas, the short lifetime of NO_2 limited the degree to how well-mixed the column was through the boundary layer. The P-3B spiral data showed that the boundary layer was not well-mixed with respect to NO_2 even though it might be with other trace-gases, such as ozone. However, the shape of the vertical distribution of NO_2 was quite complex and varied temporally and spatially (Crawford et al., 2014).

Investigations into a common profile shape from the NASA P-3B spirals were inconclusive as this shape changed vastly from day-to-day due to varying boundary layer dynamics. An exponential profile shape assumption from a exponential-fit between the surface and 70 m NO_2 *in situ* measurements was also found to be a significant underestimation of a boundary layer column.

The correlation between surface conditions to column measurements was not as apparent at the Galveston site ($r^2 = 0.22$ Figure 2-10 (middle)), as the boundary layer was less polluted and, therefore, a smaller fraction of the tropospheric column. In fact, in the morning, there was often evidence of NO_2 aloft, possibly from the urban Houston residual layer that was advected in the nighttime residual layer toward the Gulf of Mexico.

To investigate the degree of mixing in the boundary layer with respect to NO_2, the well-mixed derived profiles were compared to the NASA P-3B integrated NO_2 from 0-3.5 km. Figure 2-10 (bottom) shows how the well-mixed derived columns compared to the integrated NASA P-3B spirals. Considering all the aircraft spirals, the data exhibited a slope = 0.55, indicating that the column was approximately half of a well-mixed column at Moody Tower ($r^2 = 0.64$). However, this dataset suggested that this degree of mixing was dependent on time of day. During the first spiral of the day, the well-mixed assumption overestimated the column density the most (slope = 0.6, $r^2 = 0.82$). However, the midday spiral seemed to be much closer to well-mixed through the boundary layer (slope = 0.82, $r^2 = 0.92$). By later in the afternoon, there was no

correlation, however the columns of both products had a smaller range when compared to the morning and midday data. There was less of a pattern in Galveston with the well-mixed assumption scattering around the 1:1 relationship with the P-3B spirals no matter the time of day. In conclusion, NO_2 surface-level concentrations can be best derived from column observations in urban regions if boundary layer height is incorporated into the retrieval. This relationship was weaker in the cleaner environment of Galveston.

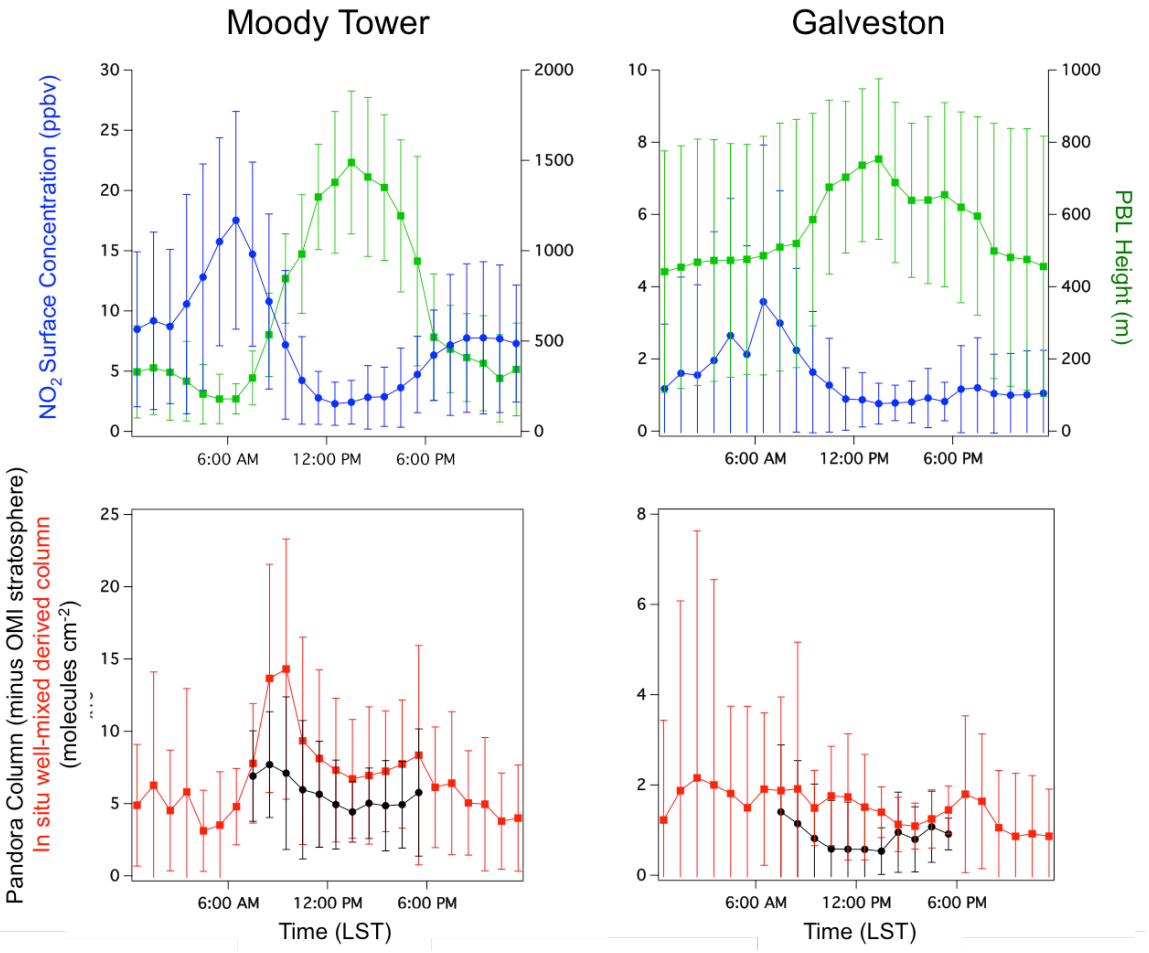

Figure 2-9: Diurnal profile in LST at the Moody Tower (left) and Galveston (right) of NO_2 concentrations at the surface (blue), boundary layer height (green), Pandora minus an OMI stratosphere (black), and in situ well-mixed derived boundary layer column (red) during the DISCOVER-AQ Texas deployment. Error bars indicate the standard deviation of the diurnal average.

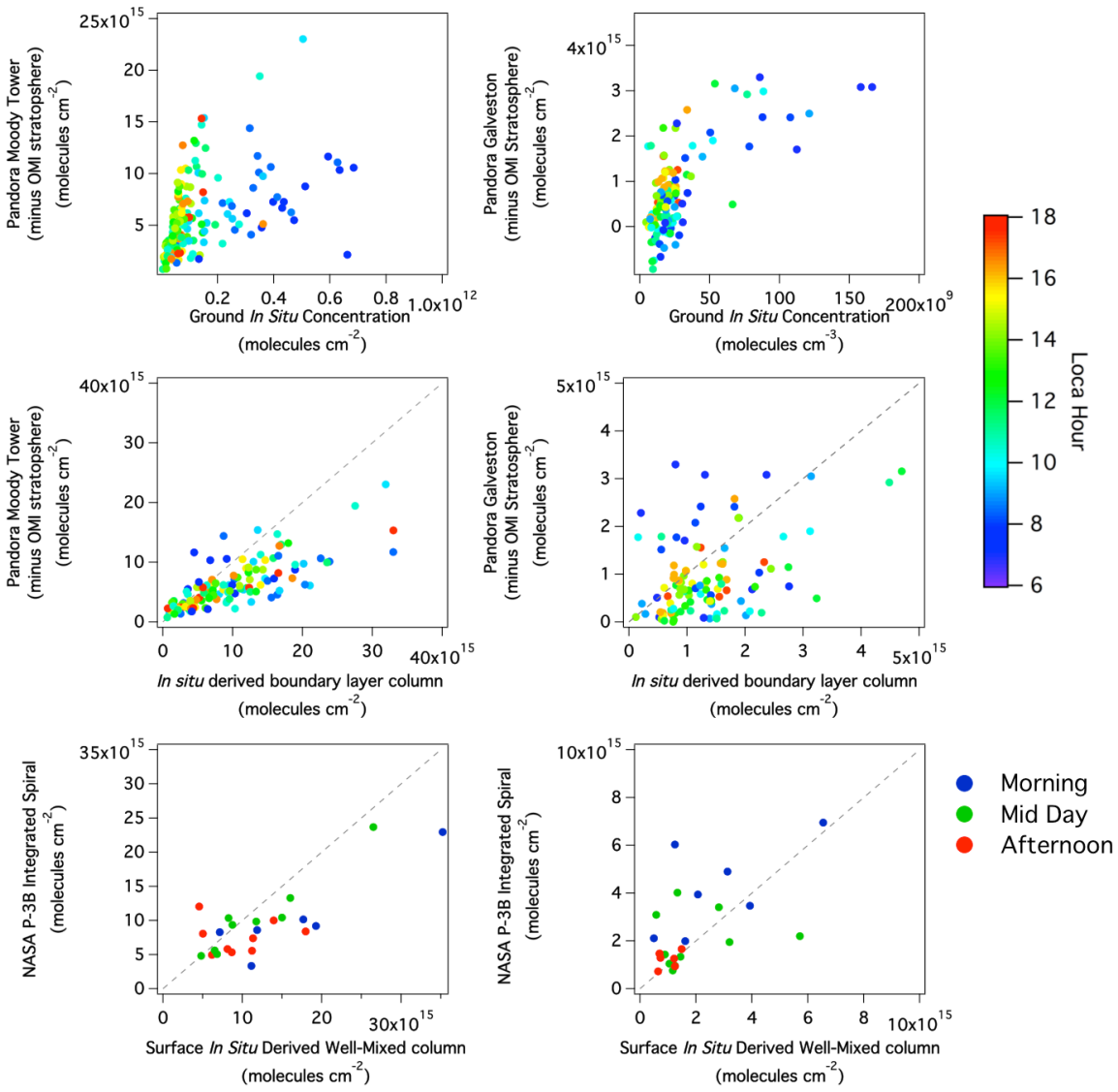

Figure 2-10: Moody Tower Pandora tropospheric columns vs. surface in situ concentrations of NO_2 (top) and in situ derived well-mixed boundary layer NO_2 columns (middle). Data in the top four graphs are colored by local hour of the day. The bottom graphs show scatter plots comparing the in situ derived well-mixed boundary layer NO_2 columns and the NASA P-3B integrated spirals colored by spiral time.

2.4 SUMMARY

This chapter presented results from the comparisons of all NO_2 measurements to a network of Pandora spectrometer observations from DISCOVER-AQ Texas. The analysis focused on how the spatial heterogeneity of NO_2 and measurement footprint influenced the comparison. OMI measurements often overestimated in cleaner regions due to its large field of view often encompassing portions of the urban plume not seen by Pandora's field of view. At urban sites, the relationship between OMI and Pandora was often scattered across the 1:1 relationship, but at times compared well with a transition across the 1:1 line around Pandora observations of ~ 6×10^{15} molecules cm^{-2}. The scatter depended on the placement of the Pandora in relation to the urban plume on that day. The OMI pixels were large enough to encompass both polluted and unpolluted environments, and its comparison to Pandora depended on the instrument's location with respect to the NO_2 plumes within the OMI pixel.

GeoTASO's 250×250 km^2 footprint was able to capture the range and variability of NO_2 in the Houston region; however, this comparison encompassed a larger range of Pandora measurements. When only looking at the smaller dynamic range of GeoTASO observations, the data did not have as strong of correlation. These results were possibly due to noise from retrieval errors and a stray-light problem within GeoTASO's spectrometer. Despite this noise, the slope between Pandora and GeoTASO was closer to one when compared to the OMI results. GeoTASO results exhibited how finer-scale

measurement will allow for future in-depth studies on the spatial distribution and magnitude of NO_2 in urban areas.

The smaller scale P-3B spiral-derived columns showed better agreement than OMI results due to the more localized observations, but there was a distinct pattern between NO_2 variability within the 100 m bins in the lowest 1 km and the RMSE of the Pandora and P-3B comparison from the 1:1 line. In the case of large outliers, the P-3B often measured plumes that were not within the Pandora's field of view. For future sensors, such as TEMPO, Pandora will be a helpful continuous measurement in which to validate NO_2 retrievals, as the spatial resolution of this space-based sensor will be closer to the spatial range that Pandora views. All these results suggest that Pandora compared well to other column measurements, but the differing field of views caused differences between the measurements at times.

One of the goals for future sensors like TEMPO is the idea of space-based air quality monitoring. The challenge of this is relating the space-based column measurements to what is occurring at the surface with respect to NO_2. This often requires information on boundary layer height and the degree of mixing near the surface, as NO_2 is not well-mixed throughout the boundary layer in polluted regions. Measurements during DISCOVER-AQ Texas showed that 10-40% of the NO_2 total column can be found below 70 m in central Houston and that the boundary layer column was often about 50% of a well-mixed column from surface measurements. This pattern did not apply everywhere. In Galveston, free tropospheric NO_2 became a larger

portion of the tropospheric column and boundary layer information did not assist in relating column observations to surface conditions. Examples at these two sites displayed the complexities of relating surface NO_2 to space-based column measurements, and the need for boundary layer information in order to derive surface conditions in NO_2-polluted urban regions in the future.

3. INFLUENCES OF ENVIRONMENTAL HETEROGENEITY ON OMI NO_2 MEASUREMENTS AND IMPROVEMENTS USING DOWNSCALING

3.1 INTRODUCTION

Haze layers visible along the urban horizon get their brown hue due to the absorption properties of nitrogen dioxide (NO_2), which is a product of combustion in motor vehicles, power plants, and industry. Due to its short lifetime and diverse distribution of sources, mixing ratios of NO_2 can vary orders of magnitude in short distances and time. It is important to monitor NOx concentrations and distributions because of their role in the net production of ozone and harmful secondary aerosols.

In the last two decades, satellite measurements have studied the spatial distribution of NO_2 globally with GOME (Burrows et al., 1999), SCIAMACHY (Bovensmann et al. 1999), OMI (Levelt et al., 2006), and GOME-2 sensors (Callies et al., 2000; Valks et al., 2011). The Ozone Monitoring Instrument (OMI) sensor currently has the highest spatial resolution of any of these sensors (13×24 km^2), which allows for the assessment of NO_2 in near-urban scale environments (Levelt et al., 2006). Although this sensor has the highest spatial resolution to date, the sensor misses sub-pixel spatial patterns in urban regions, especially when *a priori* inputs for the retrievals are larger than the OMI footprint. Heckel et al. (2011) and Valin et al. (2011) demonstrated how increasing the spatial resolution of *a priori* information can decrease retrieval errors, especially in areas where there are strong gradients in NO_2 distribution, such as in urban

coastal areas. Improvements in this area may result in more accurate applications of this data in the future, especially with future launches of sensors with higher spatial resolution than OMI—TROPOMI at 7 × 7 km^2 (van Geffen et al., 2016) and TEMPO at 2 × 4.5 km^2 (Zoogman et al., submitted).

Aircraft *in situ* data has the benefit of studying the vertical and horizontal spatial distribution of NO_2. Previously, NO_2 aircraft *in situ* measurements during ICARTT (Martin et al., 2006), PAVE and INTEX-A (Bucsela et al., 2008), INTEX-B (Boersma et al., 2008; Bucsela et al., 2008; Bucsela et al., 2013; Hains et al., 2010) and ARCTAS-CA (Russell et al., 2011) were compared to the OMI satellite retrievals. Each study made comparison assumptions including profile extrapolations to the surface and tropopause, difference in satellite and aircraft overpass times, and cloud fractions. Most validations focused on getting the full extent of the vertical profile (Boersma et al., 2008; Bucsela et al., 2008; Hains et al., 2010; Martin et al., 2006), whereas Russell et al. (2011) focused on getting as much NO_2 data within boundary layer as possible, since in urban regions this is primarily where NO_2 resides within an atmospheric column.

Past validations used a variety of techniques for comparison in vastly differing environments ranging from very clean to extremely polluted. During the DANDELIONS campaign, a NO_2 LIDAR, MAX-DOAS, Pandora spectrometer, and *in situ* data were used to compare to the OMI satellite retrievals (Brinksma et al., 2008; Celarier et al., 2008). These measurements helped study the spatial and temporal variability of NO_2 concentrations and also showed how the boundary layer NO_2

dominates the tropospheric column according to *in situ* and NO_2 lidar measurements. Boersma et al. (2009) also used *in situ* measurements in Israel along with the assumption that most tropospheric NO_2 resides in and is well-mixed throughout the boundary layer. During CalNex 2010, the OMI Standard Product retrieval was compared to airborne MAX-DOAS (Oetjen et al., 2013). This study saw an underestimation of NO_2 in the urban Los Angeles region, indicating further intercomparisons need to be applied in this region.

In this chapter, aircraft *in situ* measurements of NO_2 from CalNex 2010 were compared to three OMI tropospheric NO_2 column retrievals: the NASA Standard Product, KNMI Dutch OMI NO_2 (DOMINO), and Berkeley High Resolution (BEHR). These products used radiance measurements from the OMI sensor, and had varying assumptions about stratospheric/tropospheric separation and air mass factor (AMF) calculations resulting in differences in the calculation of tropospheric NO_2 columns. This chapter focused on the differences in *a priori* input for the tropospheric AMF calculation in each retrieval, as well as how environmental heterogeneity influenced the comparison between aircraft and OMI retrievals. These results showed that the most densely polluted regions measured by aircraft were vastly underestimated by the OMI retrievals mostly due to the difficulty for the aircraft to sample all environments represented by OMI's wide field of view. Therefore, a technique for downscaling the OMI DOMINO product to a CMAQ based resolution was tested during CalNex 2010 and DISCOVER-AQ Texas to improve the satellite-to-aircraft comparisons.

3.2 SATELLITE PRODUCTS AND MEASUREMENTS

3.2.1 OMI RETRIVALS

The Ozone Monitoring Instrument (OMI) was launched in July 2004 aboard the EOS-Aura satellite. This polar-orbiting sun-synchronous satellite crosses the equator on the ascending node around 13:30 LST capturing an early-afternoon snapshot of the trace-gas distribution (Levelt et al., 2006). The OMI instrument is a nadir-viewing spectrometer, which measures the solar backscatter in the ultraviolet/visible range with a spectral resolution of around 0.5 nm ranging from 270 - 500 nm in three separate channels (Levelt et al., 2006). The 2600 km swath, divided into 60 across track pixels, is wide enough to observe global coverage daily with a nadir resolution of 13×24 km^2. Measurements of NO_2 are processed using Differential Optical Absorption Spectroscopy (DOAS) in the wavelength range of 405-465 nm (Bucsela et al., 2006; Bucsela et al., 2013). This study investigated three different NO_2 tropospheric vertical column retrievals: the NASA Standard Product (SP), the KNMI DOMINO Product, and the Berkeley High Resolution (BEHR) retrieval. Each product was similar in their DOAS spectral fit, but each used different tropospheric/stratospheric separation algorithms and *a priori* assumptions for the calculation of the tropospheric air mass factor (AMF). Additionally, each product used a de-striping algorithm to correct for across track sensor bias (Boersma et al., 2011; Bucsela et al., 2013). More details about each product are discussed below.

3.2.1.1 NASA STANDARD PRODUCT (SP)

This study used the most recent released version of the NASA Standard Product (SP)—Version 2.1—Level 2 tropospheric NO_2 vertical column data. Details on the product, as well as information on the most recent updates to the retrieval, can be found in Bucsela et al. (2013). Below is a brief description of the algorithm and the newest improvements.

The normalized radiance/irradiance spectrum was used to obtain an initial estimate of the total slant column. After de-striping, an initial vertical column was estimated using the stratospheric AMF, which is a good assumption for most of Earth as most areas are dominated by stratospheric NO_2 (minimal surface sources). The stratospheric/tropospheric separation algorithm was one major improvement from the previous versions of the SP (Bucsela et al., 2006; Bucsela et al., 2013). The previous version used a wave-2 stratospheric model (Bucsela et al., 2006) to estimate stratospheric NO_2, where as the this version estimated it by subtracting a model-derived tropospheric column in unpolluted regions from the initial slant column. Areas where there was substantial NO_2 pollution in the troposphere were masked, and the remaining pixels were extracted to a 1° × 1° grid and then interpolated to fill in the masked portions using a weighting scheme from the ± 7 closest orbits with the greatest weight attributed by the most current orbit. Next, stratospheric hot spots (caused by additional tropospheric pollution not masked) were removed using averaging windows replacing values that

deviated more than 1.5 σ from the mean. Finally, the geographic stratospheric vertical columns were interpolated back to the native OMI resolution.

The final tropospheric slant column was computed by subtracting the stratospheric component from the initial slant column, and derived tropospheric AMFs were applied to estimate a vertical tropospheric column. *A priori* inputs for the calculation of the tropospheric AMF used OMI-derived monthly albedo 0.5° × 0.5° resolution, terrain pressure from a 3 km Digital Elevation Model (DEM) from Aura (Boersma et al., 2011), and NO_2 profiles from the Global Modeling Initiative Chemical Transport Model (GMI CTM) monthly averages at 2° × 2.5° resolution (Bucsela et al. 2013).

3.2.1.2 KNMI DOMINO:

Dutch OMI NO_2 (DOMINO) tropospheric product (Version 2.0) was discussed by Boersma et al. (2011). As stated above, this product used the same DOAS spectral fitting for the slant column estimation as the SP. However, the stratospheric separation assimilated the total slant column with the TM4 chemistry-transport model during the closest time step to the overpass time (Boersma et al., 2007).

The DOMINO product AMFs were improved for version 2.0 by expanding the look-up table (LUT) for the radiative transfer calculations, as well as applied better representative terrain heights, albedo, and modeled profiles for the AMF calculations (Boersma et al., 2011). The LUT expansion decreased interpolation errors. Similar to SP, the *a priori* inputs were also from the same OMI-derived monthly albedo measurements

and global 3 km digital elevation model (DEM) incorporated with Aura data. However, the DEM was used with the most recent TM4 model run driven by European Center for Medium range Weather Forecasting (ECMWF) data and the hypsometric equation to compute the surface pressure. Profile shapes of NO_2 were derived from the TM4 model, but the model alone has had issues mixing NO_2 throughout the boundary layer. The newer version of the product improved boundary layer mixing, leading to increased AMFs in regions with higher emissions.

Overall, in the Los Angeles region, Boersma et al. (2011) showed that version 2.0 calculated smaller tropospheric columns in comparison to the previous DOMINO version due to higher resolution terrain and albedo inputs, as well as improved mixing for the TM4 NO_2 profiles. This decrease was on the order of -39% in the winter and -30% in the summer on average.

3.2.1.3 BERKELEY HIGH RESOLUTION (BEHR)

Details on the algorithm and validation of the BEHR product can be found in Russell et al. (2011). The BEHR product used the same methods as SP for the estimation and subtraction of the stratosphere from the slant column. BEHR differed from SP in the calculation of the tropospheric AMF by using higher resolution *a priori* assumptions, which can be beneficial in regions where the environmental variables are changing on scales smaller than the OMI field of view.

Previous studies investigated the errors from coarser resolution *a priori* inputs. Heckel et al. (2011) found that the biggest contributors to AMF error were NO_2 profile

shape and albedo, indicating a need for higher resolution inputs especially as spatial resolution improves with future launches of NO_2 measuring space-based sensors. Valin et al. (2011) also found that improving the resolution of NO_2 profiles decreased the bias of satellite-measured retrievals.

For the AMF calculation, the BEHR product used Moderate Resolution Imaging Spectroradiometer (MODIS) Aqua 16-day derived-surface albedo at 0.05° × 0.05° resolution, GLOBE 1×1 km^2 topographical database, and a WRF-Chem monthly average profile shape at 12×12 km^2 resolution. The three different *a priori* assumptions for the BEHR product were all at a higher spatial resolution than SP and DOMINO and were smaller than the OMI field of view.

Using the BEHR product, Russell et al. (2011) saw a difference on average of ± 40%, ± 20%, and -29% from the changes between the albedo, terrain pressures, and NO_2 profile shape, respectively, when compared to the SP, especially over areas with heterogeneous environments (urban/rural boundaries, mountains, and other sub-pixel features). Although it should be noted that this comparison was with a previous version of SP (1.0.5), and the NO_2 profile shape in that version was an annual average instead of monthly averages in the current product (Bucsela et al., 2006; Bucsela et al., 2011, Russell et al., 2011).

3.2.2 AIRCRAFT NO_2 MEASUREMENTS

This study utilized *in situ* aircraft NO_2 data measured aboard the NOAA WP-3D during the California Research at the Nexus of Air Quality and Climate Change

(CalNex) field study. As the name suggests, the purpose of this campaign was to study the relationship between air quality and climate change in California. The campaign overview was discussed by Ryerson et al. (2013). Only three days of aircraft data were used in this analysis (May 4th, 7th, and 16th, 2010).

NO_2 along the flight path was measured at 1 Hz using a photolysis-chemiluminescence (P-Cl) system to measure NOx and NO through two channels of a four-channel P-Cl instrument. NOx was measured by using Nichia LEDs (peak wavelength 365nm with 10nm FWHM) to photolyze NO_2 to NO prior to the chemiluminescence reaction (Pollack et al., 2011). The resultant NO (background NO + converted NO_2) was then measured via the chemiluminescence chamber. Because of the identical flow paths between the NO and NOx channel in the aircraft instrument, the measurement of NO_2 was inferred from the difference between the NOx and NO measurements (Pollack et al., 2011). All measurements were in ppbv and later converted to molecules cm^{-3} using ambient temperature and pressure measured aboard the aircraft and later integrated to column densities in order to compare to OMI column measurements.

3.2.3 METHODS

3.2.3.1 AIRCRAFT-DERIVED TROPOSPHERIC NO_2 COLUMN

Comparing aircraft *in situ* measurements to remotely sensed trace-gas column densities was a challenge, as the aircraft did not fly the entire vertical/horizontal extent of the satellite-derived column. *In situ* measurements were used to derive a tropospheric

column for each OMI pixel the aircraft entered. These aircraft observations showed that most of the tropospheric NO_2 molecules resided within the boundary layer with little found within the free troposphere. As a result, the focus was on measurements within the boundary layer.

Boundary layer height was flagged by appropriate gradients in NO_2 concentrations, relative humidity, and potential temperature as the aircraft entered or exited this layer (typically 500-3000 m depending on location). A linear interpolation filled in the gaps between entrances and exits of the boundary layer to obtain a continuous estimate of boundary layer height. These heights were analyzed spatially to ensure that this method produced realistic values and did not result in large discontinuities. Next, the OMI pixel polygon was used to subset aircraft data inside the boundary layer. An average concentration (excluding outliers $\pm 2\ \sigma$) over the pixel area was integrated over the height of the boundary layer. This followed the assumption that NO_2 is well-mixed throughout the boundary layer during these hours when averaged over the whole pixel area. Results in Chapter 2 and other DISCOVER-AQ campaigns demonstrated how NO_2 was often not well-mixed in the polluted regions of Houston, but the CalNex aircraft samples lacked profiles through the lower boundary layer to sufficiently capture the NO_2 vertical gradient. Assuming that NO_2 was well-mixed within the boundary layer, particularly in urban regions, may be a source for error in the aircraft-derived columns. However, the differing relationships between the aircraft-derived columns and the OMI retrievals were still apparent for different environments.

Finally, a free tropospheric column was added to the boundary layer column, however the aircraft did not measure high enough to get a full representation of the typical free tropospheric concentration of NO_2. Instead of deducing it from aircraft measurements, the value was inferred from OMI tropospheric columns over the ocean adjacent to the coast of California. The assumption was that the free tropospheric value is similar to a region where there were minimal surface sources of NO_2 to the air in a nearby region (aka the ocean). Standard atmospheric temperatures and pressures were used to find average concentrations throughout the free troposphere. In this case, the average was ~ 25 pptv. For each aircraft-derived column, this value was integrated from the top of the boundary layer to the tropopause level using standard atmospheric temperature and pressure.

Since the OMI pixel was quite large in comparison to the NO_2 sources, much of the horizontal variability was lost in urban areas. However, if aircraft sampling was sufficient enough to represent the sub-pixel variability then the aircraft-inferred column should have been comparable to the satellite. Pixels without aircraft data or affected by the row anomaly were not considered in this analysis (http://www.knmi.nl/omi/research/product/rowanomaly-background.php).

The final aircraft-inferred columns were further filtered by difference in overpass time, number of aircraft data points in the OMI pixel, cloud fractions, pixel size, pollution level, and heterogeneous terrain (Section 3.3.1-2).

3.2.3.2 Downscaling OMI retrieval

In urban areas, OMI often underestimates the urban center and overestimates the urban outskirts due to the spatial averaging over the OMI pixel area (Chapter 2; Kim et al., 2015). Our results showed similar patterns. The OMI DOMINO retrieval was downscaled to a CMAQ resolution. NO_2 mass within an OMI pixel was conserved, and CMAQ was used to simulate the distribution of NO_2 in the area of interest (in this case the National Air Quality Forecasting Capability (NAQFC) 12 km CMAQ was used). Next, CMAQ data within the OMI pixel of interest was normalized to create a spatial weighting kernel to quantify the relative distribution of NO_2. This kernel was used to distribute the OMI measured NO_2 throughout the pixel according to the relative distribution computed by the CMAQ model. More details about this technique were discussed by Kim et al. (2015). This technique assumed that OMI correctly observed NO_2 over the pixel's spatial area, and additionally gave sub-pixel spatial distribution details. The absolute amount of NO_2 simulated by CMAQ did not matter since it only used the relative distribution of the trace-gas. However, problems can arise in the downscale if the emission source locations or wind fields in the modeled meteorology were incorrect.

3.3 RESULTS AND DISCUSSION

3.3.1 DATA SELECTION

Before making conclusions about the relationship between aircraft and satellite, the best combination of filters was determined to get the closest 'apples to apples' comparison. Table 3-1 shows the statistical comparison between the aircraft-inferred columns and the three NO_2 OMI products by varying the time difference between aircraft and satellite measurements, number of aircraft data points within each OMI pixel, and the OMI cloud fraction observed. Decisions for appropriate filters were determined by a balance between dataset correlations, changes in slope (not the magnitude of slope), and the number of valid data points.

When investigating how the comparison changed between times difference of measurements (Table 3-1), the best correlations were within an hour of the OMI overpass with r^2 values for SP, BEHR, and DOMINO of 0.92, 0.91, and 0.95, respectively. However, going from a one-hour to a two-hour difference increased the number of data points available for analysis by over 100%, with minor changes in the slopes at the expense of slightly decreased correlations (Table 3-1). Aircraft data taken more than two hours from the OMI overpass was not considered for further analysis in this study given the lower observed correlations due to the fact that concentrations of NO_2 changes quickly in urban areas.

The minimum number of *in situ* data points inside the each OMI pixel had minimal effect on the statistical comparison. Previous work by Russell et al. (2011) used

a data point threshold of 20 in the boundary layer for each pixel. Increasing further to 120 data point did little to improve comparisons, as most the data points had hundreds or even thousands of aircraft measurements within the OMI pixel. A threshold of 60 data points was used for the rest of this analysis, as the slope changed the most between 30 and 60 data points, but was consistent with higher thresholds.

		Standard Product		DOMINO		BEHR	
Overpass Time[1]	**N**	**Best Fit**	**r^2**	**Best Fit**	**r^2**	**Best Fit**	**r^2**
± 1 hour	34	$0.40x+4.6x10^{14}$	0.92	$0.55x+1.6x10^{14}$	0.91	$0.62x+2.9x10^{14}$	0.95
± 2 hours	75	$0.40x+8.0x10^{14}$	0.75	$0.57x+6.6x10^{14}$	0.74	$0.61x+6.2x10^{14}$	0.86
± 3 hours	80	$0.37x+8.6x10^{14}$	0.70	$0.56x+6.9x10^{14}$	0.73	$0.58x+6.9x10^{14}$	0.80
± 4 hours	96	$0.40x+7.4x10^{14}$	0.65	$0.59x+5.3x10^{14}$	0.69	$0.63x+5.0x10^{14}$	0.71
Data Points[2]							
30	90	$0.34x+6.6x10^{14}$	0.76	$0.54x+6.3x10^{14}$	0.76	$0.59x+5.1x10^{14}$	0.85
60	75	$0.40x+8.0x10^{14}$	0.75	$0.57x+6.6x10^{14}$	0.74	$0.61x+6.2x10^{14}$	0.86
90	71	$0.40x+8.6x10^{14}$	0.75	$0.57x+7.4x10^{14}$	0.75	$0.61x+6.8x10^{14}$	0.86
120	64	$0.39x+9.0x10^{14}$	0.75	$0.56x+8.1x10^{14}$	0.75	$0.60x+7.2x10^{14}$	0.86
Clouds[3]							
OMI 0%	59	$0.37x+6.5x10^{14}$	0.85	$0.57x+2.8x10^{14}$	0.88	$0.58x+5.3x10^{14}$	0.87
OMI 20%	75	$0.40x+8.0x10^{14}$	0.75	$0.57x+6.6x10^{14}$	0.74	$0.61x+6.2x10^{14}$	0.86
MODIS 0%	24	----------	------	----------	-------	$0.58x+1.4x10^{15}$	0.92
MODIS 20%	75	----------	------	----------	-------	$0.61x+6.2x10^{14}$	0.86

[1]OMI Cloud Fraction < 20% and > 60 data points

[2]OMI Cloud Fraction < 20% and < 2 hours between overpass times

[3]> 60 data points and < 2 hours between overpass times

Table 3-1: Comparison statistics of the three OMI NO_2 tropospheric column products filtered by difference in overpass time and aircraft measurement, number of data points per pixel, and cloud fraction from OMI.

Finally, the data was filtered by OMI cloud fraction. Past work used a threshold of 20% (Brinksma et al., 2008; Celarier et al., 2008; Kramer et al., 2008; Russell et al., 2011). There was little reason to use any threshold higher than this because all the pixels involved were either under the 20% threshold or close to 100%. The correlation between the satellite products and aircraft-inferred columns improved when the OMI cloud fraction threshold was decreased to 0%. However, the slope did not vary much between the two (less than 2%). The BEHR product also assimilated the OMI pixels with the cloud fraction from MODIS Aqua. When MODIS data was used as a cloud flag, there were large improvements in correlation for cloud-free environments ($r^2 = 0.92$) when compared to cloud-free environments measured by OMI's cloud algorithm ($r^2 = 0.87$). However, a greater number of OMI pixels were flagged by the MODIS, which decreased the number of useable cloud-free data points by over 50%.

For the rest of the data analysis, thresholds of two hours between aircraft and satellite measurements, 60 aircraft data points per OMI pixel, and OMI cloud fractions less than 20% were used. Scatter plots of this data are presented in Figure 3-1 (a-c). The more polluted a pixel, the more the aircraft and OMI retrievals disagreed. Zero polluted aircraft-derived columns were greater than OMI-derived columns, no matter which product was used. In cleaner environments the data was scattered around a 1:1 relationship, except for the SP results, which had a lower satellite bias than the other two products. The level of pollution was examined in section 3.3.2.2. SP showed the lowest slope in comparison to the other two products (slope = 0.40, $r^2 = 0.75$, RMSE = 6.6×10^{14})

(Figure 3-1a), with BEHR exhibiting the best comparison (slope = 0.61, r^2 = 0.86,RMSE = 4.5×10^{14}) (Figure 3-1c). The DOMINO product comparisons fell close to BEHR in slope, but DOMINO had an r^2 similar to the SP (Figure 3-1b) (slope = 0.57, r^2 = 0.74,RMSE = 5.1×10^{14}). BEHR and SP only varied in their calculation of the tropospheric AMF. The better correlation between BEHR and aircraft demonstrated how higher resolution *a priori* inputs matter in regions where the environment was heterogeneous with respect to terrain and pollution environments.

Another way to view this comparison was to investigate the ratio of the aircraft-inferred columns to each OMI product (A:S ratio). If the A:S ratio is around one, the two datasets compared well, whereas if it was greater than one, then the aircraft measured higher than the satellite and vise versa. A histogram of these values for each product is shown in Figure 3-1(d-f) with a bin size of 0.25. SP had local maximums at 1.25 and 2.25, BEHR at 1.5 - 1.75, and DOMINO at 1.00 and 1.5. Only 29%, 45%, 42% of the data comparisons fell between ± 50% error for the SP, BEHR, and DOMINO, respectively. A closer look into possible reasons for these deviations was investigated in section 3.3.2.

3.3.2 HETEROGENITY INFLUENCES ON COMPARISONS

Aircraft data was collected three separate days with one flight focused on the southern Central Valley (May 7th) and two flights in the Los Angeles region (May 4th and 16th). The maps in Figure 3-2 show the location and size of each OMI pixel from Figure 3-1, and the aircraft data included in the aircraft-inferred columns. The data were

compared while considering the pixel size, pollution level, and homogeneity with respect terrain surface pressure used in the satellite products.

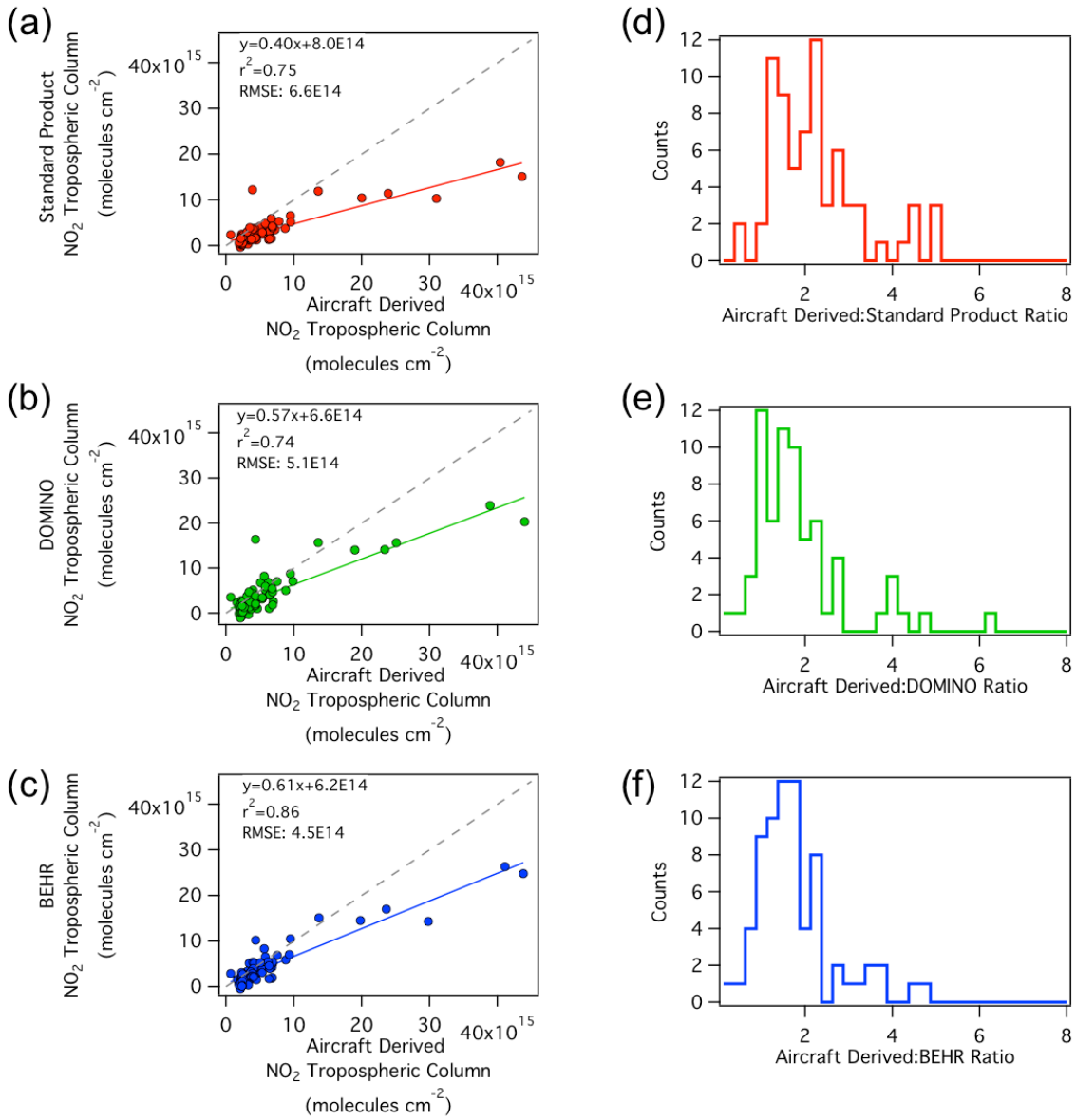

Figure 3-1: (left) Scatter plots showing the comparison between the aircraft-derived columns and the three OMI products: Standard Product (a), DOMINO (b), and BEHR (c). The grey dashed line indicates a 1:1 relationship, and the colored lines are the best linear fit to the data. (right) Histograms of the aircraft:satellite (A:S) ratio for the Standard Product (d), DOMINO (e), and BEHR (f).

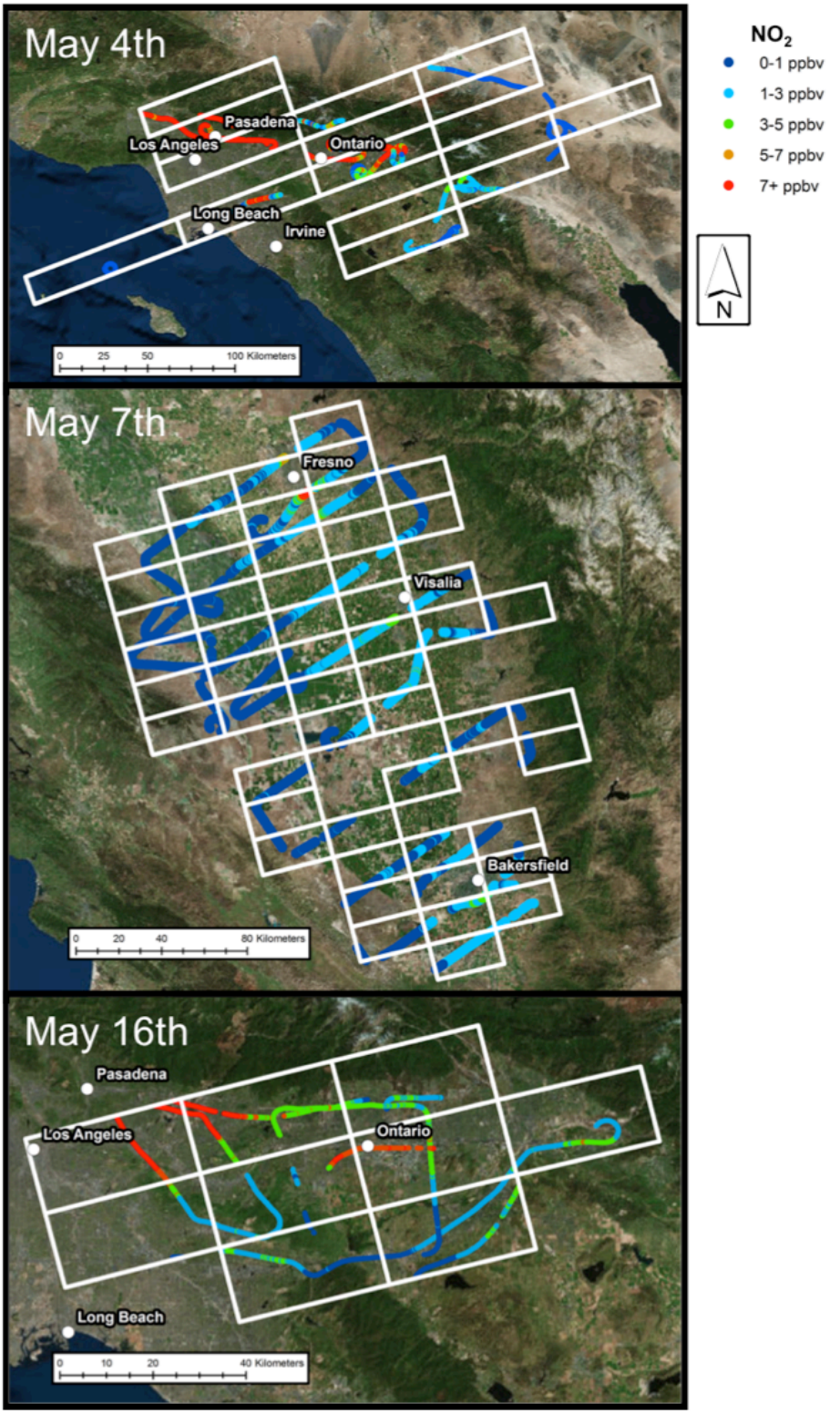

Figure 3-2: Maps representing the data in Figure 3-1 for all three flight days. OMI pixel outlines are the white boxes. The flight data is colored by NO_2 concentration and only includes data incorporated into the aircraft-derived column.

3.3.2.1 PIXEL SIZE

On May 4th, the aircraft data was collected inside OMI pixels far from nadir, with pixel area ranging from ~ 900 km^2 to 1600 km^2 (Table 3-2). During this time, the aircraft measured much higher pollution levels than the satellite, resulting in relatively low slopes ranging between 0.36 (SP) and 0.56 (BEHR) and higher RMSE values. When compared to the other Los Angeles flight with near-nadir OMI measurements (May 16th), the comparisons were in better agreement with higher slopes and smaller RMSEs. This was likely due to the smaller pixel size of ~ 400 km^2, resulting in less chance of spatial heterogeneity within the pixel area. Multiple environments influenced all pixels on May 4th (ocean, urban, desert, mountains, etc.), however the flights focused primarily on the urban measurements. Therefore, aircraft measurements were not representative of all environments within the OMI FOV. For this study, the Los Angeles region was mainly influenced by the May 4th measurements because of the larger number of valid pixels after filtering. More clouds influenced the May 16th OMI measurements. However, the pixels that were clear on the 16th were still a lower range of value than what the aircraft measured in all cases, most likely due to the weekend vs. weekday effect; May 16th was a Sunday.

3.3.2.2 POLLUTION LEVEL

In the cleaner environment of Central Valley, SP showed the worst comparison. This comparison improved dramatically for the DOMINO (slope = 0.82) and BEHR

(slope = 0.72). BEHR had a much lower RMSE in this region in comparison to DOMINO and SP (Table 3-2).

Previous aircraft validations (Boersma et al., 2008; Bucsela et al., 2008; Bucsela et al., 2013; Hains et al., 2010) focused on cleaner environments where the majority of data was less than 1×10^{16} molecules cm^{-2}. To look at this comparison closer, data were divided into polluted columns (measurements greater than 1×10^{16} molecules cm^{-2}) and unpolluted columns (measurements less than 1×10^{16} molecules cm^{-2}). Unpolluted data had a higher slope and lower RMSEs (Table 3-3).

The slopes between the aircraft-inferred columns and satellite products were much lower for pollution levels above 1×10^{16} molecules cm^{-2} (between 0.12 from Standard Product and 0.39 from BEHR (Table 3-3)). This indicated a strong mismatch between the measurements. The aircraft often only measured one type of environment. Terrain and urban heterogeneity led to partially clean and partially polluted pixels, and if only one environment was sampled in this process then the aircraft profile was not representative of the OMI FOV. BEHR did a slightly better job than DOMINO and SP in these polluted areas, as expected with the finer resolution *a priori* inputs for the tropospheric AMF calculation. BEHR's sub-pixel resolution *a priori* inputs were also averaged over the entire pixel to capture all environments occurring in the region, whereas the other two products interpolated *a priori* input information to the center of the OMI pixel (Russell et al., 2011). Future retrievals would benefit from higher resolution *a priori* inputs in areas with spatial heterogeneity.

				NASA Standard Product			DOMINO			BEHR		
Date	**Pixel Size**	**Aircraft-Derived Column Range (molecules cm^{-2})**	**N**	**Best Fit**	**r^2**	**RMSE**	**Best Fit**	**r^2**	**RMSE**	**Best Fit**	**r^2**	**RMSE**
4-May	900-1600 km^2	$7.1x10^{14}$-$4.7x10^{16}$	15	$0.36x-1.4x10^{15}$	0.91	$3.0x10^{15}$	$0.49x+2.5x10^{15}$	0.92	$2.1x10^{15}$	$0.56x+1.7x10^{15}$	0.92	$2.0x10^{15}$
7-May	360-430 km^2	$1.9x10^{15}$-$7.7x10^{15}$	51	$0.51x-3.6x10^{13}$	0.49	$3.1x10^{14}$	$0.82x-9.1x10^{14}$	0.47	$3.0x10^{14}$	$0.72x-2.8x10^{14}$	0.52	$2.5x10^{14}$
16-May	380-430 km^2	$3.9x10^{15}$-$1.4x10^{16}$	9	$0.59x+1.6x10^{15}$	0.23	$1.2x10^{15}$	$0.87x+1.4x10^{15}$	0.27	$1.5x10^{15}$	$0.89x+9.4x10^{14}$	0.55	$3.3x10^{14}$

Table 3-2: Comparison statistics of the three OMI NO_2 tropospheric column products to the aircraft-derived tropospheric columns separated by flight day.

	Standard Product			DOMINO			BEHR		
	Best Fit	**r^2 (N)**	**RMSE**	**Best Fit**	**r^2 (N)**	**RMSE**	**Best Fit**	**r^2 (N)**	**RMSE**
Unpolluted	$0.54x+4.7x10^{12}$	0.54 (68)	$2.3x10^{14}$	$0.76x-4.1x10^{14}$	0.49 (68)	$2.6x10^{14}$	$0.71x-1.3x10^{13}$	0.49 (67)	$2.3x10^{14}$
Polluted	$0.12x+9.7x10^{15}$	0.36 (7)	$6.5x10^{15}$	$0.18x+1.3x10^{16}$	0.49 (7)	$4.8x10^{15}$	$0.39x+7.4x10^{15}$	0.85 (8)	$3.8x10^{15}$

Table 3-3: Comparison statistics of the three OMI NO_2 tropospheric column products separated by pollution level. The cutoff between polluted and unpolluted was $1x10^{16}$ molecules cm^{-2}

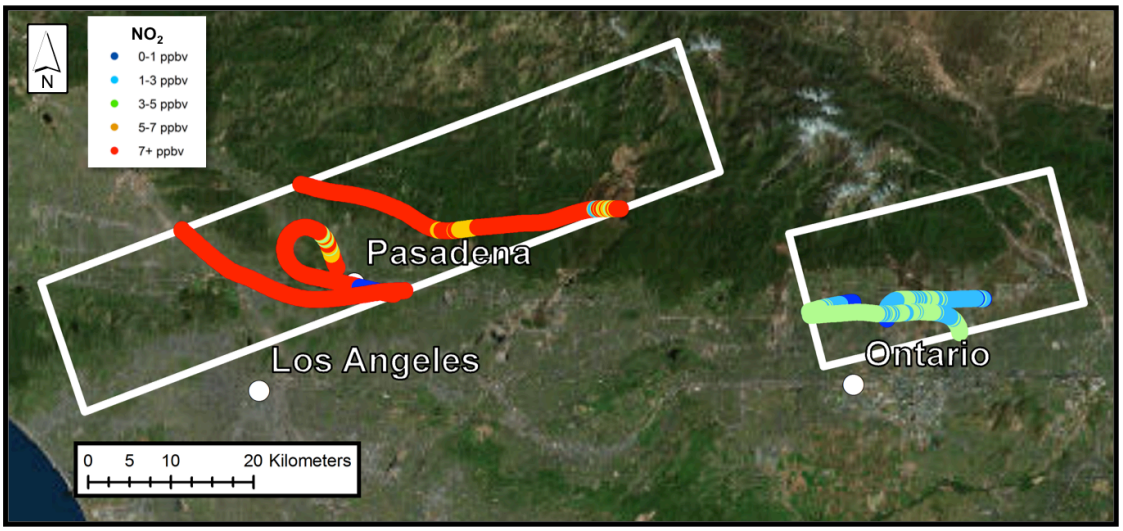

Figure 3-3: Two examples exhibiting the sampling bias in pixels with heterogeneous terrain from May 4th (left pixel) and May 16th (right pixel). OMI pixels are outlined in white and aircraft data included in the aircraft-derived column are colored by NO_2 concentration.

3.3.2.3 HOMOGENOUS TERRAIN

When considering environmental heterogeneity and aircraft sampling, it was easy to remove those pixels that had obvious mismatches due to the terrain influences. For example, Figure 3-3 shows two pixels where the aircraft-inferred columns deviated

far from the satellite measurements due to heterogeneous terrain. The aircraft sampled in the urban boundary layer, but approximately half of each pixel was covered by mountainous terrain, which in comparison should have had less NO_2 pollution. In these two examples, the A:S ratio ranged from 1.7 (BEHR) to 2.55 (SP) on May 16th (the smaller pixel). The larger pixel from the May 4th overpass had the A:S range between 1.7 (BEHR) and 2.9 (SP). Although there was aircraft sampling bias for the urban region, the higher resolution *a priori* inputs for BEHR compared better.

To minimize the influence from heterogeneous terrain, pixels were separated and evaluated by whether the environment changed due to terrain within the OMI FOV. Pixels were considered to have homogeneous terrain if the difference between the SP terrain pressure and BEHR terrain pressure for the AMF calculation for each pixel was less than 10 hPa. SP only considered the terrain pressure at the pixel center, whereas BEHR averaged over the entire pixel area. Therefore, if they were similar then the terrain should be relatively homogeneous within the pixel. This was confirmed by mapping considered pixels on a terrain map (not shown). DOMINO's terrain pressure included information from the TM4 model, and therefore was not considered in this filter. Thirty-two pixels were relatively homogenous with respect to terrain. The slopes for these pixels were higher (Figure 3-4) than all the pixels combined (Figure 3-1). However, there was a difference between homogenous pixels in the Los Angeles region vs. Central Valley. The sample size in the Los Angeles region was extremely small (only 4 pixels

spanning a large range of column densities). This made it difficult to conclude whether the homogenous terrain compared better than all the data in the Los Angeles region.

Figure 3-5 shows an example where the terrain was relatively homogeneous but the A:S ratio deviates far from 1. This map shows a pixel in the Central Valley near Fresno, CA. Even though Fresno was not within the pixel area, it was downwind of the city and the aircraft showed a concentrated NO_2 plume in the northeast portion of the pixel. This pixel was primarily agricultural with the exception of the freeway to the northeast. The aircraft flew low for the northeast to southwest transect of the pixel before spiraling out of the boundary layer. This was a case where the aircraft measurements were representative of the pixel area, but was up to 4.6 times more than the satellite retrieval in the case of DOMINO (2.1 for BEHR and 3.7 for SP). This underestimation from OMI was hypothesized to be due to the loss of spatial information across the OMI pixel, as pollution was averaged over the pixel area. This motivated the use of downscaled OMI data when comparing to smaller scale measurements such as aircraft *in situ* data.

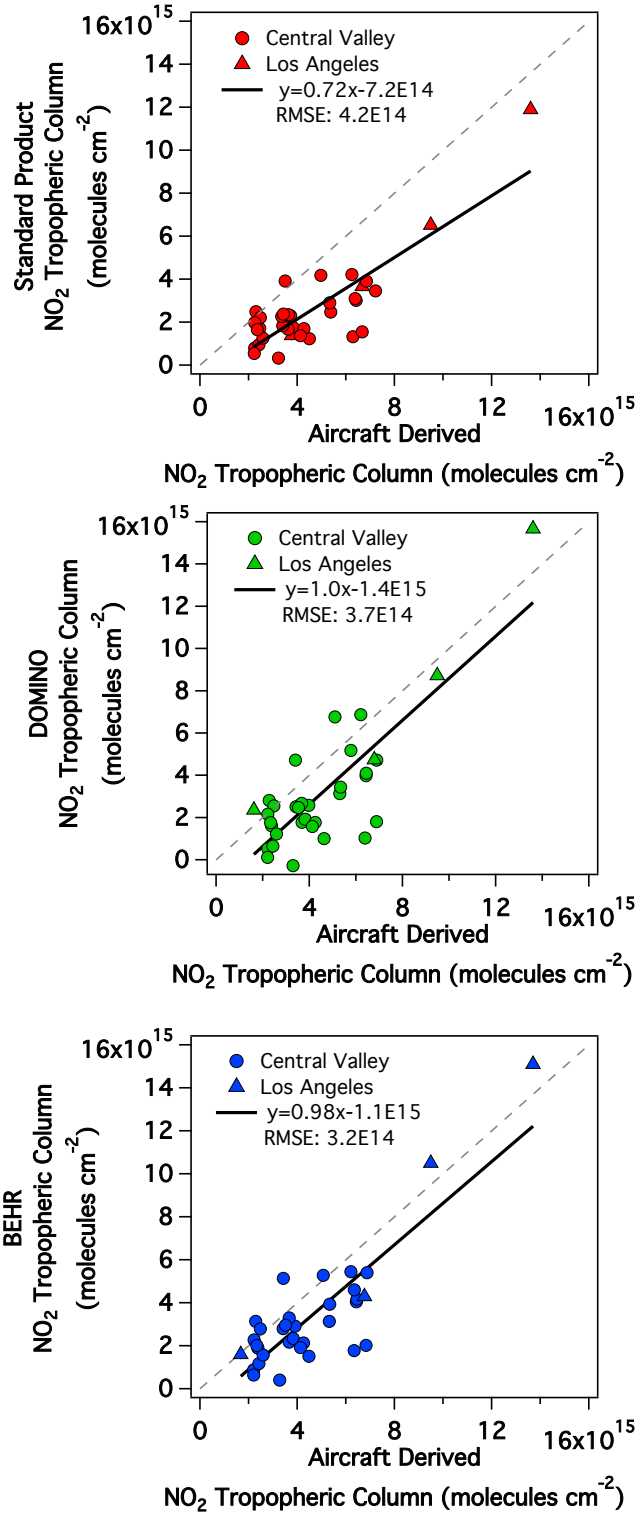

Figure 3-4: Scatter plots showing the comparison between the Standard Product, DOMINO, and BEHR and the aircraft-derived tropospheric NO_2 columns for pixels in areas with homogeneous terrain.

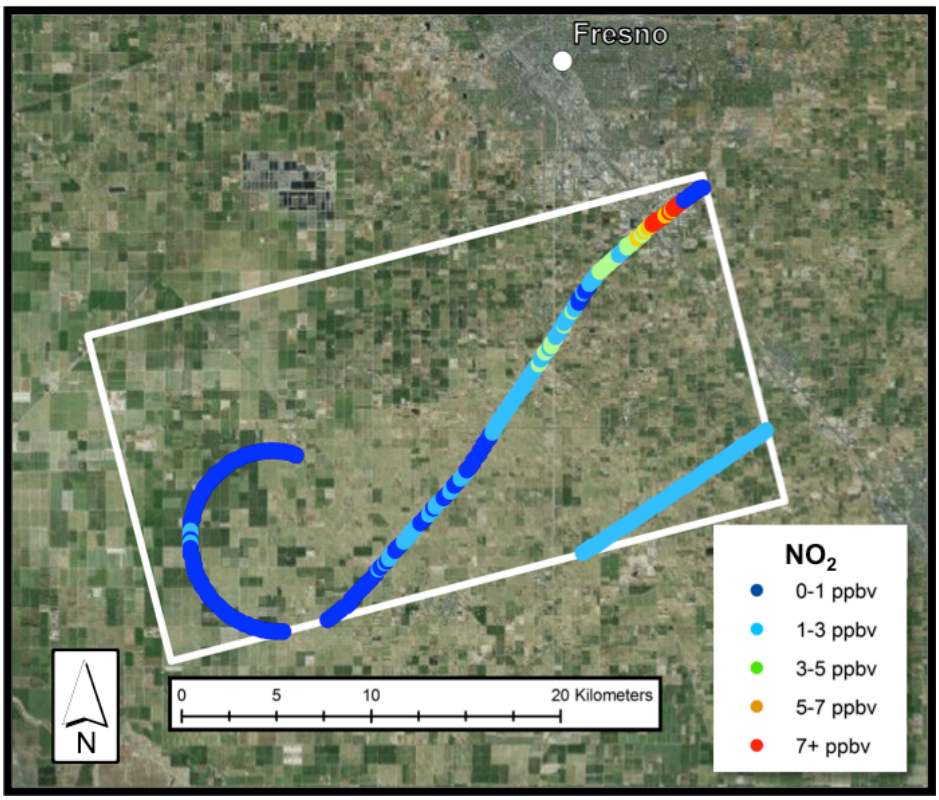

Figure 3-5: Example where the aircraft sampled throughout the pixel southwest of Fresno, CA. The OMI pixel is outlined in white and aircraft data included in the aircraft-derived column are colored by NO_2 concentration.

3.3.3 OMI DOWNSCALE

To lessen sampling bias of the aircraft and satellite comparisons, the OMI DOMINO retrieval was downscaled using CMAQ-derived spatial weighting kernels to distribute NO_2 to a smaller spatial scale. Over the large area of the OMI pixel, the spatial detail was averaged out leading underestimated observations in urban centers near Los Angeles. The downscale results for the CalNex 2010 aircraft comparisons are shown in Figure 3-6. Overall, the downscale and aircraft measurements had a closer relationship than compared to the original DOMINO product in the most polluted regions of Los

Angeles. There was little improvement in the cleaner regions, which was expected due to the lack of NO_2 spatial heterogeneity. There were a few distinct outliers that decreased the correlation between aircraft and satellite and did little to improve the RMSE when compared to the original OMI DOMINO data. Results over a longer period of time may show clearer outcomes on how well the downscale tool recreates a realistic distribution of NO_2. Improvements were visible in the majority of the polluted pixels, as they were shifted closer to agreement with the aircraft (Figure 3-6). The pixel in the map from Figure 3-5 went from an A:S ratio of 4.6 to 2.4 from the downscale. A few profiles showed worse relationships between the aircraft and satellite, but the one that did can be explained by assumptions made when aircraft profiles were derived and possible errors in model transport.

There were three high downscale outliers in the polluted pixels that were caused by assumptions made while deriving aircraft columns (boxed in Figure 3-6 and visible in Figure 3-7 on May 4th and 16th as the green/blue circles surrounded by warmer colored downscaled areas). In two cases, the aircraft entered the boundary layer adjacent to the Santa Ana Mountains, and then proceeded above the top of the mountains and out of the boundary layer. This region was likely not as polluted as the rest of the 12 km downscaled area, as the majority of that grid-box encompassed an urban environment and the aircraft did not sample far enough down in the urban boundary layer. The final outlier was located in the Inland Empire. In this case, the aircraft entered the boundary layer (~800m) and stayed in the upper portions of the boundary layer for the entire

duration of the pixel transect. These outliers were cases where the aircraft did not sample within the denser parts of the urban plume within the boundary layer, and therefore led to an underestimation by the aircraft-derived column.

The one other clear outlier is also boxed in Figure 3-6. In this case, the downscale technique did not distribute more NO_2 to the region where the aircraft measured dense NO_2 pollution. It is seen in the May 4th downscaled map of Figure 3-7 as a red circle to the north of Los Angeles. A transport error due to winds was the likely cause, as the grid-box to the east exhibited the correct amount of pollution as the aircraft-derived column. Without these four outliers, slope in Figure 3-6 increased to 0.8, r^2 increased to 0.85, and RMSE decreased to 3.6×10^{14} molecules cm^{-2}.

The downscaled data was compared for the same areas discussed in Section 3.3.2 by separating data by polluted, unpolluted, and homogenous terrain. While the unpolluted regions saw no significant change in their slope and correlation statistics, there was a larger improvement in the polluted pixels. The slope increased from 0.18 to 0.30 and the RMSE decreased by 1×10^{15} molecules cm^{-2}. In areas with homogenous terrain, there was a decrease in the RMSE and a lower slope for the downscale, but the worsening in statistics was likely due to the explained outliers. Without the outliers, slope increased to 0.98 and $r^2 = 0.71$ for areas with homogeneous terrain.

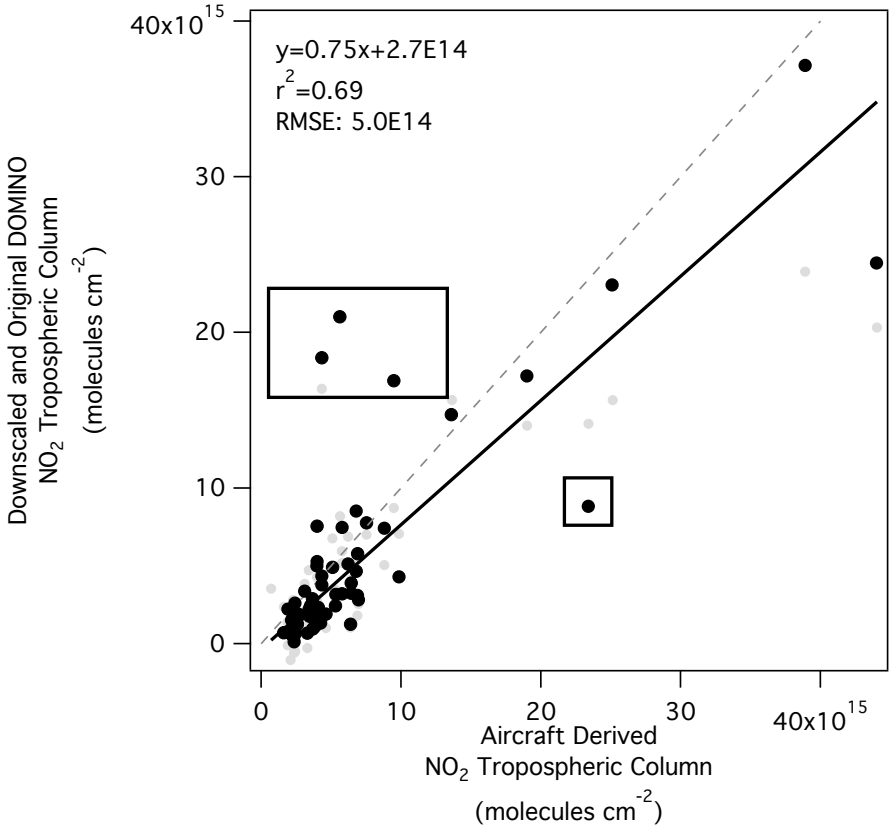

Figure 3-6: Scatter plot comparing the original and downscaled OMI retrievals to the aircraft-derived tropospheric NO_2 columns. Black dots indicate the downscaled DOMINO results, and grey points show the original DOMINO data.

DOMINO Downscale				
Subsets	**N**	**Best Fit**	**R^2**	**RMSE**
Polluted ($> 1x10^{16}$ molecules cm^{-2})	9	$0.31x+1.4x10^{15}$	0.30	$3.7\ x10^{15}$
Unpolluted ($< 1x10^{16}$ molecules cm^{-2})	65	$0.76x-4.1x10^{14}$	0.48	$2.5\ x10^{14}$
Homogeneous Terrain	47	$1.3x-2.9x10^{15}$	0.37	$5.5\ x10^{14}$

Table 3-4: Statistics of downscaled DOMINO for varying pollution levels and terrain environments.

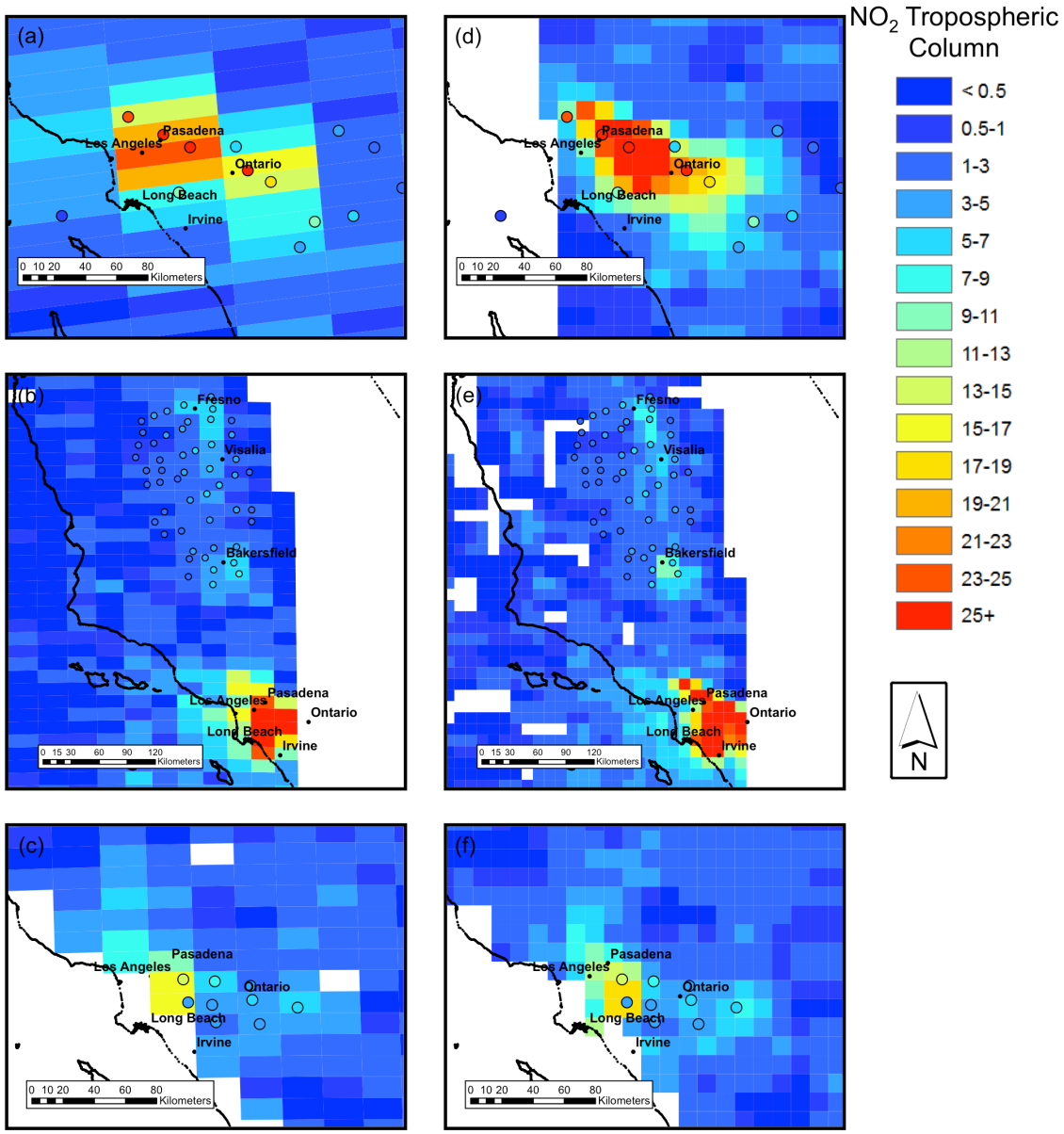

Figure 3-7: Maps of the OMI DOMINO NO_2 tropospheric column measurements on (a) May 4th, (b) May 7th, and (c) May 16th, and their OMI downscaled counterparts (d, e, f). The filled circles represent the mid-point of each aircraft profile colored by the aircraft-derived tropospheric NO_2 column. All values are in x10^{15} molecules cm^{-2}.

3.3.3.1 HOUSTON, TEXAS CASE STUDY

To test OMI downscaling in an additional environment, this technique was applied during the times of DISCOVER-AQ Texas 2013. The NASA P-3B spirals

mentioned in Chapter 2 were matched to downscaled DOMINO results. Spirals within two hours of the OMI overpass were considered in this analysis and OMI pixels must have had cloud fractions less than 20% and free of the row anomaly. Unfortunately, only 21 spirals from the NASA aircraft coincided with downscaled OMI results due to convective cloud conditions and the row anomaly lining up with Houston, Texas on some flight days. Most of the coinciding data occurred on September 24th and 26th, 2013. On the four other flight days included in this downscale analysis, the most polluted regions of Houston did not coincide with valid downscaled data and only a few points in cleaner environments were added to the dataset (Galveston, Smith Point, Manvel Croix).

Figure 3-8 compares both the DOMINO OMI product and the downscaled DOMINO to the aircraft-derived columns. A few patterns emerged as this data was displayed. The most unpolluted environments (less than 3×10^{15} molecules cm^{-2}) showed a high bias from DOMINO and the downscale. In this case, the downscale tool did not improve the results. However, for polluted regions (greater than 7×10^{15} molecule cm^{-2}), the downscale tool brought the compared datasets into closer agreement. These locations included results from Channelview and Deer Park near the Houston Ship Channel, which were among some of the most NOx-polluted sites in the city (see Chapter 4). These results suggested that the downscale tool could help in areas that are under constant heavy pollution from NOx emissions, similar to the Los Angeles region.

In the mid-range of NO_2-polluted columns, there was a lot of variability in the results. The two most extreme results coincided with the downscale at the Moody Tower (black crosses in Figure 3-8). This region of the city is unique as it is at the junction of 3 major freeways near downtown Houston and also near the Ship Channel. In every downscale result in Houston, the grid-box containing the Moody Tower location was the most NO_2 pollution grid-box of the region (Figure 3-9). This pattern also appeared in the past. Couzo et al. (2015) found that emissions inventories overestimated NO_2 by over 300% during the daytime hours at Moody Tower. The majority of the emissions in this area are marked as non-mobile Ship Channel activity. Similar to Couzo et al. (2015), the downscale grid-box to the south of Moody Tower was used to compare to the aircraft. While the values were closer to the value of the aircraft spiral, the differences were still on the order of $3\text{-}4\times10^{15}$ molecules cm^{-2} and this grid-box was not representative of where the spiral occurred.

Other outliers besides Moody Tower were apparent where the downscale significantly overestimates NO_2. These data points all occurred on September 24th, 2013 (as outlined in red in Figure 3-8). Upon further examination of the conditions, it appeared that the Houston region was under the cover of a thick cumulus field on this day, but OMI estimated the cloud fraction between 10-20%. These OMI observations were near the edge of the swath where pixels encompassed a much larger area than just the Houston region. Although there were clouds over Houston, clearer conditions to the east may have averaged the cloud fraction out over the large area of the OMI pixel. On

this day, most the results overestimated NO_2 when compared to the aircraft measurements. Transport error was ruled out as modeled wind directions show that these sites were upwind of most NOx sources. It was likely not a good day for OMI observations in the region.

Overall, there was little improvement in the RMSE between the DOMINO measurements and the downscale in Houston, as they both had RMSE = 2.9×10^{15} molecules cm^{-2}. However, if results from September 24th were removed from the dataset, RMSE decreased from 3.3×10^{15} molecule cm^{-2} from DOMINO to 2.1×10^{15} molecules cm^{-2} from the downscale. Overall, these results suggested that the downscale tool will likely help in areas constantly underestimated by the satellite (locations with consistently heavy NOx emissions), and likely should only be used over longer time periods where singular result errors from transport, emissions, and unfavorable observation conditions could be averaged out.

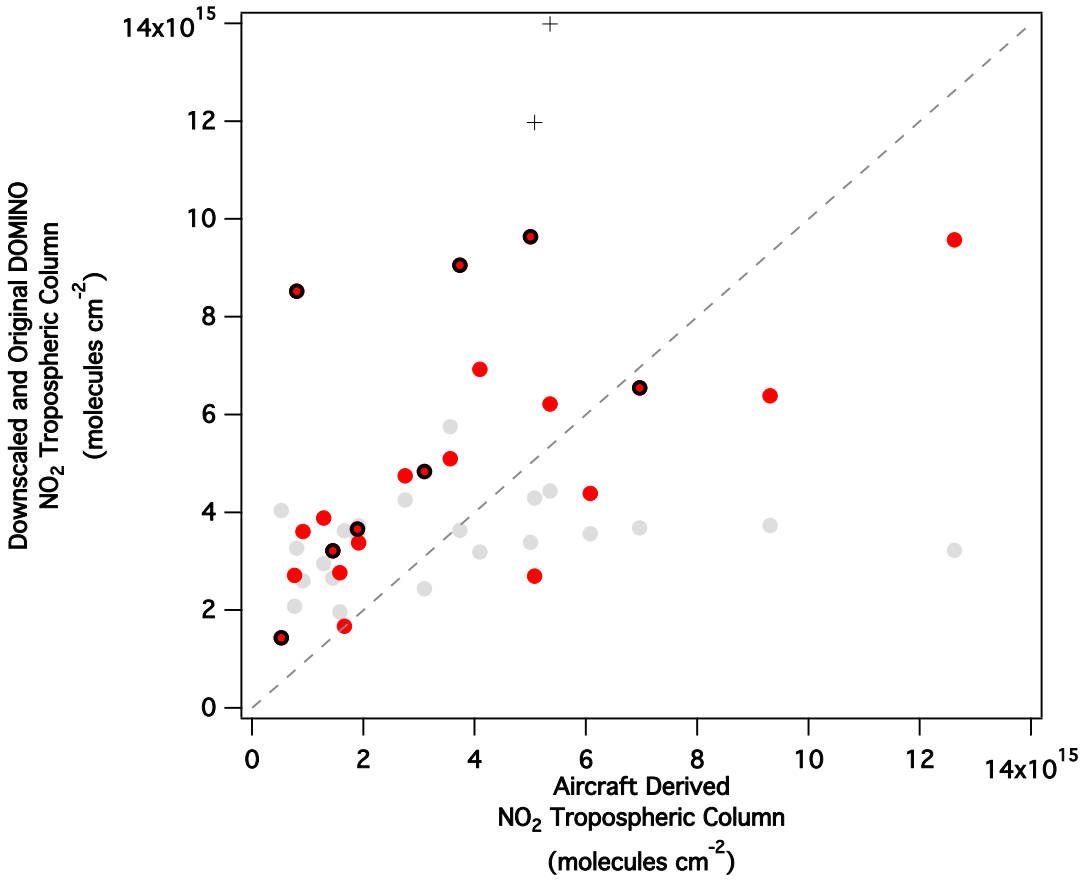

Figure 3-8: Scatter plot displaying the comparisons between aircraft-derived columns from DISCOVER-AQ Texas and the DOMINO tropospheric column product (grey) and the downscaled DOMINO results (red). The black crosses are downscaled DOMINO results from Moody Tower, however marked as an area where emissions were thought to be overestimated. Red circles outlined in black indicate data occurring on September 24th, 2013.

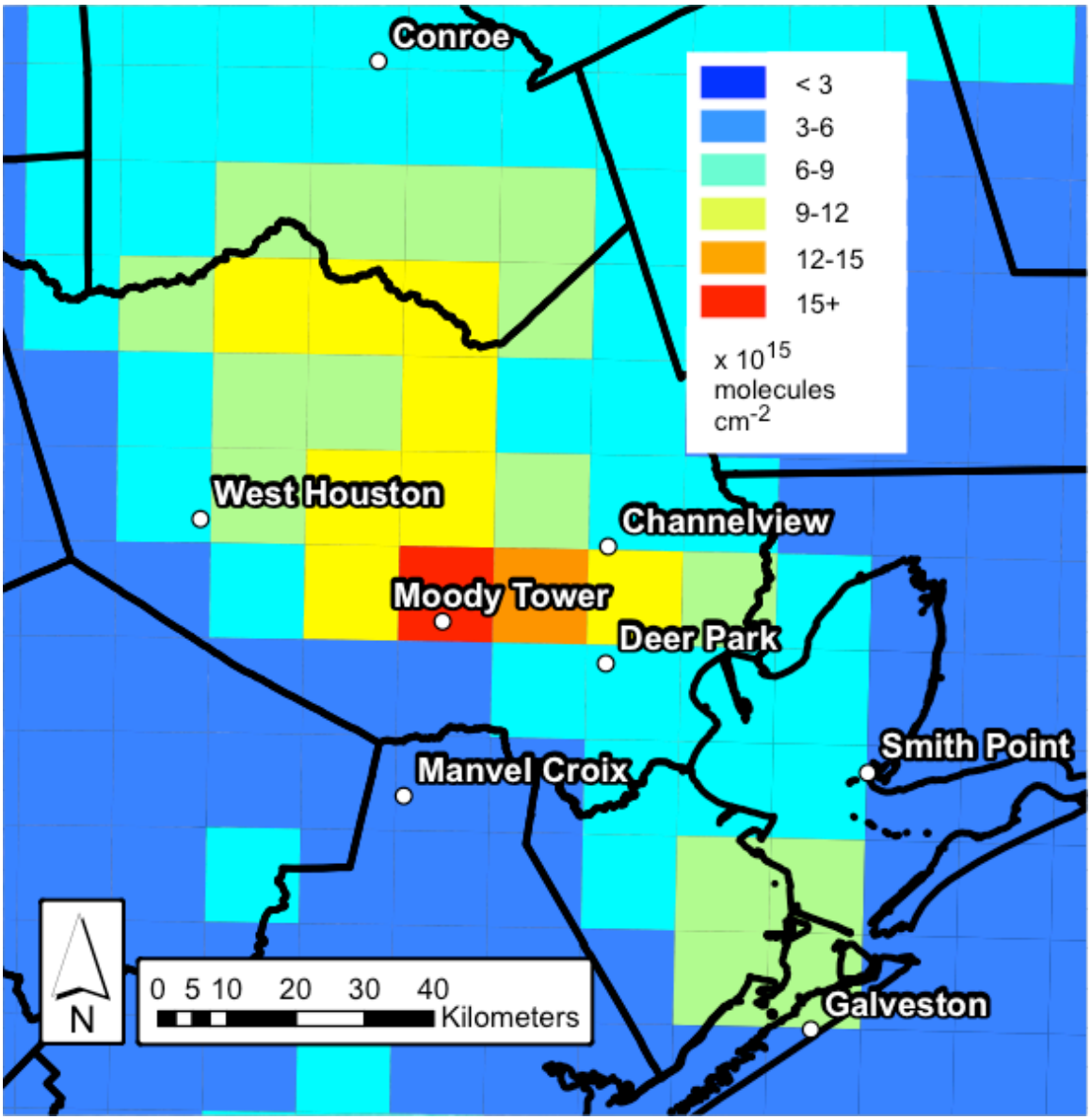

Figure 3-9: Map displaying the results from the downscaled DOMINO on September 26th, 2013. Moody Tower is found within the most polluted grid-box.

3.4 SUMMARY

This chapter investigated how well the NASA Standard Product, BEHR, and DOMINO OMI retrievals captured the distribution of NO_2 in the Los Angeles and Central Valley regions of California by comparing to aircraft-derived column measurements during CalNex 2010. Comparisons showed that in the most polluted regions, OMI measurements were not representative of the aircraft observations due to spatial resolution mismatch and environmental spatial heterogeneity. The higher resolution *a priori* inputs for the AMF calculation in BEHR showed a better comparison to the aircraft measurements, suggesting that future retrievals would benefit from these algorithm improvements.

The level of heterogeneity in each pixel was influenced by the pixel size, the level of pollution, and terrain. The OMI results from smaller pixels were closer in comparison to aircraft-derived columns because their area covered more a homogeneous environment and the aircraft sampling was more representative. The more polluted a pixel, the larger the difference between the satellite retrieval and the aircraft observation. In these cases, the aircraft was sampling primarily urban air, and the OMI footprint often encompassed both urban and mountainous terrain. To investigate terrain influences, only pixels with homogenous terrain were analyzed. Data for these pixels compared better, but the Los Angeles region only had four homogeneous terrain pixels during this experiment, so it was difficult to make conclusions about OMI results in the urban environments.

Downscaling OMI observations showed improvement in the data comparisons by lessening sampling bias of the aircraft and added information on sub-pixel distribution of NO_2. However, there were instances where the comparison worsened. Many of these California cases were outliers caused by failed assumptions for deriving the aircraft column and model transport errors.

In Houston, similar improvements from downscaling OMI were also found in the most polluted areas of the region. Outliers from the downscale results proved to be due to either emission estimation errors or imperfect observation conditions from OMI due to clouds. Despite potential errors and lack of improvement in cleaner regions, the use of this downscaling method allows for potential smaller scale studies of NO_2 heterogeneity in the most polluted areas near urban cores and likely would be more beneficial over longer periods of time.

4. TRENDS AND SPATIAL DISTRIBUTION IN NO_x AND VOC CONCENTRATIONS AND THEIR EFFECTS ON OZONE PHOTOCHEMISTRY

4.1 INTRODUCTION

While stratospheric ozone is necessary for life to live on Earth, ground level ozone is considered detrimental to human health, especially to those populations with health problems, such as asthma or lung disease. Ground level ozone can also harm ecosystems by inhibiting plants' ability to produce food and affects the physical appearance of the vegetation (http://www3.epa.gov/ozonepollution/).

Ozone has two primary pathways for production. Reaction 1.1 and 1.3-1.4 shows the first pathway of ozone production. This pathway leads to zero net production of ozone (null cycle), as an ozone molecule must be destroyed to produce the NO_2 necessary to make another ozone molecule. The net ozone-producing pathway (Reactions 1.2-1.4) requires peroxy radicals formed from the oxidation of volatile organic carbons (VOCs). These peroxy radicals can react with NO to create the NO_2 necessary for ozone production.

Urban regions often have excess NOx ($NO+NO_2$) and VOCs, as they are emitted from mobile and stationary sources. Due to transportation and industry dominating Houston's economy, local air quality is in non-compliance according to EPA NAAQS for ozone. The ozone NAAQS uses a 'design value', which is defined as the maximum daily 8-hr average ozone on the fourth highest day annually averaged over the last three

years. Policy-makers and industries have worked together to decrease reactive hydrocarbon and NOx emissions in an attempt to bring the area into attainment of the ozone NAAQS in terms of the number and severity of ozone events in the Houston region. The design value in the Houston-Galveston-Brazoria (HGB) region has decreased from 112 ppbv in 1999 to 80 ppbv in 2015 (Figure 1-1), but is still higher than the newest 2016 8-hr NAAQS standard of 70 ppbv. Fortunately, the numbers of ozone-exceedance events were cut in half from approximately two months to less than a month each year from 2000-2014.

Urban Houston sits to the northwest of Galveston Bay and consists of a dense network of freeways heavily traveled by the millions of people residing within the region. The Ship Channel is located to the east of urban Houston as an inlet from Galveston Bay. The Houston Ship Channel is one of the busiest seaports in the United States and home to numerous petrochemical facilities and other industries. The release of reactive hydrocarbons from this localized region complicates the understanding and study of Houston's air quality.

This study explored the changes in the photochemical environment in the Houston Ship Channel by using continuous air monitoring data from TCEQ at Deer Park in the south, Clinton Drive in the west, and Channelview to the north (Figure 4-1). Analysis was also expanded out the Ship Channel to explore photochemical changes spatially throughout the city. Emissions in these areas decreased since 2000 (Figure 4-2) and were linked to the decreasing ozone NAAQS exceedances in the Houston region

(Figure 1-1). At the long term monitoring sites of interest, NOx has decreased 20-44% since 2000. Other sites in Houston have seen even larger decreases in NOx, such as Aldine with an annual mean NOx decrease of ~ 60% since the late 1990s. Alkanes and alkenes had also decreased 25-45% and 65-72%, respectively, in the Ship Channel. However, in the last few years, alkanes have started to increase, likely due to the boom in hydraulic fracturing boosting the use of natural gas in industrial processes. Decreases in alkenes have also flattened out, with most changes occurring before 2010.

Through the years, the complexity of Houston's air quality motivated numerous intensive research campaigns. In 2000, the Texas Air Quality Study (TexAQS) involved both aircraft and surface measurements of atmospheric parameters to get a better understanding of the relationship between emissions, air quality, and meteorology in the region (Banta et al., 2005; Daum et al., 2003; Jiang et al., 2004; Mao et al., 2010; Ryerson et al., 2003). Scientists from NOAA, the Department of Energy, and universities had a common goal of learning about pollution in Houston and determining the best strategy to combat poor air quality. Similar to 2000, TexAQS II and the Gulf of Mexico Atmospheric Composition and Climate study (GoMACCS) took place in 2006 with similar goals to TexAQS 2000 with the additional study on air quality influences on climate (Parrish et al., 2009). Aircraft data from these two campaigns are used to analyze how photochemistry changes spatially in the Houston region in section 4.3.5.

This study involved the photochemical modeling of data from three long-term monitoring sites (Figure 4-1) in the Houston Ship Channel (2000-2014) to assess how

emissions and photochemistry have changed in the most polluted region of the city. Modeled aircraft data from TexAQS 2000 and TexAQS II/GoMACCS 2006 demonstrated how photochemistry changed outside the Ship Channel region to more urbanized and rural portions of the region. Additionally, during Moody Tower 2010 (Flynn, 2013) and DISCOVER-AQ Texas 2013 (https://www.nasa.gov/mission_pages/discover-aq/), measurements at Moody Tower (Figure 4-1) in urban Houston were used to show how urban photochemical characteristics changed after the TexAQS campaigns. Attributes investigated include ozone production rates, hydrocarbon reactivity, NOx/VOC sensitivity regimes, and ozone production efficiency.

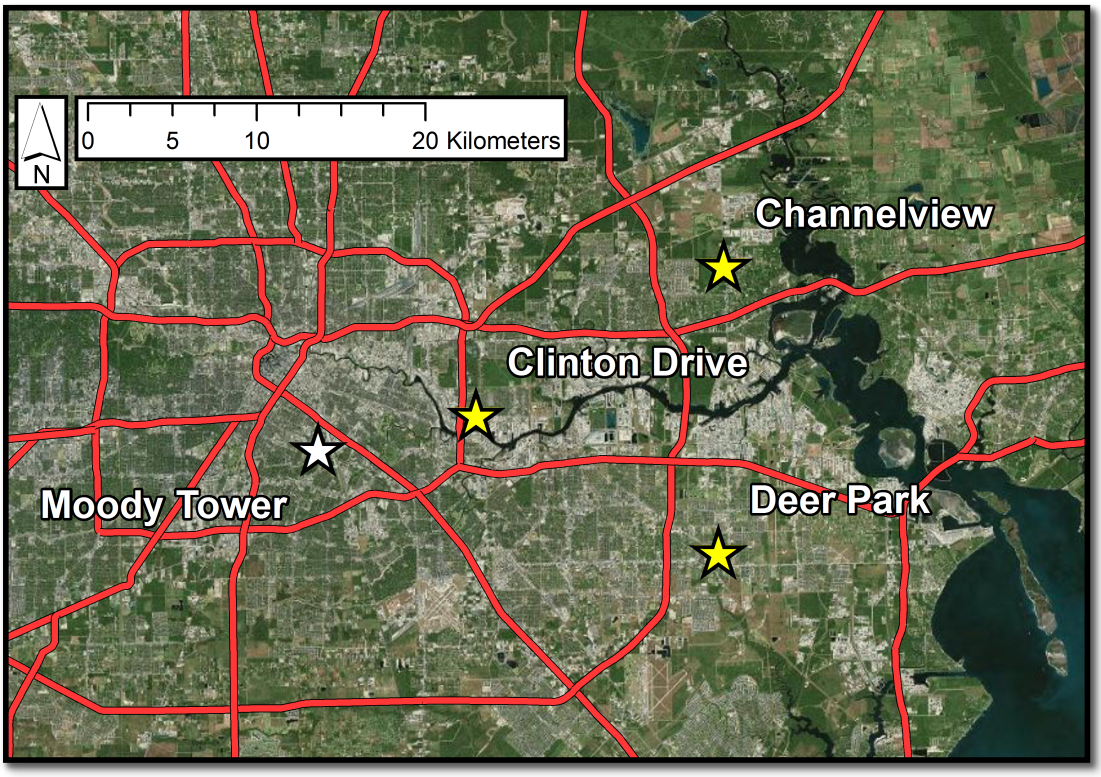

Figure 4-1: Map of the Houston area. Red lines indicate the location of freeways, and the stars highlight the locations of the University of Houston's Moody Tower and the long-term monitors from which the data is modeled to study photochemistry trends in the Houston Ship Channel (the inlet extending from Galveston Bay toward central Houston).

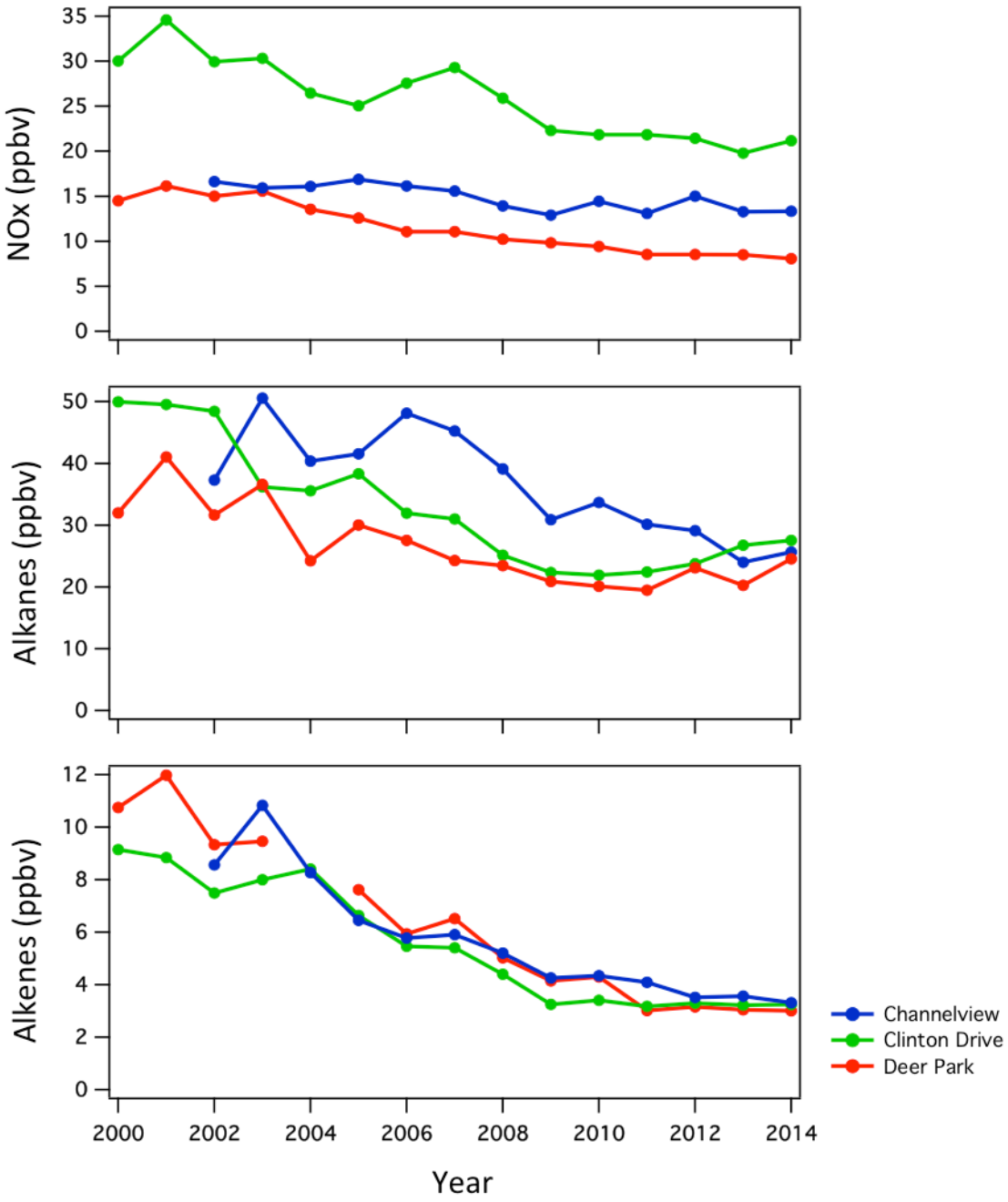

Figure 4-2: Annual average of the concentrations of NOx, Alkanes, and Alkenes at the three long-term monitoring sites used in this study.

4.2 METHODS AND DATA

4.2.1 LARC MODEL

The Langley Research Center (LaRC) model is a zero dimensional photochemical box model, and it was executed in time-dependent diurnal steady state (Crawford et al., 1999; Olson et al., 2006). This model simultaneously solved 251 chemical and 36 photolytic reactions. The chemical reactions and kinetics were from Sanders et al. (2006) with hydrocarbon chemistry based on Lurmann et al. (1986). Non-methane hydrocarbons were lumped as shown in Table 4-1, where all alkanes, alkenes, and aromatics measured, but not explicitly handled in the model, are assumed as a chemical family. Previously, the LaRC compared well to other well-known chemical mechanisms (CB05, RACM2, SAPRC-07, and MCM v3.1) in Houston (Chen et al., 2010; Ren et al., 2013).

The minimum input required the following data parameters: temperature, dew point, O_3, CO, NO, NO_2, NMHCs, jNO_2, and overhead O_3 columns. Flynn et al. (2010) showed the importance of constraining to PAN, formaldehyde, and HONO when studying ozone production in Houston. Unfortunately, these parameters were not monitored in the Ship Channel. However, general photochemistry trend were still apparent in the model output.

The LaRC model output contained reaction rates for all 251 chemical reactions and 36 photolysis frequencies, as well as other modeled gas species. It also quantified ozone formation and destruction rates and their individual components. In these

results, net production of ozone (PO_3) was calculated as ozone formation (FO_3) minus ozone destruction (DO_3).

4.2.2 LONG TERM MONITORING DATA

All long-term data were from the Continuous Ambient Monitoring Sites (CAMS) from Texas Commission for Environmental Quality (TCEQ), with the exception of ozone column inputs into the LaRC model. Hourly averaged data were used for each time-step in the model. The number of sites in this analysis was limited by data availability from long-term automatic gas chromatograph (auto-GC) monitors. All auto-GC monitors were located near the Ship Channel region in Houston. The three sites in this analysis were spread throughout the Ship Channel with Channelview in the north, Clinton Drive in the west, and Deer Park in the south (Figure 4-1).

O_3, CO, NO, and NO_2 data were all QA/QC evaluated monitoring data. Although detection limits and measurement uncertainties were not quantified for the monitoring sites, the data quality was investigated and erroneous looking data points were filtered out. Most of this filtered data included NOx data, where the NO_2/NO ratios exceeded reasonable values. During the active photochemical hours (9am-3pm) at Moody Tower during the DISCOVER-AQ campaign in September 2013, the NO_2/NO ratio was a maximum of ~ 30 and an average of 3.4. Outliers may have resulted from interferences within the molybdenum converter from other reactive nitrogen species (Dunlea et al., 2007; Sather et al., 2006).

There were no measurements of carbon monoxide (CO) at the Channelview site, so CO was assumed to be proportional to the concentration of NO_2. A correction factor was applied from the linear best fits at Clinton Drive (the nearest site): CO = 9.3061 ± 0.109 [NO_2] + 138.69 ± 1.89, r^2 = 0.21. Ozone production was not very sensitive to the concentration of CO. Varying CO from 100 ppbv (cleaner onshore flow) to 500 ppbv (polluted-continental flow) only influenced ozone production on average of ~3%.

At the monitoring sites, jNO_2 was not directly measured. Instead, jNO_2 was inferred from a calibration coefficient applied to data from pyranometers at Deer Park and Channelview and a UV radiation photometer at Clinton Drive. These calibration coefficients were determined using the quick TUV model (http://cprm.acom.ucar.edu/Models/TUV/Interactive_TUV/). Solar and UV radiation data from the sites were compared to the quick TUV data output on days that were shown to be cloud free and correction factors were calculated and applied.

The input for ozone column was determined from measurements from polar-orbiting spectroradiameter instruments: Total Ozone Mapping Spectrometer aboard Earth Probe (Jan. 2000-Oct. 2004) (McPeters et al., 1998), Ozone Monitoring Instrument aboard EOS-Aura (Oct. 2004-Jan. 2012) (Levelt et al., 2006), and Ozone Mapping and Profiling Suite (OMPs) aboard Suomi NPP (Jan. 2012-Dec.2014) (Dittman et al., 2002;Flynn et al., 2014b; Seftor et al., 2014; Wu et al., 2014).

Explicit	Alkanes	Alkenes	Aromatics
Ethane	N-butane	Propene	m/p xylene
Propane	Isobutane	Trans-2-butene	Toluene
Ethene	N-pentane	Cis-2-butene	Ethylbenzenes
Benzene	Isopentane	1,3-Butadiene	1,3,5-trimethylbenzene
Isoprene	N-hexane	1-pentene	1,2,4-trimethylbenzene
Acetone#	N-heptane	Trans-2-pentene	1,2,3-trimethylbenzene
	N-octane	Cis-2-pentene	N-propylbenzene
	N-nonane	1-butene	Isopropylbenzene
	N-decane	cyclopentene*	Styrene
	2,2-dimethylbutane	3-methyl-1-	a-pinene*
	2,4-dimethylpentane	butene*	o-xylene*
	3-methylhexane	2-methyl-1-	2-ethyltoluene@
	2,2,4-	butene@	3-ethyltoluene@
	trimethylpentane	2-methyl-2-	4-ethyltoluene@
	3-methylheptane	butene*	d-limonene#
	2-methylhexane		
	2,3-dimethylpentane		
	2-methylheptane^		
	Cyclopentane		
	Cyclohexane		
	Methylcyclohexane		
	Methylcyclopentane		
	2-methylpentane*		
	3-methylpentane@		
	3-dimethylbutane@		
	3-methylhexane*		

*Table 4-1: Hydrocarbon Lumping for LaRC. The suite of the speciated hydrocarbons differed between the TCEQ continuous monitoring sites and the aircraft missions. Those with symbols only occurred within the marked datasets: ^TCEQ and TexAQS 2000, #TexAQS 2000, @TexAQS 2006, *TexAQS 2000 and 2006*

4.2.3 SPATIAL ANALYIS DATA

Data from NOAA Electra during TexAQS 2000 and the NOAA WP-3D during TexAQS II/GoMACCS 2006 were used as input into the LaRC model described in section 4.2.1. Information about data used from the aircraft can be found in Parrish et al. (2009),

Ryerson et al. (2003), and Zhou et al. (2014). As this data was research grade with lower detection limits, higher sensitivity, and lower uncertainties, it was used to verify the trends found from the long-term data results in the Houston Ship Channel. This data was primarily used to assess how photochemistry changed spatially through the rural, urban, and Ship Channel regions of the HGB area.

Whole Air Sample (WAS) cans were collected aboard the flights for hydrocarbon analysis. O_3, CO, NO, NO_2, and jNO_2 data were averaged over the time of the WAS samples for coincident measurements. All data for analysis were only considered during the daytime hours while flying below 1 km, although most measurements were taken at ~500m.

Between 2006 and 2014, there were no aircraft measurements available with the minimum inputs required for the LaRC model. However, to extrapolate the urban region temporal coverage, data from Moody Tower 2010 (Flynn, 2013) and DISCOVER-AQ Texas 2013 (https://www.nasa.gov/mission_pages/discover-aq/) at Moody Tower (Figure 4-1) were used in the LaRC model and showed how urban photochemical characteristics changed since the TexAQS campaigns. Data from Study of Houston Atmospheric Radical Precursors (SHARP) 2009 (Flynn, 2013; Ren et al., 2013) was not included in this analysis as it was during the spring season instead of late-summer and fall like the rest of the spatial analysis data.

4.3 RESULTS

Emissions occur daily, but only days with suitable meteorology (strong sunlight and light winds) will produce elevated levels of ozone in this region. For this analysis, the data were broken up into five-year increments (2000-2004, 2005-2009, 2010-2014). Data from the top 5% maximum daily average 8-hr (MDA8) ozone days for each five-year increment were considered for this analysis. These results showed what happened photochemically when meteorological conditions allowed for the production of ozone from 2000-2014.

Efficient ozone producing days typically ranged from the spring until fall following the strength of sunlight due to the decreased solar zenith angles. The bi-modal shape of the data distribution by month (Figure 4-3) shows how weather systems played a role for when most ozone events occurred. In the summer months, frontal systems typically did not make it far enough south to push through the city and onshore flow dominated the flow patterns. However, when fronts pushed through the area, post-frontal conditions often coincided with light winds out of the north. These conditions lead to stagnation events where pollution built up over the Houston region, encouraging the photochemical production of ozone (Lefer et al., 2010). This was further complicated and enhanced by the sea/bay-breeze circulation (Banta et al., 2005).

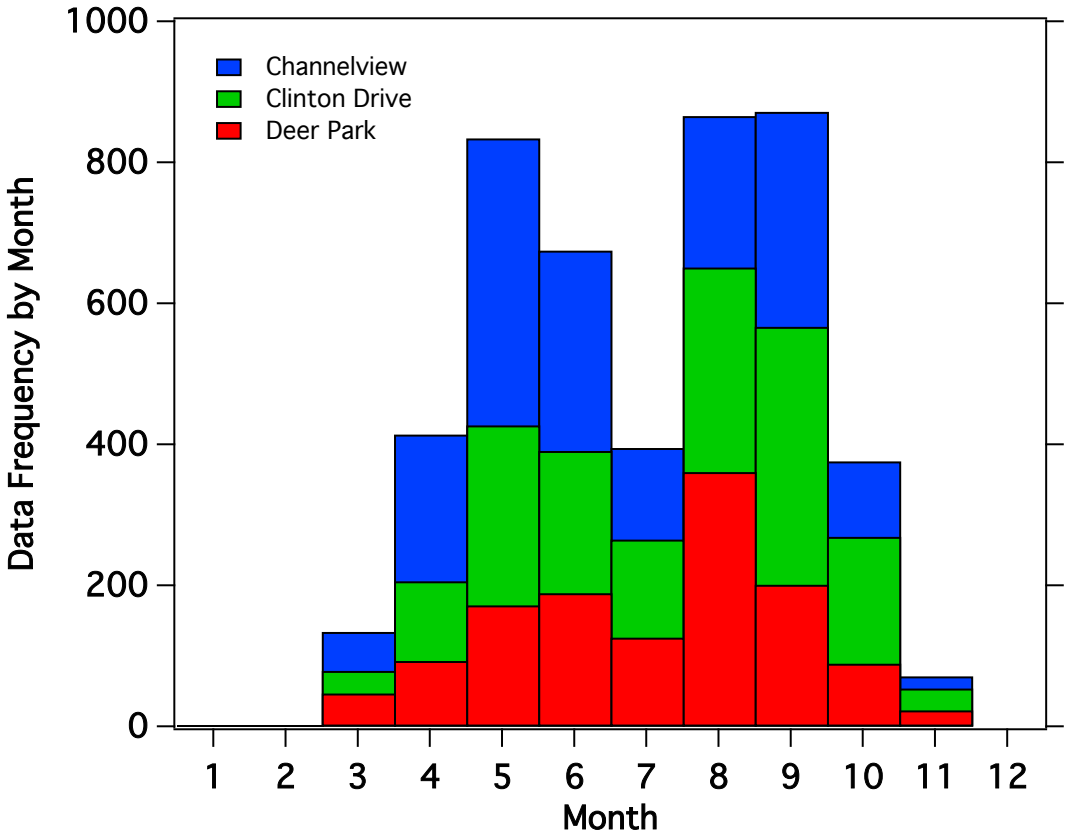

Figure 4-3: Histogram of the top 5% ozone-polluted day data points by month colored by location.

Analyzing the top 5% ozone-polluted days instead of days exceeding the NAAQS 8-hr standard of 75 ppbv was an attempt to evaluate the same volume of data over time. However, the amount of data was at a minimum in the first five years of monitoring and increased through time. Subsequent figures in this analysis used the same data points from the top 5% ozone-polluted days for all diurnal profiles and box plot distributions. The temporal distribution of these data points is shown in Figure 4-4. As the model was only executed for time steps in which all parameters had valid data, the amount of data for investigating diurnal patterns coinciding with the top 5% ozone-

polluted days increased through the years due to more efficient monitoring strategies. The least robust dataset was from Deer Park during 2000-2004, leading to less clear diurnal patterns at that time. For box plot distribution graphs by year, the number of points correlated to the severity of ozone pollution that year (Figure 1-1 and Figure 4-4).

Figure 4-5 is similar to Figure 4-2; however, it only included data from monitoring data during the top 5% ozone-polluted days in this analysis. NOx concentrations had not decreased as much over time on polluted days, and Clinton Drive saw increased NOx after 2006. Alkanes and alkenes still decreased over the years on polluted days, but the magnitude is less than all days due to the data in Figure 4-5 only including daytime data. Often, concentrations of NOx and hydrocarbons can accumulate at night due to the shallow boundary layer and lack of photochemistry. The severity of ozone has decreased over time, with MDA 8-hr ozone averaging between 90-100 ppbv at the turn of the century, and it decreased to ~70 ppbv in 2014.

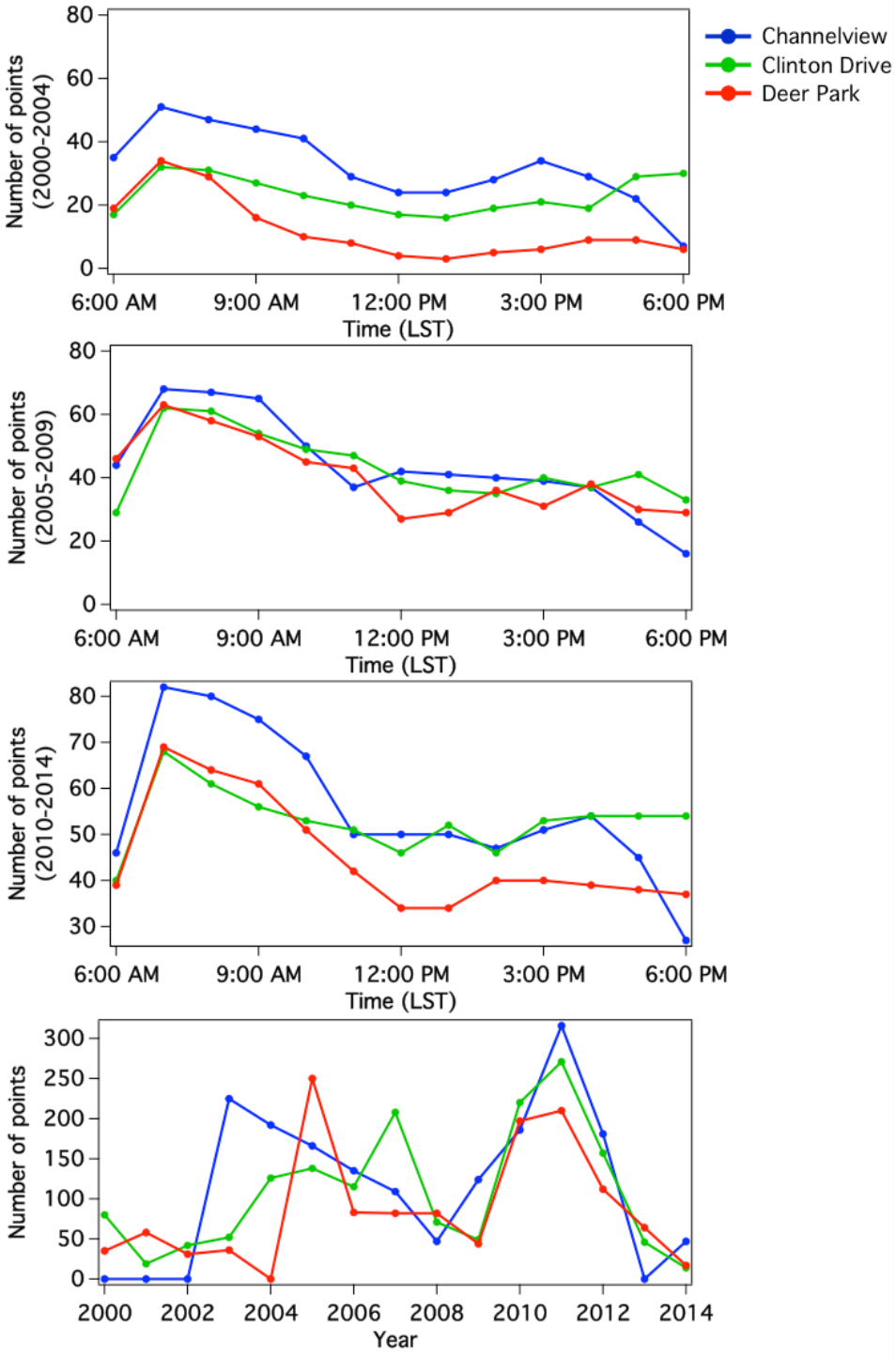

Figure 4-4: Number of data points per hour for each of the subsequent diurnal profiles 2000-2004, 2005-2009, and 2010-2014 and the number points per year in each of the following Ship Channel box plots for Channelview (blue), Clinton Drive (green), and Deer Park (red) on the top 5% ozone-polluted days.

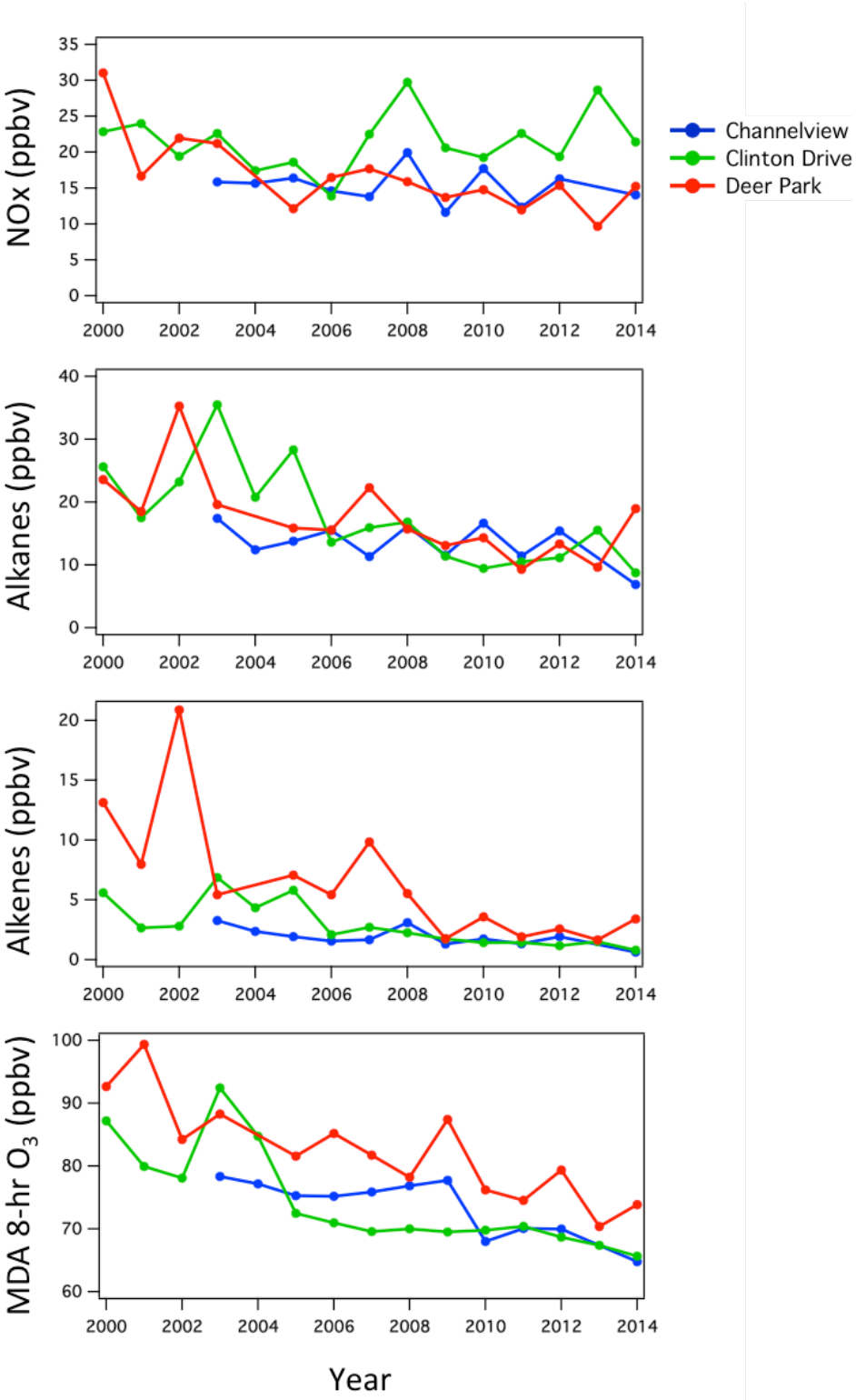

Figure 4-5: Average concentrations of NOx, alkanes, and alkenes and the maximum daily average (MDA) 8-hr ozone during the top 5% ozone-polluted days analyzed in this study at the three long-term monitoring.

4.3.1 OZONE PRODUCTION TRENDS

The number of ozone exceedances and the average concentration of ozone precursors have decreased since 2000 in the Houston Ship Channel (Figure 1-1, Figure 4-2, and Figure 4-5). Therefore, it was unsurprising that the median magnitude of net ozone production rates diurnally had also decreased at all three Ship Channel sites (Figure 4-6 top). The range of net ozone production rates had also decreased, with fewer occurrences of extreme production rates above 100 ppbv/hr (Figure 4-6 bottom). The largest decreases occurred at Deer Park, where the median diurnal peak for 2010-2014 was half of what it was in the early 2000s. Deer Park also had a different diurnal profile shape in comparison to Channelview and Clinton Drive. The peak in ozone production occurred near solar noon at Clinton Drive and Channelview. This suggested that sunlight was a limiting factor for ozone production throughout the day. However, Deer Park's peak in the mid-morning was typical for a strong emission source site, where peak production was a balance between the precursor concentrations (peaking in the morning due to rush hour and a shallow boundary layer trapping emissions throughout the night) and the increasing strength of the sunlight throughout the morning. At Moody Tower, near downtown Houston, ozone production has been shown to also peak near noon in previous studies from research campaigns (Flynn, 2013; Ren et al., 2013).

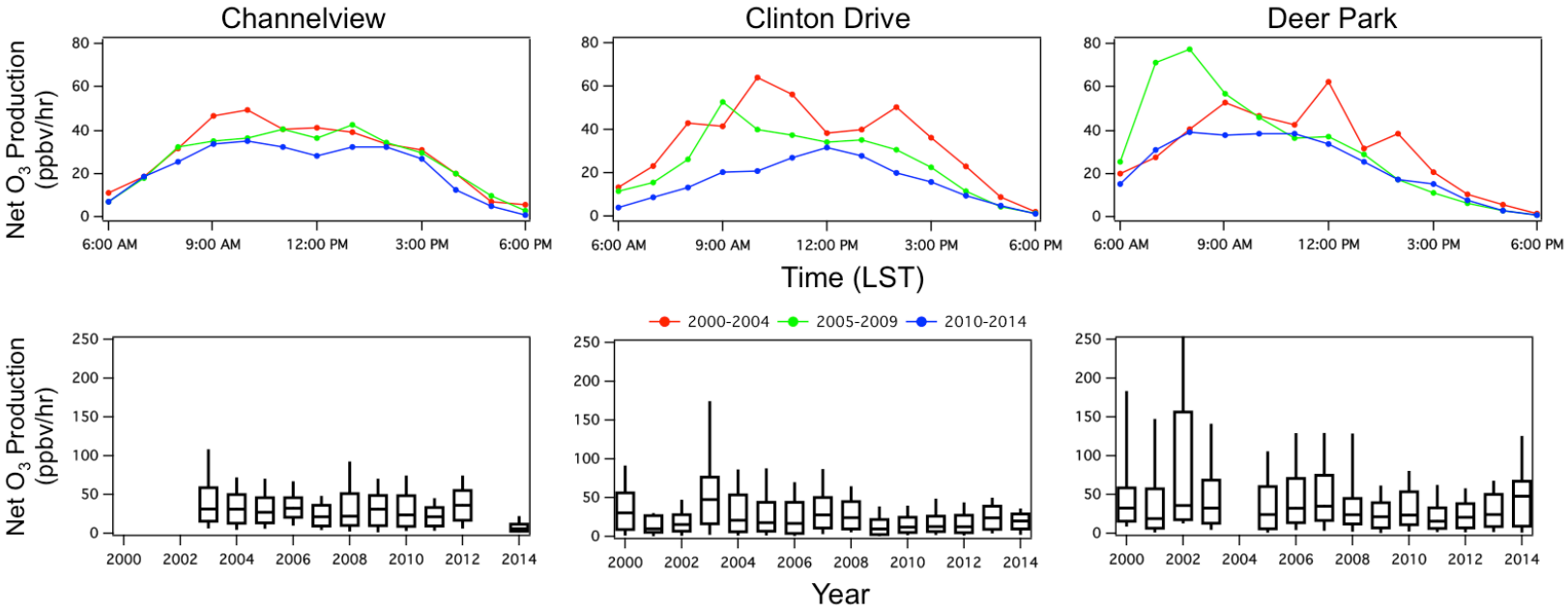

Figure 4-6: Median diurnal profiles of net ozone production rates (top), box plots of net ozone production rates data for each year (bottom) for each Ship Channel site. Number of points incorporated into the diurnal profile average and the box plots are found in Figure 4-4.

The relative contribution of ozone formation reactions to the total had not changed much between 2000-2014 (Figure 4-7), but the absolute magnitude of ozone production rates decreased through time. At Clinton Drive, peak ozone production has dropped from ~ 70 ppbv/hr to less than 40 ppbv/hr, and at Deer Park it has dropped from ~ 80 ppbv/hr to 40 ppbv/hr (Figure 4-6). Reductions at Channelview were less pronounced. The model results showed that most of the Ship Channel's ozone formation (~45-50%) was from the reaction between HO_2 and NO to produce NO_2. The reaction with CH_3O_2 made up the next 15%, and the remainder of formation was due to the larger peroxy radicals. This percent contribution had not changed much through time, was consistent between all three sites, and showed little diurnal variation (Figure 4-7). These components were similar to ozone formation at Moody Tower (Flynn, 2013).

The destruction components for ozone had a much more interesting diurnal profile. The primary ozone destructor for all sites was the loss of NOx to HNO_3. Ozone destruction increased with a solar zenith angle centered near solar noon, which influenced the rate of OH production. This was correlated to the increase in the reaction rate of $O^1D + H_2O$, where the source of O^1D came from the photodissociation of O_3. In percent contribution, the formation of HNO_3 was at a maximum in the morning with the excess NOx from rush hour and decreased throughout the day (Figure 4-7). The rest of the components were ozone reactions and were small in absolute magnitude, but became a larger percent component as the day went on, as they were correlated with the increased ozone concentrations in the late-afternoon hours.

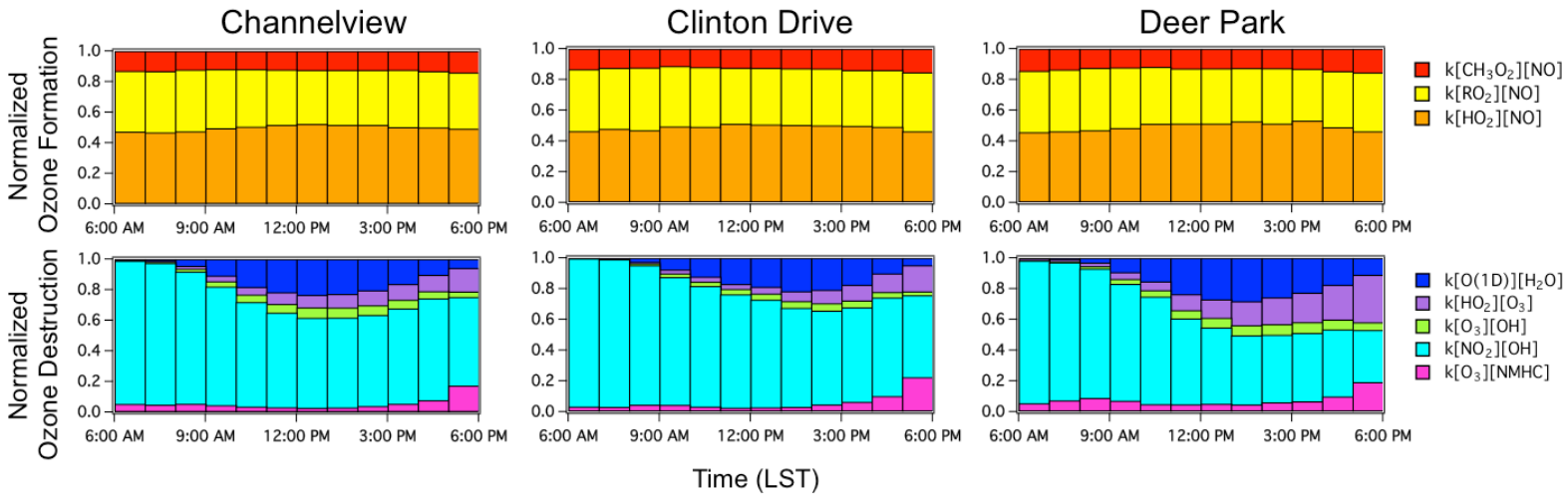

Figure 4-7: Normalized median diurnal profile of the components of ozone formation (top) and destruction (bottom) during all years for the three Ship Channel sites. Number of points incorporated into the diurnal profile average is found in Figure 4-4.

4.3.2 HYDROCARBON REACTIVITY

As some hydrocarbons species are more reactive than others, a measure of hydrocarbon reactivity with respect to OH was used to determine the most important contributors to Houston's ozone problem. Reactivity was defined similar to Steiner et al. (2008) and Flynn (2013):

$$R_{VOC+OH} = k_{OH+ethane}[ethane] + k_{OH+propane}[propane] + k_{OH+alkanes}[alkanes] + k_{OH+ethene}[ethene] + k_{OH+alkenes}[alkenes] + k_{OH+isoprene}[isoprene] + k_{OH+benzene}[benzene] + k_{OH+aromatics}[aromatics] + k_{OH+formaldehyde}[formaldehyde] \quad \textit{(Eq. 4.1)}$$

Deer Park was the site most influenced by reactive hydrocarbon sources (Figure 4-8). This site also saw the largest hydrocarbon reactivity decrease, markedly from the 2005-2009 subset to 2010-2014 subset. Clinton Drive was the next most polluted with respect to hydrocarbon reactivity, followed by Channelview. All sites showed maximum hydrocarbon reactivity in the morning, due to the encouragement of emission buildup under a shallow and stable nocturnal boundary layer before the mid-morning boundary layer growth and increase in photochemistry. Clinton Drive and Channelview had a secondary maximum later in the afternoon, most likely correlating to influences from rush-hour traffic. In the late afternoon, Deer Park was downwind of Galveston Bay and was less influenced from the surrounding mobile sources.

Although the absolute magnitude of reactivity had decreased through time, the relative contributions had been mostly consistent. The two biggest components included alkenes and formaldehyde. In the vicinity of the Ship Channel, past studied

showed that most of the formaldehyde (> 90%) was secondarily produced from highly reactivity VOCs (HRVOCs) emitted from the petrochemical industry (Parrish et al., 2012). In Harris country, HRVOCs are defined as ethene, propene, butenes, and 1,3-butadiene (Title 30, Texas Administrative Code, Chapter 115).

Research from intensive air quality measurement campaigns had also attributed alkenes and formaldehyde as the largest contributors to ozone production (Daum et al, 2003; Parrish, et al. 2012). As a result, the State Implementation Plan for meeting the NAAQS ozone standard includes a rule for controlling HRVOC emissions (30 Texas Administration Code, Chapter 115). This rule was first adopted in 2004 and involved reducing HRVOC emissions and additional monitoring in the area. Unfortunately, formaldehyde was not measured at the monitoring sites and may have been overestimated by this model. These results strongly suggest benefits from monitoring formaldehyde for future photochemical modeling studies to quantify the contribution of formaldehyde to ozone production in the Ship Channel.

Other components of hydrocarbon reactivity included approximately 10% from alkanes, another 10% from aromatics (excluding isoprene) at all sites. The contribution from isoprene differed between the three sites, with a maximum contribution at Channelview. Isoprene at Channelview had decreased since 2000, suggesting a close industrial source as opposed to changes in biogenic activity.

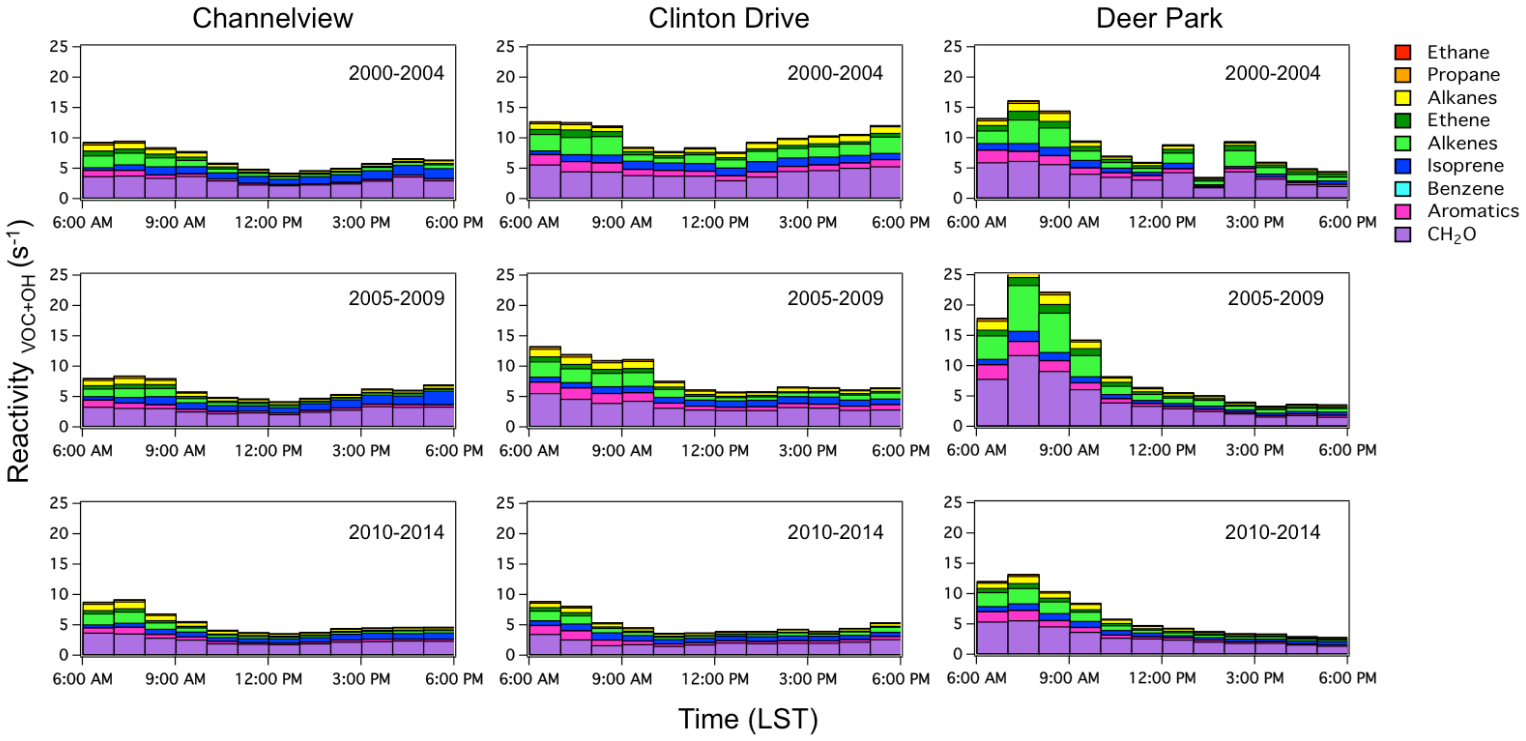

Figure 4-8: Median diurnal profile of the components of reactivity for each five-year increment for the top 5% ozone-polluted days at three Ship Channel sites. Number of points incorporated into the diurnal profile average is found in Figure 4-4.

4.3.3 NOx/VOC SENSITIVITY

In the presence of strong sunlight, O_3 production is limited by the emissions of either NOx or peroxy radicals produced from VOCs. From a policy standpoint, addressing whether an environment is NOx or VOC-sensitive is an important step to addressing what is limiting the ozone production and the quickest way to improve air quality with respect to ozone. Urban areas lacking significant VOC sources from industry are often in excess of NOx and are VOC-sensitive throughout the entire day. In TexAQS 2000, urban Houston was shown to be VOC-sensitive in the urban region due to excess NOx and the lack of strong VOC sources, however the Ship Channel was more complicated due to the complexity of both NOx and VOC sources (Daum et al., 2003). In studies from 2006 and 2009, Moody Tower showed a VOC-sensitive environment in the morning, however it often transitioned to a borderline NOx-sensitive environment later in the afternoon (the degree to which was dependent on whether it was a high or low ozone producing day) (Ren et al., 2013). The same pattern showed up in Mexico City in 2003 (Mao et al., 2010).

The top three graphs in Figure 4-9 show that the fastest ozone production rates occurred over large ranges of NOx concentrations and hydrocarbon reactivity. However, if hydrocarbon reactivity decreased to less than 10 s^{-1}, ozone production rates decreased quickly. This suggests that the area was relatively VOC-sensitive on the top 5% ozone-polluted days.

To quantify the NOx/VOC sensitivity regime, a ratio of Ln/Q quantified an environment as NOx or VOC-sensitive, where Ln was calculated as the loss rate of radicals to produce NOz (NOy-NOx) in the system, and Q was free radical production, (Kleinman et al., 2005). Neuman et al. (2009) demonstrated that HNO_3 and PAN in Houston was the bulk of the reactive nitrogen reservoir (NOz), with only a few percent made up by alkyl nitrates. In this study, Ln = R4.4 + (R4.5-R4.6) and Q = 2*(R4.1) + 2*(R4.2) + (R4.3).

Radical Production

(R4.1) $O(^1D) + H_2O \rightarrow 2OH$

(R4.2) $CH_2O + h\nu \rightarrow 2HO_2$

(R4.3) Alkenes + $O_3 \rightarrow$ Radicals

Net NOz Production

(R4.4) $NO_2 + OH \rightarrow HNO_3$

(R4.5) $RCO_3 + NO_2 \rightarrow PAN$

(R4.6) $PAN \rightarrow RCO_3 + NO_2$

If Ln/Q is above 0.5, the environment is NOx-saturated/VOC-sensitive, as the environment is losing more radicals to the production of HNO_3 and PAN. If Ln/Q is less than 0.5, the environment is limited by the amount of NOx in the system (Kleinman et al., 2005, Mao et al., 2010; Ren et al., 2013).

The bottom of Figure 4-9 shows how Ln/Q varied as a function of NOx and hydrocarbon reactivity for all days over the 15-year period (polluted and unpolluted). Ln/Q is largely determined by the ratio of NOx and reactivity. The black dots in Figure 4-9 indicate the position of the data during the top 5% ozone-polluted days. The bulk of the points were located in a VOC-sensitive regime with Ln/Q values mostly at or above

1. This indicates that the region of the Ship Channel had excess NOx and the ozone production was limited by VOCs on the most ozone-polluted days.

Although Figure 4-10 demonstrates that the Ship Channel was VOC-sensitive when the area was producing high levels of ozone, the magnitude of VOC sensitivity had changed over the last 15 years and varied by site. Channelview and Clinton Drive had transitioned from a mix of VOC and NOx-sensitivity, to a completely VOC-sensitive regime on the most ozone-polluted days, with the strongest transition from 2006-2008 at Clinton Drive. Out of the three sites, Clinton Drive was the most NOx-polluted due to its proximity to the 610 freeway and being located on a heavily used road for trucks entering and leaving the Ship Channel. After 2006, its NOx concentrations increased. The strong transition at Clinton Drive was influenced by the increase in NOx and the decrease in hydrocarbon reactivity both working to increase its VOC-sensitivity. Deer Park's regime had changed the least out of the three sites, but the occurrences of Ln/Q below 0.5 disappeared through time on the top 5% ozone-polluted days. Deer Park's lower Ln/Q, in comparison to the other sites, coincided with the greater VOC emissions in the area.

These results along with the study on reactivity components suggest the importance in further addressing HRVOC emissions and formation of formaldehyde as a plan to further reduce the severity and number of ozone events through time in the Houston Ship Channel.

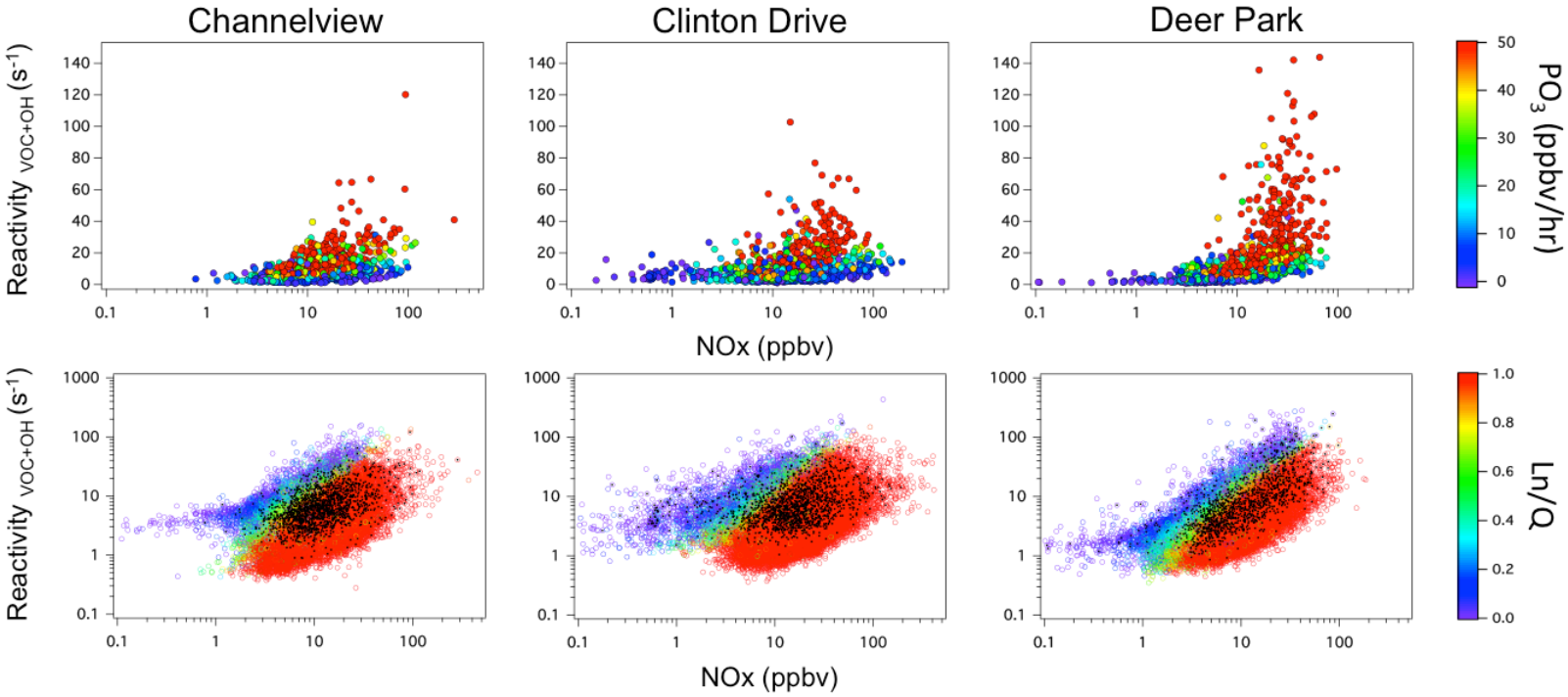

Figure 4-9: Hydrocarbon Reactivity (s^{-1}) vs. NOx (ppbv) for the three sites colored by net ozone production on polluted days (top) and Ln/Q on the bottom for all days (bottom). The black dots indicate the location of the data on the top 5% ozone-polluted days.

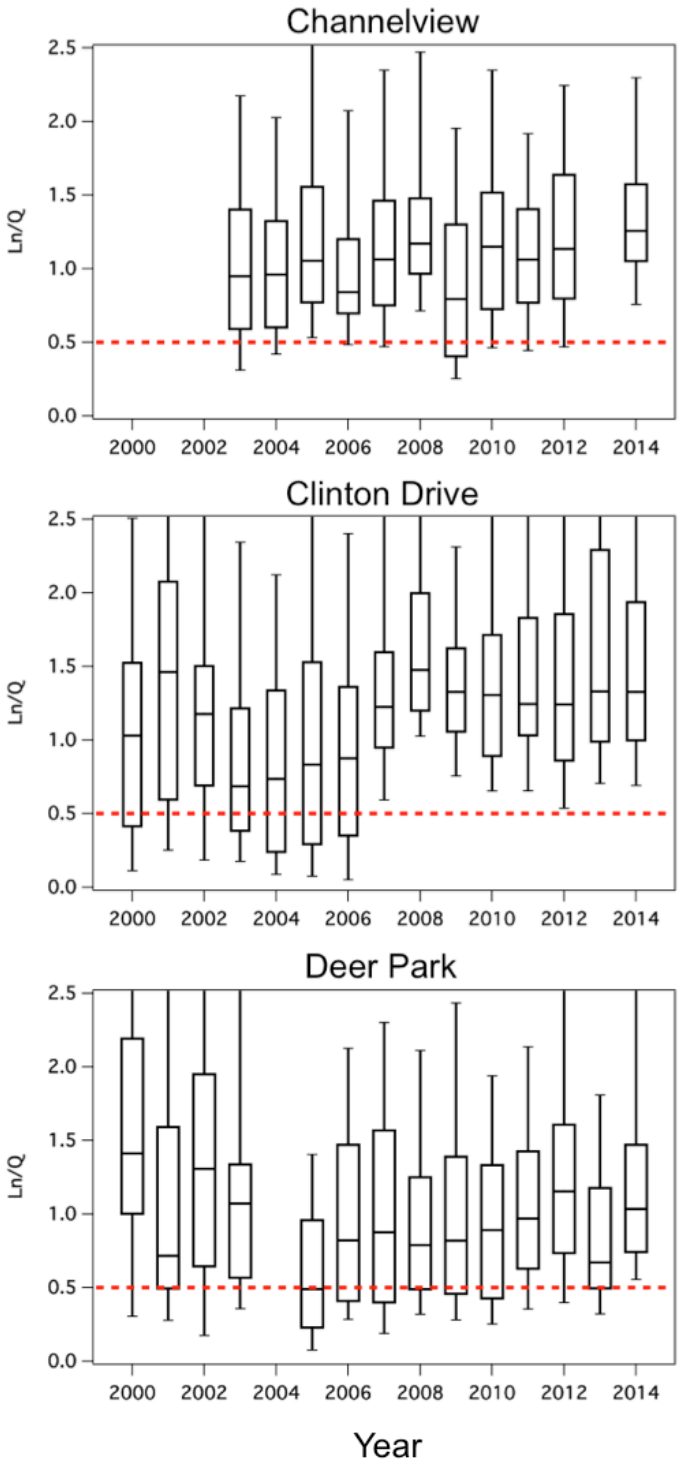

Figure 4-10: Box plots demonstrating the distribution of Ln/Q for the data points on the top 5% ozone-polluted days for the three monitoring sites. The dashed red line indicates the transition from NOx to VOC-sensitive regimes. Number of points incorporated into the box plot distribution is found in Figure 4-4.

4.3.4 OZONE PRODUCTION EFFICIENCY

Ozone production efficiency (OPE) is defined as the number of ozone molecules made per NOx consumed to NOz. In Houston, OPE changes radically depending on the environment. The petrochemical plumes in the Ship Channel have a substantially higher OPE than the urban environments due to the abundance of highly reactive VOCs boosting ozone production (Ryerson et al., 2003). Typically, OPE is quantified by plotting Ox ($O_3 + NO_2$) vs. NOz. Out of the three long-term sites, only Deer Park had NOy data available for the NOz calculation. Data from 9 am - 3 pm on the top 5% ozone-polluted days were considered for the OPE analysis to ensure active photochemistry. Data was also filtered for stagnant winds (below 2 mph).

When considering all wind quadrants, Deer Park showed an OPE of 4.7 ± 0.4 over the last 15 years ($r^2 = 0.17$). The correlation value of this relationship was low, which was likely due the large uncertainty in the monitoring site measurements at this pollution scale, as well as the complexity of OPE from varying sources. To investigate further, the data was subset by wind quadrant (Figure 4-11). The highest OPE values were in the northeast quadrant (OPE = 7.43 ± 0.91; $r^2 = 0.32$), which was the source region with the most photochemical facilities in relation to the monitoring site. The western two quadrants showed very low correlation values for the Ox vs. NOz relationship. The most prominent wind quadrant was from the Gulf of Mexico and Galveston Bay, which included a clean marine background with industrial and ship sources picked up along the way. This region showed an OPE of 4.81 ± 0.53 ($r^2 = 0.23$). The correlation is further

improved in the subset for the dominating wind direction lobe from 115-135° ($r^2 = 0.30$). However, OPE from this subset quadrant was unchanged. Although there was much scatter in this dataset, similar values of OPE were measured at a nearby site in La Porte during TexAQS 2000 with OPE = 4.7 ($r^2 = 0.76$) from samples between August 19th and September 14th (Jiang et al., 2003). All of these values were found to be lower than the OPE calculated from aircraft data from Ryerson et al. (2003) within petrochemical plumes. However, at a stationary site, not all measurements are going to be within pure plumes from one source, but rather a mixing of sources over the study period.

With the LaRC model, instantaneous net ozone production efficiency (IOPE) was calculated and analyzed for all three sites (Kleinman et al., 2002).

$$IOPE = \frac{PO_3}{PNOz} \qquad (Eq.\ 4.2)$$

PNOz was assumed to be the same as Ln in the Ln/Q calculation. IOPE demonstrates how efficiently ozone is produced at a snapshot in time.

IOPE depended on source region at the three sites (Figure 4-12). All three sites showed the dominance of the bay/sea breeze with large lobes to the southeast on the most ozone-polluted days in the region. The source regions with the highest IOPE occurred differently between the three sites. In Channelview, the highest IOPE appeared during a northerly wind. Although this wind quadrant did not occur frequently, it indicated influence of ethene emissions from a plant to the immediate northeast of the monitoring site. Most the data at these sites were in the IOPE range of

10-20. Clinton had large calculations of IOPE from its easterly quadrant, with values exceeding 50 at times. As Clinton Drive was located on the western side of the Ship Channel, this shows how the industrial emissions were more efficient at producing ozone than urban emissions to the west. When winds were out of the north at Deer Park, IOPE was never below 10, with the largest peak from the northeast toward petrochemical facilities.

Kleinman et al. (2005) demonstrated how IOPE increases as NOx decreases; however, Figure 4-13 demonstrates the importance of hydrocarbons in addition to NOx concentrations in the study of IOPE. IOPE not only increased at decreasing NOx, in general, as hydrocarbon reactivity increased, IOPE also increased. As indicated in Figure 4-5, the amount of NOx on the top 5% of ozone-polluted days had not changed much in the Houston Ship Channel, and had even increased at Clinton Drive; therefore decreased hydrocarbon reactivity was expected to decrease the values of IOPE through time. This is shown in Figure 4-14 as a decrease in the magnitude and range of IOPE at Clinton Drive and Deer Park. This decrease was most pronounced at Clinton Drive, which was the region with large IOPE in its eastern quadrant occurring prior to 2006. Prior to this time, the 95th percentile of IOPE was calculated above 80 at Clinton Drive. After 2006, there was an increase in NOx concentrations and a decrease in VOCs that worked together to decrease IOPE at the site. The decrease at Deer Park was more gradual than Clinton Drive, as Deer Park had a decline in NOx concentrations and hydrocarbon reactivity, which worked to offset each other's influence on IOPE. Channelview had the

weakest decline of them all. Reducing IOPE is a delicate balance between NOx and hydrocarbon emission reductions. Reducing NOx may worsen ozone in the future by increasing the efficiency of ozone production; therefore it is crucial to decrease VOCs to make an impact on ozone productions rates and efficiency in the Houston Ship Channel.

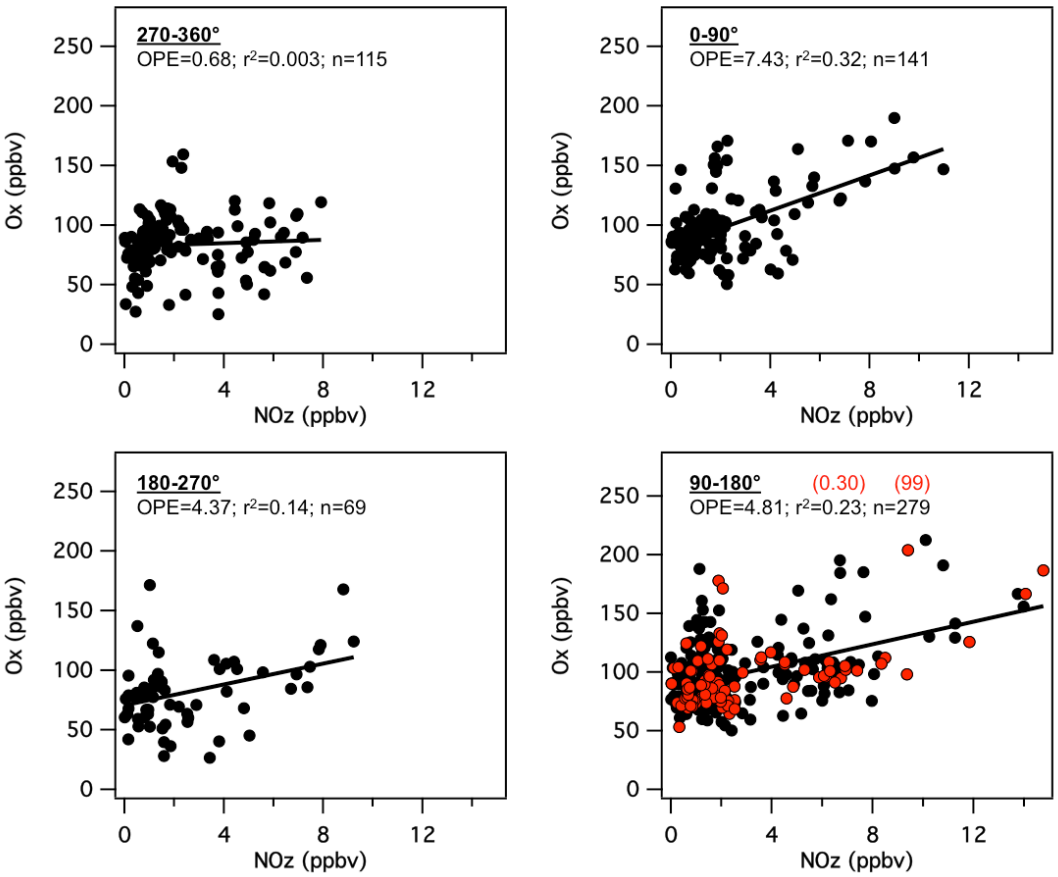

Figure 4-11: In situ measured Ox (O_3 + NO_2) vs. NOz (NOy-NOx) by wind quadrant at Deer Park for the 5% ozone-polluted days during all years of the study from 9 am – 3 pm. The linear best-fit exhibits OPE. The red data depict the points in the most common wind quadrant from 115-135°.

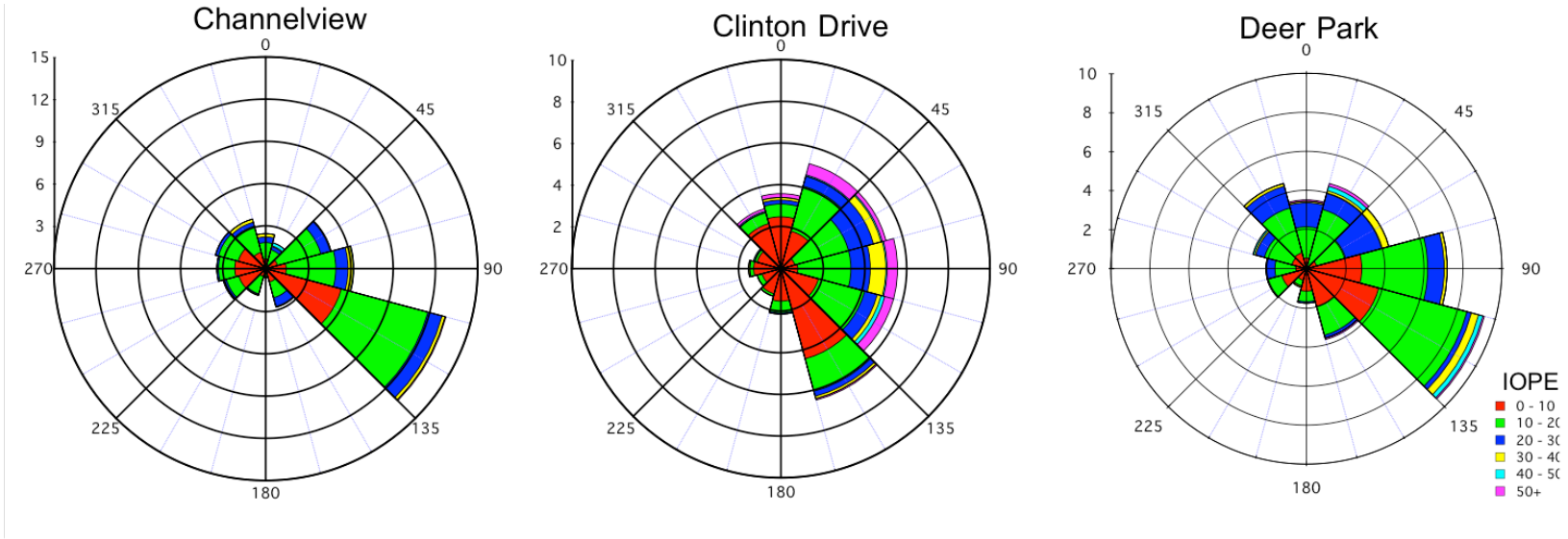

Figure 4-12: Wind roses at the three Ship Channel sites showing the range of IOPE by wind quadrant. This data is only for polluted days with wind above 2mi/hr to exclude stagnation.

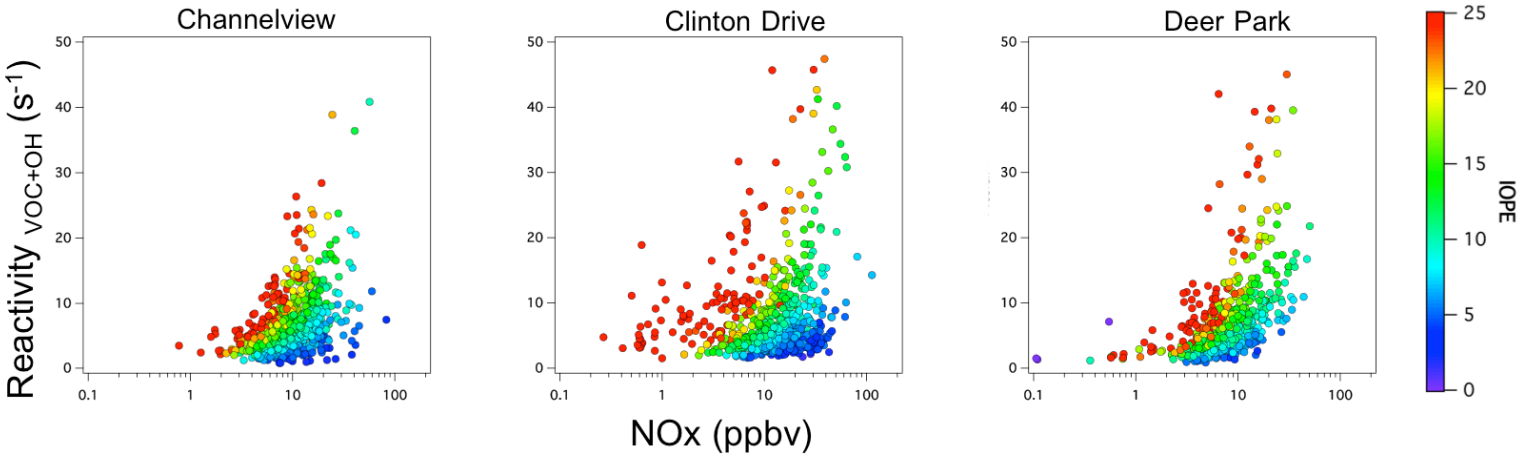

Figure 4-13: The relationship between NOx and hydrocarbon reactivity for the three long-term sites. Data is colored by the IOPE.

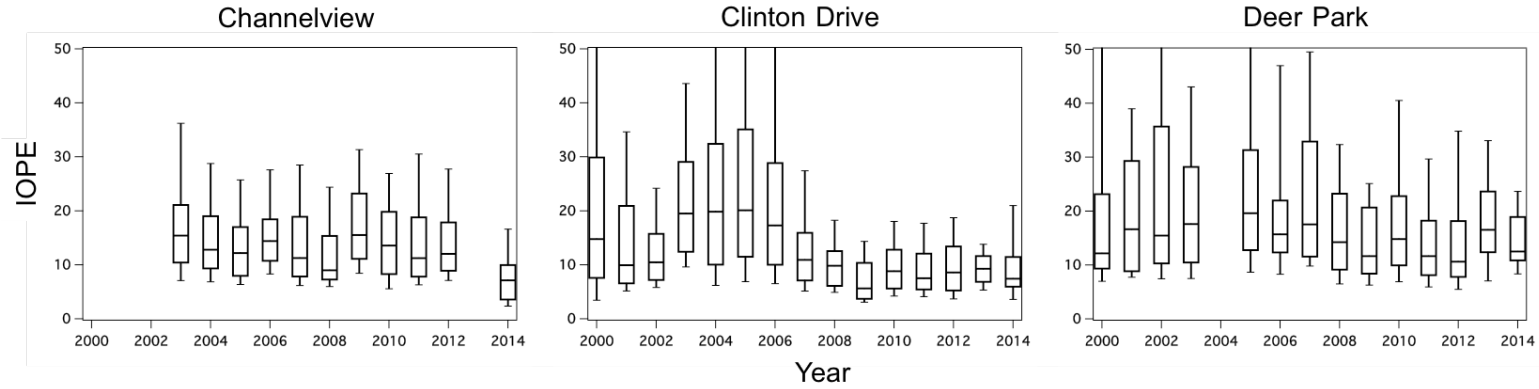

Figure 4-14: Box plot showing the distribution of IOPE modeled measurements each year for long-term monitoring sites. Number of points incorporated into the box plot distribution is found in Figure 4-4.

4.3.5 SPATIAL VARIABILITY OF OZONE PRODUCTION PARAMETERS

The spatial analysis of photochemistry in Houston was limited by the extent of hydrocarbon data available outside the Ship Channel, as there are currently no continuous auto-GC monitors outside this region. During TexAQS 2000 and TexAQS II/GoMACCS 2006, the NOAA Electra and WP-3D aircrafts measured both hydrocarbons and other required data for photochemical modeling over the spatial extent of Houston. Although the NASA P-3B flew during DISCOVER-AQ in 2013 over the same region, the lack of speciated hydrocarbon data limited the study of the characteristics discussed in this chapter.

The spatial analysis in this study was limited to days where the aircraft flew and the NAAQS ozone 8-hr standard was exceeded. Aircraft samples were taken around 500 m for many of the areal transects, but a 1 km threshold was applied for this analysis. During TexAQS 2000, the NOAA Electra flew during eight ozone-exceedance days. On these days, monitors exceeded 100 ppbv throughout the city. Many of these 100+ ppbv concentrations were located near the Ship Channel, including Deer Park, La Porte, Baytown, and others. Approximately 200 data samples were included in this analysis.

During the TexAQS II/GoMACCS 2006 campaign, the NOAA WP-3D flew during seven ozone-exceedance days. These days often only saw 8-hr averages of ozone ranging from 80-90 ppbv, in which the peak was at Conroe on October 6th with 97 ppbv of ozone. This campaign had more data samples than TexAQS 2000 with over 500 points included in this analysis. All data points from the aircraft ranged from the

Houston Ship Channel, urban Houston, and the rural parts of the region and occurred from 10am-6pm.

These flights also included additional constraints for the LaRC model, however, they were not consistent between the two campaigns. Even though both aircraft included HNO_3 measurements, Flynn et al. (2010) demonstrated that constraining to this parameter did not significantly influence the net ozone production rates in Houston. However, PAN and CH_2O were important to ozone production rates and not constraining to these trace-gases often lead to an overestimation in the morning with less impact during the afternoon hours (Flynn et al., 2010). However, the 2000 data included CH_2O but not PAN, and 2006 included PAN but not CH_2O. Therefore, these model runs could not be constrained similarly to each other. Luckily, most the data during these flights were during the afternoon hours where the influences of these constraints are less significant. The model was constrained the same as the long-term measurements in the Houston Ship Channel.

Figure 4-15 and Figure 4-16 map the data samples during both campaigns for NOx, O_3, PO_3, hydrocarbon reactivity, and Ln/Q. All these parameters showed hot spots over the Ship Channel and/or urban Houston region. The exception was ozone concentrations, which could have been advected downwind from where it was produced. The most striking differences between the campaigns were the decrease in reactivity over both the Ship Channel and urban Houston and the change in the

NOx/VOC sensitivity regime from borderline NOx/VOC-sensitive in 2000 to primarily VOC-sensitive in 2006 during ozone NAAQS exceedance events.

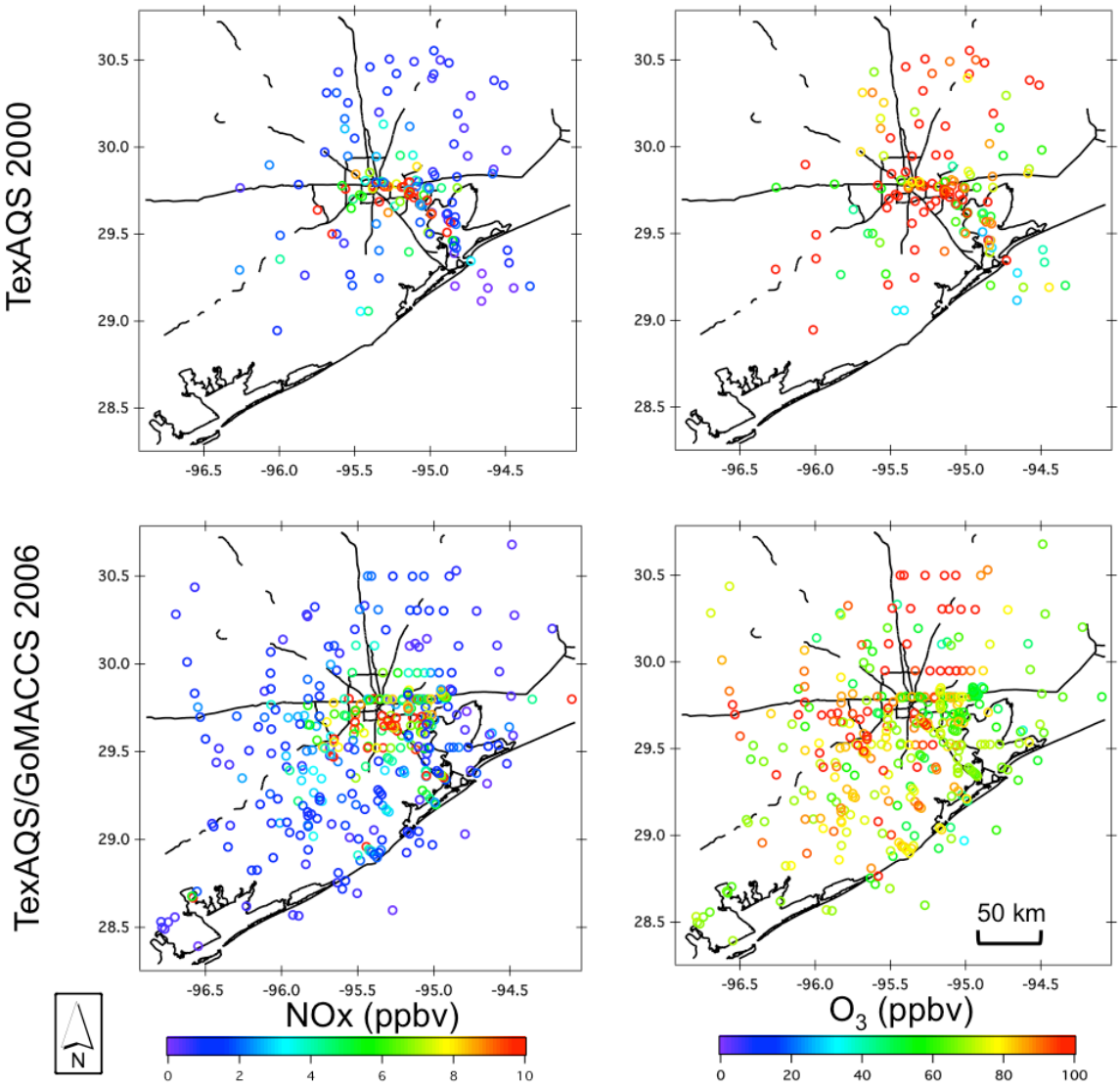

Figure 4-15: Map of the concentrations of NOx (left) and O_3 (right) during the TexAQS 2000 (top) and TexAQS II/GoMACCS 2006 (bottom).

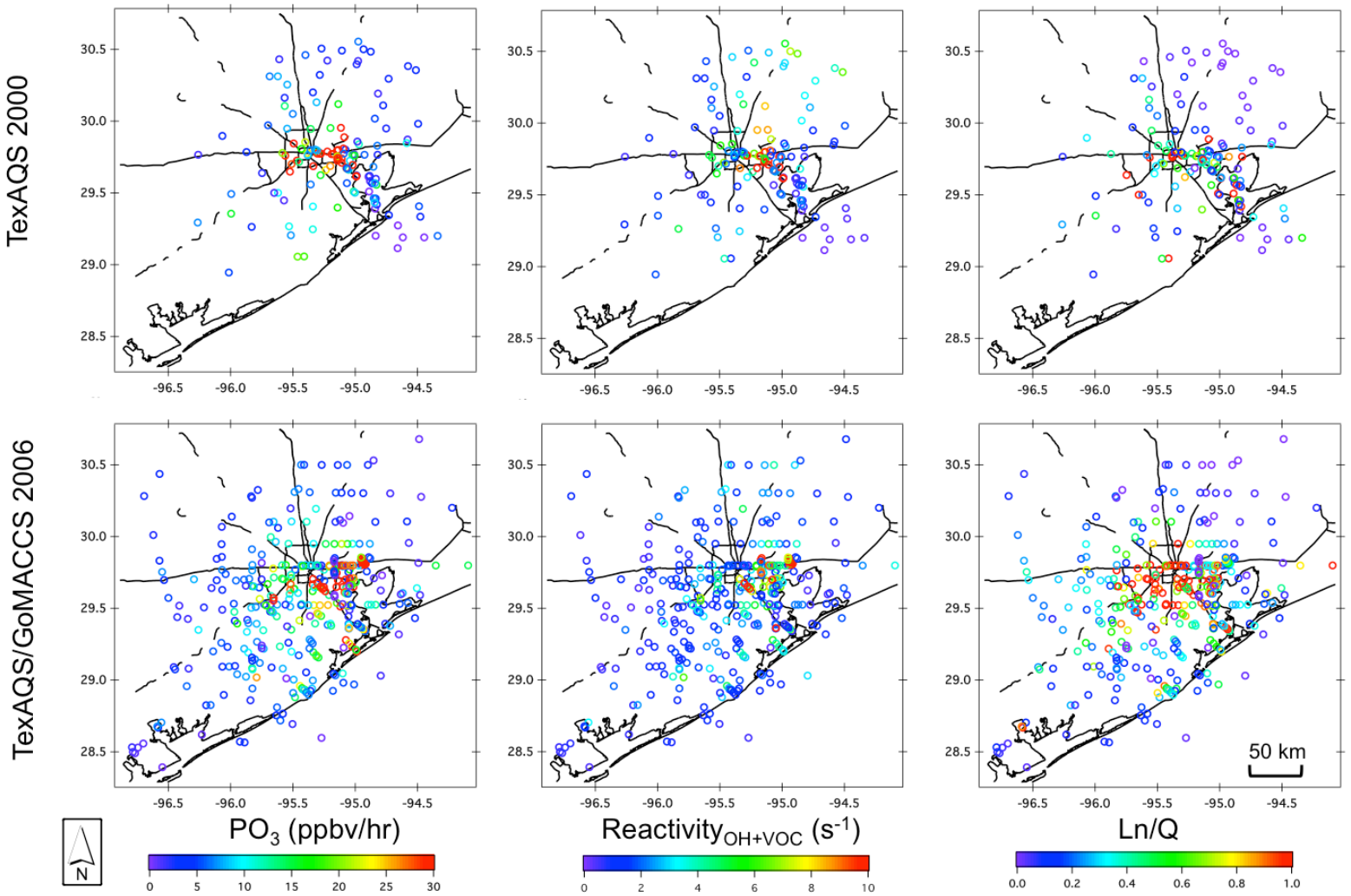

Figure 4-16: Map of net ozone production rates (left), hydrocarbon reactivity (middle), and Ln/Q (right) during the TexAQS 2000 (top) and TexAQS II/GoMACCS 2006 (bottom).

To demonstrate how photochemistry characteristics vary in different spatial environments, the data was subset by the regions as indicated by the boxes in Figure 4-17. The rural region excluded area with heavy traffic and urbanization. The box was purposely drawn to exclude marine environments, Freeport (another industrial region to the south of Houston), and Beaumont to the east. The Ship Channel region incorporated data bordering the channel to the north and east of Galveston Bay, and the urban region of Houston was in between the two other regions, and was dominated by freeways and urbanization.

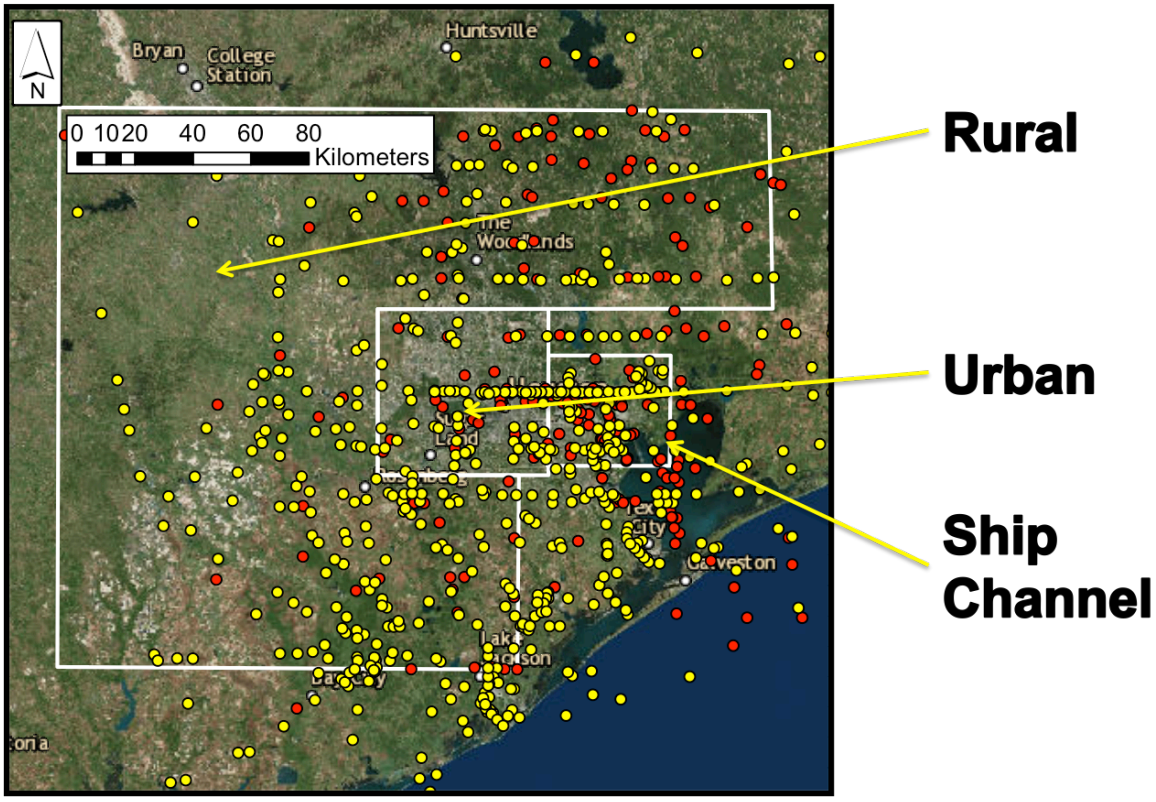

Figure 4-17: Map showing the aircraft samples from TexAQS 2000 (red) and TexAQS/GoMACCS 2006 (yellow) and the boxes used to subset the data by rural, urban, and the Ship Channel.

Figure 4-18 shows the box plot distribution of the photochemistry parameters investigated in this study for each of the region subsets. Between 2000 and 2006, the net production and concentration of ozone, hydrocarbon reactivity, and IOPE decreased for all regions. NOx decreases were not apparent between 2000-2006, demonstrating that decreases in ozone are linked to reduced hydrocarbon emissions. IOPE decreases were also tied to the decrease in hydrocarbon reactivity, which decreased the VOC/NOx ratio.

Comparing between regions, NOx, PO_3, and hydrocarbon reactivity were found to be at a minimum in the rural regions, which was expected, as there are few emission sources in rural areas. However, the rural sector still saw high levels of ozone, and was not without significant rates for ozone production or hydrocarbon reactivity. The difference between IOPE in each region can be explained by the different ratios of VOC/NOx. In the urban sector, there was comparable NOx and lower VOCs when compared the Ship Channel, which caused lower IOPE. While in the rural region, IOPEs were larger than the values in the Ship Channel. This can be linked to its low NOx concentrations, and therefore the OH needed to sink NOx to NOz often reacted with the hydrocarbons first due to the lack of NOx.

Ln/Q increased in all regions from 2000 to 2006, showing how the degree of VOC sensitivity was increasing in the urban and Ship Channel regions, rather than spanning between VOC-sensitive and NOx-sensitive at varying times. However, the rural region was in mostly a NOx-sensitive regime, as there were little NOx emissions occurring in these unpopulated areas and lower but comparable hydrocarbon reactivity to the urban

sector. This area of the city could benefit from reductions in NOx emissions. In 2000, both the urban and Ship Channel regions straddled between NOx and VOC sensitivity regimes on ozone-exceedance days. This changed by 2006, with the urban region being almost entirely VOC-sensitive, and the Ship Channel only exhibiting NOx-sensitivity ~ 25% of the time. As shown in Figure 4-10, the Ship Channel had become even more VOC-sensitive on the top 5% of ozone-polluted days after 2006. These results indicate the need for further reducing hydrocarbon emissions in the urban and Houston Ship Channel to bring the region into compliance with the NAAQS ozone standard. If NOx were decreased in Houston without reductions in VOCs, this could lead to more efficient ozone production and an increase in ozone concentrations.

In addition to the two aircraft campaigns, data from the urban region at Moody Tower (Figure 4-1) was added from measurements during ozone-exceedance events in the late summer/early fall of 2010 (18 days) and DISCOVER-AQ Texas 2013 (2 days). Ozone concentrations, net ozone production, and hydrocarbon reactivity during the two later campaigns were comparable to the 2006 measurements in the urban area. However, the NOx concentrations during high-ozone events decreased for 2010 and 2013. While Ln/Q followed the increasing trend in 2010 toward a more VOC-sensitive regime, it showed a very different range in 2013. This is likely due to the fact that DISCOVER-AQ Texas 2013 only had two days with MDA 8-hr ozone above 70 ppbv in the region (September 25th and 26th). This event was not tied to large NOx concentrations like previous events and had a larger range of hydrocarbon reactivity and higher IOPE,

leading to primarily NOx-sensitive conditions. The hot spot during this event was located in the Ship Channel with a one-hour average of ozone at La Porte peaking at over 150 ppbv and an 8-hour average of 124 ppbv, which was 24 ppbv larger than the next highest day in 2013. This suggests the possible occurrence of fugitive emissions in the area, and could be labeled an uncharacteristic event for the region.

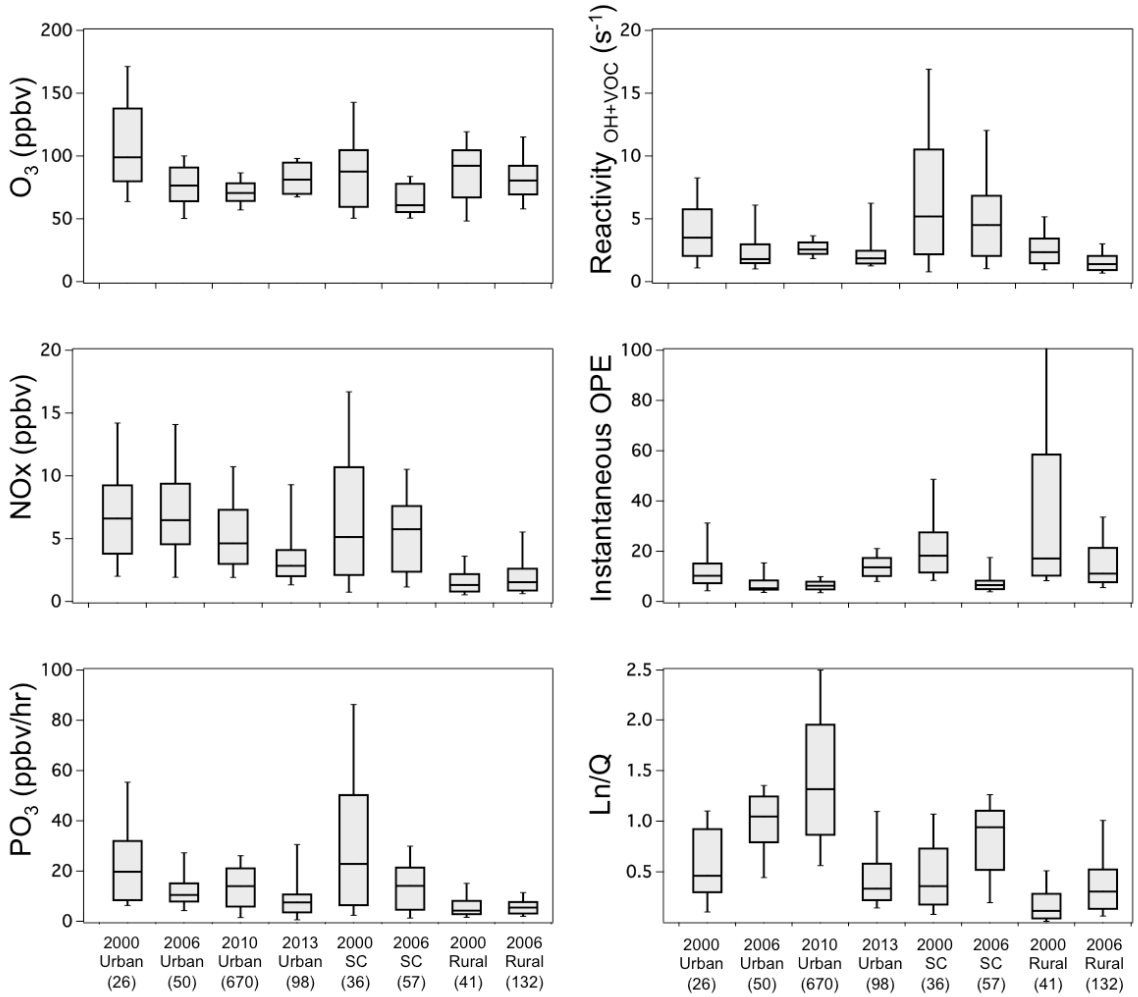

Figure 4-18: Box plots showing the distribution of data for O_3, NOx, PO_3, hydrocarbon reactivity, IOPE, and Ln/Q for the three defined regions from Figure 4-17 in 2000 and 2006 aircraft samples. Additionally, stationary measurements from Moody Tower in 2010 and 2013 were also added to the urban sector. Numbers under box plot labels indicate the number of points within the calculation of each box plot distributions.

4.4 SUMMARY

Since 2000, the annual number of ozone NAAQS exceedance days decreased from over 2 months out of the year to less than a month annually. The severity of ozone pollution has also decreased with the HGB ozone design value decreasing from 112 ppbv to 80 ppbv from 2000-2014. In the Houston Ship Channel, NOx decreased 20-44% since 2000, which was a smaller decrease than what had been seen at more urban sites in Houston. Alkanes and alkenes had also decreased 25-45% and 65-72%, respectively. Interestingly, NOx concentrations during the most polluted days had not decreased as much as the annual average of all days, and NOx even increased at the Clinton Drive site after 2006.

The LaRC photochemical box model was used to study how changes in ozone precursors had influenced the photochemical environment in Houston since 2000 on the top 5% ozone-polluted days. Over the time period of this study, net ozone production rates decreased in the Ship Channel, with diurnal median peaks declining from 50-70 ppbv/hr to less than 40 ppbv/hr. Peak ozone production rates typically occurred around solar noon, with the exception of Deer Park, which peaked in the mid morning and correlated with its higher hydrocarbon reactivity in comparison to the other two sites. Extreme production rates of over 100 ppbv/hr had also diminished over time.

Hydrocarbon reactivity in the Ship Channel peaked during the morning and decreased as the boundary layer grew and photochemistry increased in the mid-morning. The two most reactive species were alkenes and formaldehyde, and these

species saw the most reductions from 2000-2014. Due to the lack of measurements, formaldehyde could not be constrained to in the model, but current results suggest that future formaldehyde monitoring would solidify the assessment of its contribution to ozone production. Most species of incorporated in hydrocarbon reactivity decreased during the time period of this study. The most reactive site was Deer Park, followed by Clinton Drive and Channelview.

The results in the Houston Ship Channel showed a mostly VOC-sensitive environment on the top 5% ozone-polluted days, and all sites transitioned further into the VOC-sensitivity regime from 2000 to 2014. This was linked to the lack of decreasing NOx emissions on the most polluted days, but significantly decreased hydrocarbon reactivity, particularly HRVOCs. In the Ship Channel, further reductions in HRVOCs would benefit air quality with respect to ozone. It would take significant reductions in NOx to make an impact on Houston's current ozone levels, and decreasing NOx may even worsen Houston's ozone pollution due to increasing IOPE.

OPE results from direct measurements of NOz and Ox were complex, but the measurements showed an increase in OPE toward petrochemical sources at Deer Park. IOPE was calculated using results from the LaRC model, with extremely efficient ozone production plumes originating from the direction of Ship Channel's industrial sources. IOPE increases as hydrocarbon reactivity increases and NOx decreases. From 2000-2014, IOPE decreased at Deer Park as linked with decreased hydrocarbon emissions. At

Clinton Drive, both increased NOx and hydrocarbon reactivity reductions drove the most significant decrease in IOPE after 2006.

Finally, this analysis was expanded to outside the Ship Channel by incorporating available data in the urban and rural sectors of Houston into the LaRC model. Aircraft data was available from the TexAQS 2000 and TexAQS II/GoMACCS 2006 campaigns, and the urban sector dataset was expanded to more recent years with measurements during 2010 and 2013 at Moody Tower. On the ozone-exceedance days, hot spots of NOx, net ozone production rates, and hydrocarbon reactivity were located in the Ship Channel. However, elevated ozone was measured throughout the entire region. The urban sector of Houston saw less efficient ozone production in comparison to the Ship Channel and rural regions. High IOPE and NOx-sensitivity in the rural sector was linked to low NOx concentrations. Considering the rural sector still saw a median PO_3 of ~ 5 ppbv/hr, NOx reductions could benefit ozone levels in this region. However, if NOx is decreased without any reductions in VOCs in Houston, then IOPE will increase and result in more efficient ozone production in the urban and Ship Channel sectors of the city. To bring Houston metropolitan area into compliance with ozone NAAQS, these results suggest further regulations on industrial HRVOC emissions.

5. CONCLUSIONS

The first two parts of this dissertation involved the analysis of the spatial variability of NO_2 and its influences on measurement intercomparisons from a remote sensing perspective. DISCOVER-AQ Texas provided a unique opportunity to compare measurements of NO_2 with differing techniques and spatial coverage in the Houston, TX region. Analysis from this work can be used to better interpret validation results for future space-based sensors, like TEMPO, as their spatial footprint approaches a sub-urban spatial scale, as well as showed how finer-scale measurements from TEMPO will open up opportunities for more urban-scale studies with respect to the spatial distribution and magnitude of NO_2.

The spatial resolution of OMI could not capture the magnitude of pollution measured by the network of Pandora spectrometers in the urban regions of Houston. In rural areas, OMI consistently measured a larger column than Pandora due to its footprint often encompassing plumes of NO_2. In urban/industrial regions, the comparison between OMI and Pandora had no consistent pattern as OMI lacked the dynamic range of Pandora. When Pandora was located in a relatively unpolluted portion of the OMI pixel, then OMI tended to compare larger, and vice versa. The location of Pandora relative to the area of the OMI pixel changed from day to day, and variable meteorology influenced the distribution of the NO_2 throughout the urban area.

These two reasons led to deviations in the observation comparisons and demonstrated why OMI could not detect the range of pollution that occurred in the region.

When the spatial coverage was decreased from OMI's resolution to GeoTASO's 250×250 km^2 column measurements, r^2 values increased from 0.22 to 0.74 and the slope was nearer to one. However, when the GeoTASO comparison range was decreased to a scale similar to OMI/Pandora observations, the correlation was not improved due to noise within GeoTASO spectrometer ($r^2 = 0.28$). However, GeoTASO's smaller scale measurement had the capability of capturing the ranges of pollution over the urban area by observing individual plumes. The relationship between Pandora and GeoTASO was stronger on more polluted days when there were larger ranges of NO_2 over the urban region.

The 5-km diameter spirals measured by the NASA P-3B were the closest spatial coverage to TEMPO's expected spatial resolution. Aircraft *in situ* data was binned and integrating from 0-3.5 km to derive a tropospheric column for comparisons. The P-3B-derived column compared closely to Pandora, and the scatter between these datasets was correlated to the degree of spatial heterogeneity as quantified by the average standard deviation within each 100 m bin in the lowest 1 km of P-3B NO_2 *in situ* measurements. In areas like Deer Park, the Pandora missed localized NO_2 plumes, as they were not in the field of view of the Pandora instrument. Ultimately, when Pandora is used for future retrieval validations, the degree of spatial variability of NO_2 in the region and the possibility of localized concentrated plumes need to be considered.

To address the TEMPO's goal of monitoring surface air quality from a column observation, Pandora column observations at Moody Tower and Galveston were compared to surface measurements with the assistance of boundary layer height and the P-3B spirals. Both NO_2 column and surface measurements peaked diurnally in the morning, though there was a several hour lag between maxima due to the influence of boundary layer growth and dilution at the surface. There was no significant correlation between surface concentrations and column measurements near Moody Tower; however, when the surface observations were integrated through the height of the boundary layer, the semblance of a relationship appeared with $r^2 = 0.56$. This relationship also demonstrated that the column was not thoroughly mixed through the boundary layer due to NO_2's short lifetime. At Moody Tower, the boundary layer seemed to be approximately half of a well-mixed boundary layer column. This pattern did not appear in Galveston. The range of column and surface measurements were smaller at the Galveston site, and the correlation between surface and column measurements did not appear to be as dependent on the height of the boundary layer. A smaller portion of the NO_2 column was located within the boundary layer with a larger fraction found in the free troposphere. Galveston data also suggested the presence elevated NO_2 layers in the morning, likely from offshore flow within the residual layer from urban Houston. Boundary layer dynamics, NO_2's short lifetime, and possibility of elevated layers will make monitoring the NO_2 air quality at the surface from space-based

monitors difficult. However, in urban areas, surface NO_2 can best be derived from column observations if boundary layer height is incorporated in the retrieval.

Results from Chapter 3 showed that higher resolution *a priori* inputs for the AMF calculation in tropospheric NO_2 column retrievals are necessary in areas with environmental heterogeneity. Out of the three products investigated in California, the BEHR retrieval matched closest to the aircraft-derived column measurements. BEHR was superior with its *a priori* calculations by incorporating higher resolution albedo, terrain pressure, and NO_2 profile to the calculation of the tropospheric AMF. Additionally, the BEHR product averaged *a priori* input parameters over the area of the pixel, rather than the center of the pixel in DOMINO and the NASA Standard Product. These results suggested that future operational retrievals would benefit from similar improvements over urban regions subject to environmental heterogeneity.

Despite adding higher-resolution *a priori* information to the retrieval, mismatched comparisons still occurred in California. This was mainly due to influences from varying pixel sizes, pollution level, and complex terrain. To help with this situation, the OMI DOMINO retrieval was downscaled to a 12×12 km^2 resolution with the CMAQ NAQFC 12 km model output. This tool conserved the mass of NO_2 within the OMI pixel but distributed it according to the relative distribution calculated in the model. The goal of downscaling was to capture the spatial heterogeneity at a finer scale than the satellite's field of view, and in this case, it helped decrease sampling bias between aircraft and the OMI measurements. While this tool led to problems due to

CMAQ errors in transport and emissions, it improved comparisons in the densely polluted areas of Los Angeles and Houston. If CMAQ is able to simulate realistic emission and meteorological conditions, the downscale tool can aid in air quality monitoring, updating of emissions inventories, and determining mitigation strategies for air quality by connecting older large-scale observations with the future urban-scale measurements from TEMPO and TROPOMI.

In addition to investigating NO_2 remote sensing retrievals and intercomparisons, continuous air monitoring data in the Houston Ship Channel was incorporated into the LaRC photochemical box model to analyze how emissions and the photochemical environment had changed between 2000-2014. During this time period, emission reductions in ozone precursors led to fewer ozone-exceedance events in the Houston area. Events that still do occur are less severe than they were in 2000.

On the top 5% ozone-polluted days, maximum ozone production rates decreased from 2000-2014, and extreme production rates over 100 ppbv/hr diminished in the Ship Channel region. The Houston Ship Channel saw a reduction in hydrocarbon reactivity with the biggest decrease near Deer Park; decreased ozone production rates were linked to this drop. The Ship Channel transitioned from borderline VOC-sensitive to exceedingly VOC-sensitive on the most ozone-polluted days during the study period, and model results showed that alkenes and formaldehyde were the most significant contributing VOCs for ozone production.

The most efficient ozone producing plumes originated from wind sectors toward petrochemical facilities with IOPE reaching over 50 at times, suggesting that IOPE was correlated with hydrocarbon emissions in the Houston Ship Channel. As hydrocarbon reactivity increased, IOPE also increased, and it rose at a faster rate if NOx concentrations were reduced. As NOx levels had not decreased as quickly as VOCs, plumes from the Ship Channel became less efficient at making ozone from 2000-2014. Future regulations should focus on VOC emissions in the Ship Channel due to its VOC-sensitivity. If NOx emissions are reduced without a reduction in VOCs, the ozone levels could worsen due to increasing IOPE.

In Houston's urban sector, O_3 and NOx concentrations were comparable to the Ship Channel; however its hydrocarbon reactivity and net ozone production rates were less. Similar to the Ship Channel, the urban sector was VOC-sensitive with the exception of the 2013 dataset. This event appeared to be an outlier by having much lower NOx concentrations and higher levels of hydrocarbon reactivity. The epicenter for this event was located within the Ship Channel, and the characteristics of this event suggested the possibility of fugitive emissions, and the results should not be associated with the trends since 2000.

Expanding further from emission sources to the rural region around Houston, NOx and ozone production rates were lower than the urban sector and Ship Channel counterparts. However, its O_3 concentrations were similar to the rest of the sectors and significant production rates of ~ 5 ppbv/hr were observed. This was an area not

influenced by many fresh emission sources and exhibited NOx-sensitivity with respect to ozone production. Therefore, a NOx reduction could help with ozone concentrations in the rural region in the future. However, even though NOx reductions may help in rural areas of Houston, there is a strong need for VOC reductions in the Ship Channel and urbanized sectors of the city. Decreasing NOx and not addressing VOCs will lead to worse air quality with respect to O_3 in the area. Therefore, in order to bring the Houston metropolitan area into compliance with the ozone NAAQS, these results suggest that further regulations on industrial HRVOC emissions in Houston are needed.

6. REFERENCES

Banta, R. M., C. J. Senff, J. Nielsen-Gammon, L. S. Darby, T. B. Ryerson, R. J. Alvarez, S. R. Sandberg, E. J. Williams, and M. Trainer (2005), A bad air day in Houston, Bulletin of the American Meteorological Society, 86(5), 657-+, doi:10.1175/bams-86-5-657.

Boersma, K. F., et al. (2011), An improved tropospheric NO_2 column retrieval algorithm for the Ozone Monitoring Instrument, Atmospheric Measurement Techniques, 4(9), 1905-1928, doi:10.5194/amt-4-1905-2011.

Boersma, K. F., et al. (2007), Near-real time retrieval of tropospheric NO_2 from OMI, Atmospheric Chemistry and Physics, 7(8), 2103-2118.

Boersma, K. F., et al. (2008), Validation of OMI tropospheric NO_2 observations during INTEX-B and application to constrain NOx emissions over the eastern United States and Mexico, Atmospheric Environment, 42(19), 4480-4497, doi:10.1016/j.atmosenv.2008.02.004.

Boersma, K. F., D. J. Jacob, M. Trainic, Y. Rudich, I. DeSmedt, R. Dirksen, and H. J. Eskes (2009), Validation of urban NO_2 concentrations and their diurnal and seasonal variations observed from the SCIAMACHY and OMI sensors using in situ surface measurements in Israeli cities, Atmospheric Chemistry and Physics, 9(12), 3867-3879.

Bovensmann, H., J. P. Burrows, M. Buchwitz, J. Frerick, S. Noel, V. V. Rozanov, K. V. Chance, and A. P. H. Goede (1999), SCIAMACHY: Mission objectives and measurement modes, Journal of the Atmospheric Sciences, 56(2), 127-150, doi:10.1175/1520-0469(1999)056<0127:smoamm>2.0.co;2.

Brinksma, E. J., et al. (2008), The 2005 and 2006 DANDELIONS NO_2 and aerosol intercomparison campaigns, Journal of Geophysical Research-Atmospheres, 113(D16), 18, doi:10.1029/2007jd008808.

Bucsela, E. J., E. A. Celarier, M. O. Wenig, J. F. Gleason, J. P. Veefkind, K. F. Boersma, and E. J. Brinksma (2006), Algorithm for NO_2 vertical column retrieval from the ozone monitoring instrument, Ieee Transactions on Geoscience and Remote Sensing, 44(5), 1245-1258, doi:10.1109/tgrs.2005.863715.

Bucsela, E. J., N. A. Krotkov, E. A. Celarier, L. N. Lamsal, W. H. Swartz, P. K. Bhartia, K. F. Boersma, J. P. Veefkind, J. F. Gleason, and K. E. Pickering (2013), A new stratospheric and tropospheric NO_2 retrieval algorithm for nadir-viewing satellite instruments: applications to OMI, Atmospheric Measurement Techniques, 6(10), 2607-2626, doi:10.5194/amt-6-2607-2013.

Bucsela, E. J., et al. (2008), Comparison of tropospheric NO_2 from in situ aircraft measurements with near-real-time and standard product data from OMI, Journal of Geophysical Research-Atmospheres, 113(D16), 14, doi:10.1029/2007jd008838.

Burrows, J. P., et al. (1999), The global ozone monitoring experiment (GOME): Mission concept and first scientific results, Journal of the Atmospheric Sciences, 56(2), 151-175, doi:10.1175/1520-0469(1999)056<0151:tgomeg>2.0.co;2.

Callies, J., E. Corpaccioli, M. Eisinger, A. Hahne, and A. Lefebvre (2000), GOME-2 - Metop's second-generation sensor for operational ozone monitoring, Esa Bulletin-European Space Agency(102), 28-36.

Celarier, E. A., et al. (2008), Validation of ozone monitoring instrument nitrogen dioxide columns, Journal of Geophysical Research-Atmospheres, 113(D15), 23, doi:10.1029/2007jd008908.

Chen, S. A., X. R. Ren, J. Q. Mao, Z. Chen, W. H. Brune, B. Lefer, B. Rappengluck, J. Flynn, J. Olson, and J. H. Crawford (2010), A comparison of chemical mechanisms based on TRAMP-2006 field data, Atmospheric Environment, 44(33), 4116-4125, doi:10.1016/j.atmosenv.2009.05.027.

Couzo, E., B. Lefer, J. Stutz, G. Yarwood, P. Karamchandani, B. Henderson, and W. Vizuete (2015), Impacts of heterogeneous HONO formation on radical sources and ozone chemistry in Houston, Texas, Atmospheric Environment, 112, 344-355, doi:10.1016/j.atmosenv.2015.04.048.

Crawford, J., et al. (1999), Assessment of upper tropospheric HOx sources over the tropical Pacific based on NASA GTE/PEM data: Net effect on HOx and other photochemical parameters, Journal of Geophysical Research-Atmospheres, 104(D13), 16255-16273, doi:10.1029/1999jd900106.

Crawford, J. H., et al. (2014), Challenges and opportunities for remote sensing of air quality: Insights from DISCOVER-AQ in AGU Fall Meeting, San Francisco, CA.

Daum, P. H., L. I. Kleinman, S. R. Springston, L. J. Nunnermacker, Y. N. Lee, J. Weinstein-Lloyd, J. Zheng, and C. M. Berkowitz (2003), A comparative study of O-3 formation in the Houston urban and industrial plumes during the 2000 Texas Air Quality Study, Journal of Geophysical Research-Atmospheres, 108(D23), 18, doi:10.1029/2003jd003552.

de Foy, B., Z. F. Lu, D. G. Streets, L. N. Lamsal, and B. N. Duncan (2015), Estimates of power plant NOx emissions and lifetimes from OMI NO_2 satellite retrievals, Atmospheric Environment, 116, 1-11, doi:10.1016/j.atmosenv.2015.05.056.

Dittman, M., E. Ramberg, M. Chrisp, J. V. Rodriguez, A. Sparks, N. Zaun, P. Hendershot, T. Dixon, R. Philbrick, and D. Wasinger (2002), Nadir ultraviolet imaging spectrometer for the NPOESS Ozone Mapping and Profiler Suite (OMPS), paper presented at Conference on Earth Observing Systems VII, Spie-Int Soc Optical Engineering, Seattle, Wa, Jul 07-10.

Duncan, B. N., L. N. Lamsal, A. M. Thompson, Y. Yoshida, Z. F. Lu, D. G. Streets, M. M. Hurwitz, and K. E. Pickering (2016), A space-based, high-resolution view of notable changes in urban NOx pollution around the world (2005-2014), Journal of Geophysical Research-Atmospheres, 121(2), 976-996, doi:10.1002/2015jd024121.

Dunlea, E. J., et al. (2007), Evaluation of nitrogen dioxide chemiluminescence monitors in a polluted urban environment, Atmospheric Chemistry and Physics, 7(10), 2691-2704.

Flynn, C. M., et al. (2014a), Relationship between column-density and surface mixing ratio: Statistical analysis of O-3 and NO_2 data from the July 2011 Maryland DISCOVER-AQ mission, Atmospheric Environment, 92, 429-441, doi:10.1016/j.atmosenv.2014.04.041.

Flynn, J., et al. (2010), Impact of clouds and aerosols on ozone production in Southeast Texas, Atmospheric Environment, 44(33), 4126-4133, doi:10.1016/j.atmosenv.2009.09.005.

Flynn, J. H. (2013), MEASUREMENTS AND ANALYSIS OF OZONE PRODUCTION IN HOUSTON AND LOS ANGELES, Dissertation thesis, University of Houston.

Flynn, L., et al. (2014b), Performance of the Ozone Mapping and Profiler Suite (OMPS) products, Journal of Geophysical Research-Atmospheres, 119(10), 6181-6195, doi:10.1002/2013jd020467.

Hains, J. C., et al. (2010), Testing and improving OMI DOMINO tropospheric NO_2 using observations from the DANDELIONS and INTEX-B validation campaigns, Journal of Geophysical Research-Atmospheres, 115, 20, doi:10.1029/2009jd012399.

Haman, C. L., B. Lefer, and G. A. Morris (2012), Seasonal Variability in the Diurnal Evolution of the Boundary Layer in a Near-Coastal Urban Environment, Journal of Atmospheric and Oceanic Technology, 29(5), 697-710, doi:10.1175/jtech-d-11-00114.1.

Heckel, A., S. W. Kim, G. J. Frost, A. Richter, M. Trainer, and J. P. Burrows (2011), Influence of low spatial resolution a priori data on tropospheric NO_2 satellite retrievals, Atmospheric Measurement Techniques, 4(9), 1805-1820, doi:10.5194/amt-4-1805-2011.

Herman, J., A. Cede, E. Spinei, G. Mount, M. Tzortziou, and N. Abuhassan (2009), NO_2 column amounts from ground-based Pandora and MFDOAS spectrometers using the direct-sun DOAS technique: Intercomparisons and application to OMI validation, Journal of Geophysical Research-Atmospheres, 114, 20, doi:10.1029/2009jd011848.

Jiang, G. F., and J. D. Fast (2004), Modeling the effects of VOC and NOx emission sources on ozone formation in Houston during the TexAQS 2000 field campaign, Atmospheric Environment, 38(30), 5071-5085, doi:10.1016/j.atmosenv.2004.06.012.

Kim, H. C., P. Lee, L. Judd, L. Pan, and B. Lefer (2016), OMI NO_2 column densities over North American urban cities: the effect of satellite footprint resolution, Geoscientific Model Development, doi:10.5194/gmd-9-1111-2016.

Kim, S. W., A. Heckel, S. A. McKeen, G. J. Frost, E. Y. Hsie, M. K. Trainer, A. Richter, J. P. Burrows, S. E. Peckham, and G. A. Grell (2006), Satellite-observed US power plant NOx emission reductions and their impact on air quality, Geophysical Research Letters, 33(22), 5, doi:10.1029/2006gl027749.

Kleinman, L. I. (2005), The dependence of tropospheric ozone production rate on ozone precursors, Atmospheric Environment, 39(3), 575-586, doi:10.1016/j.atmosenv.2004.08.047.

Kleinman, L. I., P. H. Daum, D. Imre, Y. N. Lee, L. J. Nunnermacker, S. R. Springston, J. Weinstein-Lloyd, and J. Rudolph (2002), Ozone production rate and hydrocarbon reactivity in 5 urban areas: A cause of high ozone concentration in Houston, Geophysical Research Letters, 29(10), 4, doi:10.1029/2001gl014569.

Knepp, T., et al. (2013), Estimating surface NO_2 and SO_2 mixing ratios from fast-response total column observations and potential application to geostationary missions, Journal of Atmospheric Chemistry, doi:10.1007/s10874-013-9257-6.

Kramer, L. J., R. J. Leigh, J. J. Remedios, and P. S. Monks (2008), Comparison of OMI and ground-based in situ and MAX-DOAS measurements of tropospheric nitrogen dioxide in an urban area, Journal of Geophysical Research-Atmospheres, 113(D16), 12, doi:10.1029/2007jd009168.

Lamsal, L. N., B. N. Duncan, Y. Yoshida, N. A. Krotkov, K. E. Pickering, D. G. Streets, and Z. F. Lu (2015), U.S. NO_2 trends (2005-2013): EPA Air Quality System (AQS) data versus improved observations from the Ozone Monitoring Instrument (OMI), Atmospheric Environment, 110, 130-143, doi:10.1016/j.atmosenv.2015.03.055.

Lamsal, L. N., et al. (2014), Evaluation of OMI operational standard NO_2 column retrievals using in situ and surface-based NO_2 observations, Atmospheric Chemistry and Physics, 14(21), 11587-11609, doi:10.5194/acp-14-11587-2014.

Lamsal, L. N., R. V. Martin, A. Padmanabhan, A. van Donkelaar, Q. Zhang, C. E. Sioris, K. Chance, T. P. Kurosu, and M. J. Newchurch (2011), Application of satellite observations for timely updates to global anthropogenic NOx emission inventories, Geophysical Research Letters, 38, 5, doi:10.1029/2010gl046476.

Lefer, B., B. Rappengluck, J. Flynn, and C. Haman (2010), Photochemical and meteorological relationships during the Texas-II Radical and Aerosol Measurement Project (TRAMP), Atmospheric Environment, 44(33), 4005-4013, doi:10.1016/j.atmosenv.2010.03.011.

Levelt, P. F., G. H. J. Van den Oord, M. R. Dobber, A. Malkki, H. Visser, J. de Vries, P. Stammes, J. O. V. Lundell, and H. Saari (2006), The Ozone Monitoring Instrument, Ieee Transactions on Geoscience and Remote Sensing, 44(5), 1093-1101, doi:10.1109/tgrs.2006.872333.

Liang, J. Y., L. W. Horowitz, D. J. Jacob, Y. H. Wang, A. M. Fiore, J. A. Logan, G. M. Gardner, and J. W. Munger (1998), Seasonal budgets of reactive nitrogen species and ozone over the United States, and export fluxes to the global atmosphere, Journal of Geophysical Research-Atmospheres, 103(D11), 13435-13450, doi:10.1029/97jd03126.

Lurmann, F. W., A. C. Lloyd, and R. Atkinson (1986), A CHEMICAL MECHANISM FOR USE IN LONG-RANGE TRANSPORT ACID DEPOSITION COMPUTER MODELING, Journal of Geophysical Research-Atmospheres, 91(D10), 905-936, doi:10.1029/JD091iD10p10905.

Mao, J. Q., et al. (2010), Atmospheric oxidation capacity in the summer of Houston 2006: Comparison with summer measurements in other metropolitan studies, Atmospheric Environment, 44(33), 4107-4115, doi:10.1016/j.atmosenv.2009.01.013.

Martin, R. V., C. E. Sioris, K. Chance, T. B. Ryerson, T. H. Bertram, P. J. Wooldridge, R. C. Cohen, J. A. Neuman, A. Swanson, and F. M. Flocke (2006), Evaluation of space-based constraints on global nitrogen oxide emissions with regional aircraft measurements over and downwind of eastern North America, Journal of Geophysical Research-Atmospheres, 111(D15), 15, doi:10.1029/2005jd006680.

McPeters, R. D., et al. (1998), Earth Probe Total Ozone Mapping Spectrometer (TOMS) Data Products User's Guide, edited, NASA Technical Publication.

Munkel, C., N. Eresmaa, J. Rasanen, and A. Karppinen (2007), Retrieval of mixing height and dust concentration with lidar ceilometer, Boundary-Layer Meteorology, 124(1), 117-128, doi:10.1007/s10546-006-9103-3.

Neuman, J. A., et al. (2009), Relationship between photochemical ozone production and NOx oxidation in Houston, Texas, Journal of Geophysical Research-Atmospheres, 114, 12, doi:10.1029/2008jd011688.

Nowlan, C. R., et al. (2015), Nitrogen dioxide observations from the Geostationary Trace gas and Aerosol Sensor Optimization (GeoTASO) airborne instrument: retrieval algorithm and measurements during DISCOVER-AQ Texas 2013, Atmospheric Measurement Techniques Discussion, 13099–13155, doi:10.5194/amtd-8-13099-2015.

Oetjen, H., S. Baidar, N. A. Krotkov, L. N. Lamsal, M. Lechner, and R. Volkamer (2013), Airborne MAX-DOAS measurements over California: Testing the NASA OMI tropospheric NO_2 product, Journal of Geophysical Research-Atmospheres, 118(13), 7400-7413, doi:10.1002/jgrd.50550.

Olson, J. R., et al. (2004), Testing fast photochemical theory during TRACE-P based on measurements of OH, HO_2, and CH_2O, Journal of Geophysical Research-Atmospheres, 109(D15), 16, doi:10.1029/2003jd004278.

Palmer, P. I., D. J. Jacob, K. Chance, R. V. Martin, R. J. D. Spurr, T. P. Kurosu, I. Bey, R. Yantosca, A. Fiore, and Q. B. Li (2001), Air mass factor formulation for spectroscopic measurements from satellites: Application to formaldehyde retrievals from the Global Ozone Monitoring Experiment, Journal of Geophysical Research-Atmospheres, 106(D13), 14539-14550, doi:10.1029/2000jd900772.

Parrish, D. D., et al. (2009), Overview of the Second Texas Air Quality Study (TexAQS II) and the Gulf of Mexico Atmospheric Composition and Climate Study (GoMACCS), Journal of Geophysical Research-Atmospheres, 114, 28, doi:10.1029/2009jd011842.

Parrish, D. D., et al. (2012), Primary and secondary sources of formaldehyde in urban atmospheres: Houston Texas region, Atmospheric Chemistry and Physics, 12(7), 3273-3288, doi:10.5194/acp-12-3273-2012.

Pollack, I., B. Lerner, and T. Ryerson (2011), Evaluation of ultraviolet light-emitting diodes for detection of atmospheric NO_2 by photolysis - chemiluminescence, Journal of Atmospheric Chemistry, 65(2-3), 14, doi:10.1007/s10874-011-9184-3.

Reed, A. J., A. M. Thompson, D. E. Kollonige, D. K. Martins, M. A. Tzortziou, J. R. Herman, T. A. Berkoff, N. K. Abuhassan, and A. Cede (2013), Effects of local meteorology and aerosols on ozone and nitrogen dioxide retrievals from OMI and Pandora spectrometers in Maryland, Journal of Atmospheric Chemistry, doi:10.1007/s10874-013-9254-9.

Ren, X. R., et al. (2013), Atmospheric oxidation chemistry and ozone production: Results from SHARP 2009 in Houston, Texas, Journal of Geophysical Research-Atmospheres, 118(11), 5770-5780, doi:10.1002/jgrd.50342.

Russell, A. R., A. E. Perring, L. C. Valin, E. J. Bucsela, E. C. Browne, K. E. Min, P. J. Wooldridge, and R. C. Cohen (2011), A high spatial resolution retrieval of NO_2 column densities from OMI: method and evaluation, Atmospheric Chemistry and Physics, 11(16), 8543-8554, doi:10.5194/acp-11-8543-2011.

Russell, A. R., L. C. Valin, and R. C. Cohen (2012), Trends in OMI NO_2 observations over the United States: effects of emission control technology and the economic recession, Atmospheric Chemistry and Physics, 12(24), 12197-12209, doi:10.5194/acp-12-12197-2012.

Ryerson, T. B., et al. (2013), The 2010 California Research at the Nexus of Air Quality and Climate Change (CalNex) field study, Journal of Geophysical Research-Atmospheres, 118(11), 5830-5866, doi:10.1002/jgrd.50331.

Ryerson, T. B., et al. (2003), Effect of petrochemical industrial emissions of reactive alkenes and NOx on tropospheric ozone formation in Houston, Texas, Journal of Geophysical Research-Atmospheres, 108(D8), 24, doi:10.1029/2002jd003070.

Sander, S. F., R. R. Ravishankara, A. R. Golden, D. M. Kolb, C. E. Kurylo,M. J. Molina, M. J. Moortgat, G. K. Keller-Rudek, H. Finlayson-Pitts, B. J.Wine, P. H. Huie, R. E., and V. L. Orkin (2006), Chemical Kinetics and Photochemical Data for Use in Atmospheric Studies Evaluation Number 15, edited, JPL Publication.

Sather, M. E., E. T. Slonecker, K. G. Kronmiller, D. D. Williams, H. Daughtrey, and J. Mathew (2006), Evaluation of short-term Ogawa passive, photolytic, and federal reference method sampling devices for nitrogen oxides in El Paso and Houston, Texas, Journal of Environmental Monitoring, 8(5), 558-563, doi:10.1039/b601113f.

Saunders, S. M., M. E. Jenkin, R. G. Derwent, and M. J. Pilling (2003), Protocol for the development of the Master Chemical Mechanism, MCM v3 (Part A): tropospheric degradation of non-aromatic volatile organic compounds, Atmospheric Chemistry and Physics, 3, 161-180.

Seftor, C. J., G. Jaross, M. Kowitt, M. Haken, J. Li, and L. E. Flynn (2014), Postlaunch performance of the Suomi National Polar-orbiting Partnership Ozone Mapping and Profiler Suite (OMPS) nadir sensors, Journal of Geophysical Research-Atmospheres, 119(7), 4413-4428, doi:10.1002/2013jd020472.

Steiner, A. L., R. C. Cohen, R. A. Harley, S. Tonse, D. B. Millet, G. W. Schade, and A. H. Goldstein (2008), VOC reactivity in central California: comparing an air quality model to ground-based measurements, Atmospheric Chemistry and Physics, 8(2), 351-368.

Tzortziou, M., J. Herman, A. Cede, C. Loughner, N. Abuhassan, and S. Naik (2013), Spatial and temporal variability of ozone and nitrogen dioxide over a major urban estuarine ecosystem, Journal of Atmospheric Chemistry, doi:10.1007/s10874-013-9255-8.

Tzortziou, M., J. R. Herman, A. Cede, and N. Abuhassan (2012), High precision, absolute total column ozone measurements from the Pandora spectrometer system: Comparisons with data from a Brewer double monochromator and Aura OMI, Journal of Geophysical Research-Atmospheres, 117, 14, doi:10.1029/2012jd017814.

Valin, L. C., A. R. Russell, R. C. Hudman, and R. C. Cohen (2011), Effects of model resolution on the interpretation of satellite NO_2 observations, Atmospheric Chemistry and Physics, 11(22), 11647-11655, doi:10.5194/acp-11-11647-2011.

Valks, P., G. Pinardi, A. Richter, J. C. Lambert, N. Hao, D. Loyola, M. Van Roozendael, and S. Emmadi (2011), Operational total and tropospheric NO_2 column retrieval for GOME-2, Atmospheric Measurement Techniques, 4(7), 1491-1514, doi:10.5194/amt-4-1491-2011.

van Geffen, J., K. F. Boersma, H. J. Eskes, J. D. Maasakkers, and J. P. Veefkind (2016), TROPOMI ATBD of the total and tropospheric NO_2 data products, KNMI technical document: S5P-KNMI-L2-0005-RP.

Wang, S. H., T. J. Pongetti, S. P. Sander, E. Spinei, G. H. Mount, A. Cede, and J. Herman (2010), Direct Sun measurements of NO_2 column abundances from Table Mountain, California: Intercomparison of low- and high-resolution spectrometers, Journal of Geophysical Research-Atmospheres, 115, 16, doi:10.1029/2009jd013503.

Washenfelder, R. A., et al. (2010), Characterization of NOx, SO_2, ethene, and propene from industrial emission sources in Houston, Texas, Journal of Geophysical Research-Atmospheres, 115, 14, doi:10.1029/2009jd013645.

Wu, X. Q., et al. (2014), Evaluation of the Sensor Data Record from the nadir instruments of the Ozone Mapping Profiler Suite (OMPS), Journal of Geophysical Research-Atmospheres, 119(10), 6170-6180, doi:10.1002/2013jd020484.

Zhou, W., D. S. Cohan, and B. H. Henderson (2014), Slower ozone production in Houston, Texas following emission reductions: evidence from Texas Air Quality Studies in 2000 and 2006, Atmospheric Chemistry and Physics, 14(6), 2777-2788, doi:10.5194/acp-14-2777-2014.

Zoogman, P., et al. (submitted), Tropospheric Emissions: Monitoring of Pollution (TEMPO), Journal of Quantitative Spectroscopy and Radiative Transfer.